Control of Wind Turbine Systems

Dao Zhou

Associate Professor
Email: zda@et.aau.dk

AALBORG UNIVERSITY
DENMARK

WinGrid

Outline

1. State-of-art of wind turbine system
   - Configuration evolution
   - Grid codes requirement
   - General control structure

2. Modeling and control of wind turbine system
   - Topology of DFIG and PMSG
   - Modeling and control of grid-side converter
   - Modelling of control of machine-side converter (DFIG and PMSG)

3. Abnormal operation of wind turbine system
   - Classification of grid faults
   - DFIG operation under symmetrical/asymmetrical grid faults
   - PMSG operation under symmetrical/asymmetrical grid faults

Outline

1. State-of-art of wind turbine system
   - Configuration evolution
   - Grid codes requirement
   - General control structure

2. Modeling and control of wind turbine system
   - Topology of DFIG and PMSG
   - Modeling and control of grid-side converter
   - Modelling of control of machine-side converter (DFIG and PMSG)

3. Abnormal operation of wind turbine system
   - Classification of grid faults
   - DFIG operation under symmetrical/asymmetrical grid faults
   - PMSG operation under symmetrical/asymmetrical grid faults

Configuration Evolution

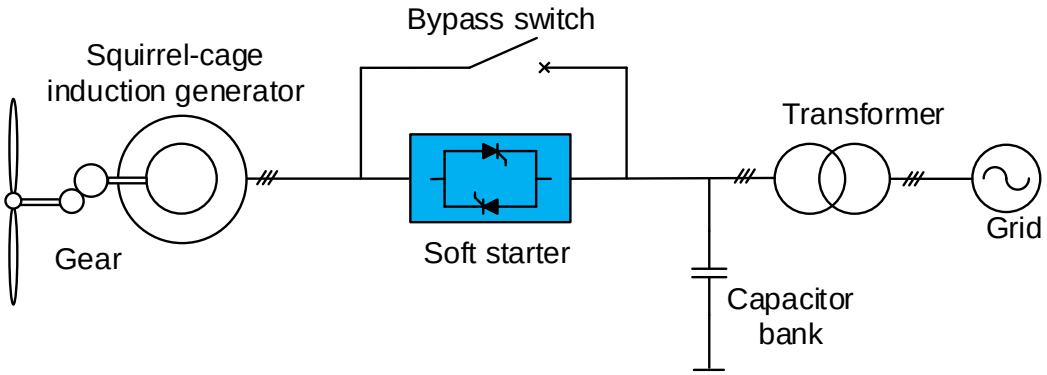

Type I – Fixed speed wind turbine

- Popular in 1980s
- Equipped with SCIG & soft starter
- Electrical power pulsations
- Cap. bank to compensate excited Q

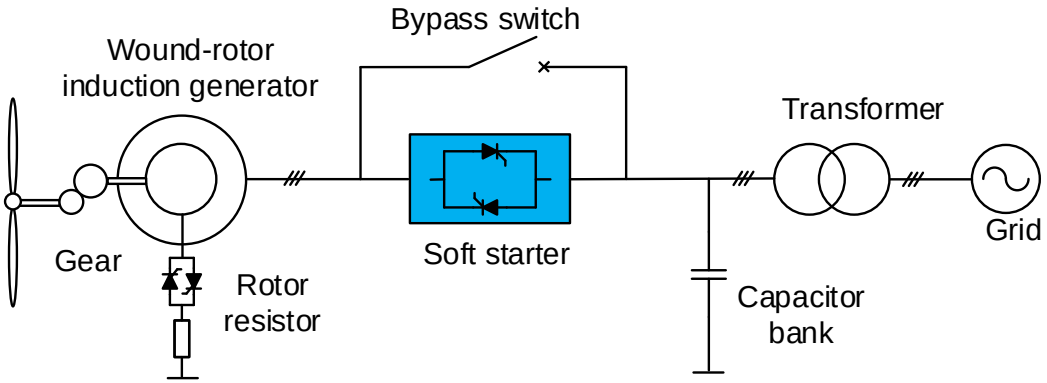

Type II – Partial variable speed wind turbine with rotor resistor

- Emerge in mid-1990s
- Equipped with WRIG & soft starter
- Limited variable speed
- Resistor power dissipation

Configuration Evolution (Cont.)

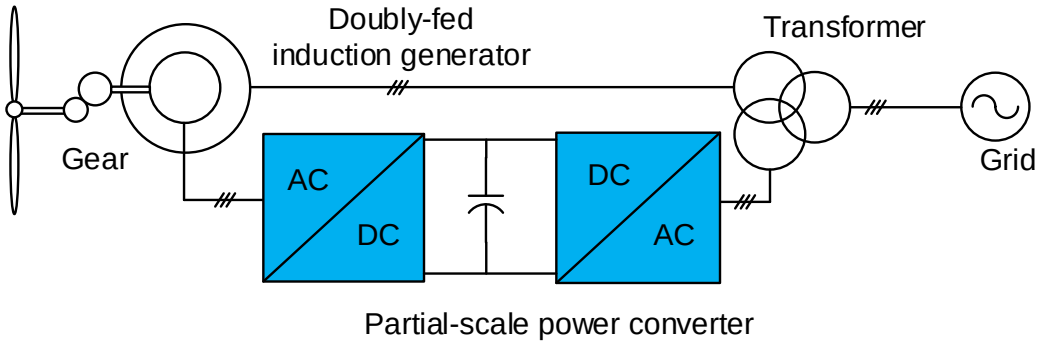

- Equipped with DFIG
- Around 30% rated power converter
- Fragile slip rings
- Crowbar for grid ride-through

Type III – Variable speed wind turbine with partial-scale converter

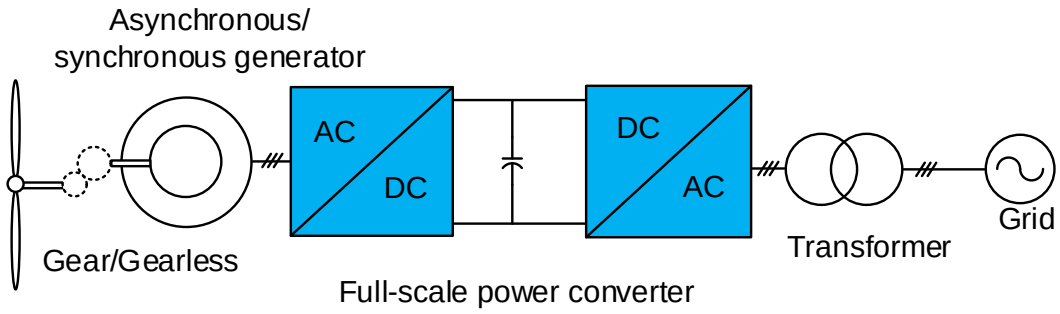

- Synchronous/asynchronous generator
- Elimination of slip rings
- Possible gear-less
- Full controllability during grid faults

Type IV – Variable speed wind turbine with full-scale converter

Grid Codes Requirements

Normal operation

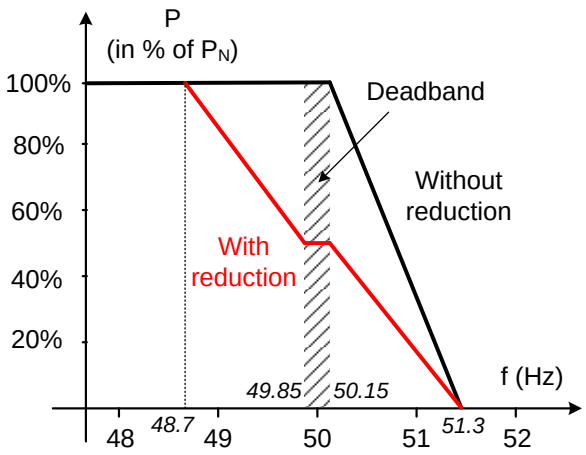

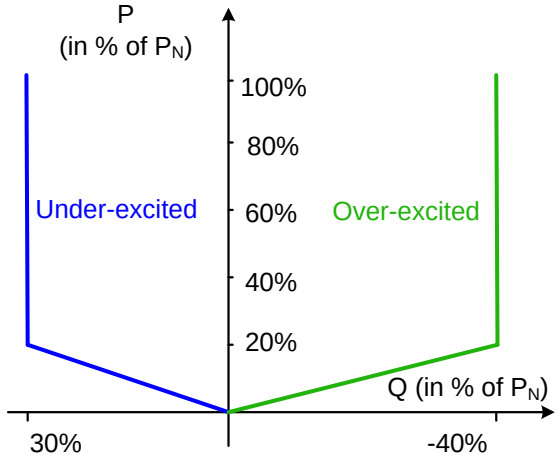

Voltage disturbances

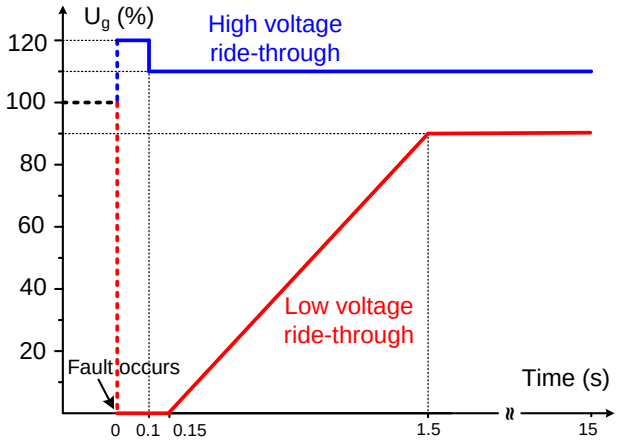

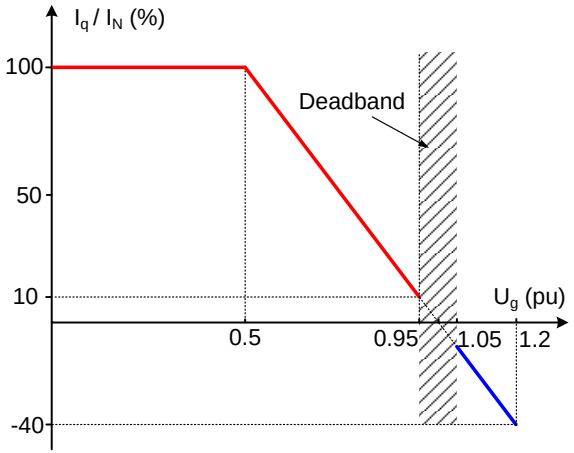

General Control Structure

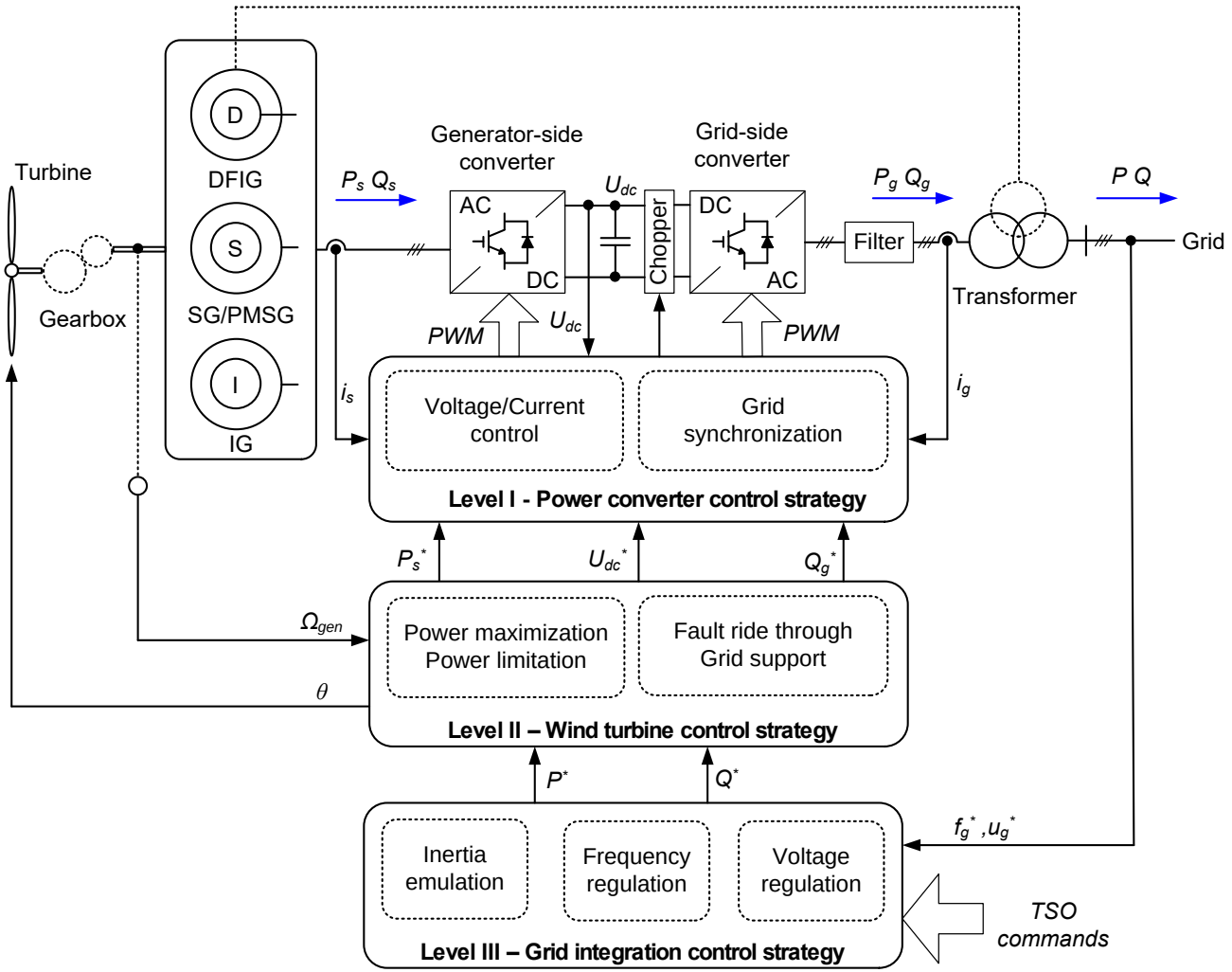

Outline

1. State-of-art of wind turbine system
   - Configuration evolution
   - Grid codes requirement
   - General control structure

2. Modeling and control of wind turbine system
   - Topology of DFIG and PMSG
   - Modeling and control of grid-side converter
   - Modelling of control of machine-side converter (DFIG and PMSG)

3. Abnormal operation of wind turbine system
   - Classification of grid faults
   - DFIG operation under symmetrical/asymmetrical grid faults
   - PMSG operation under symmetrical/asymmetrical grid faults

Configurations of DFIG and PMSG Systems

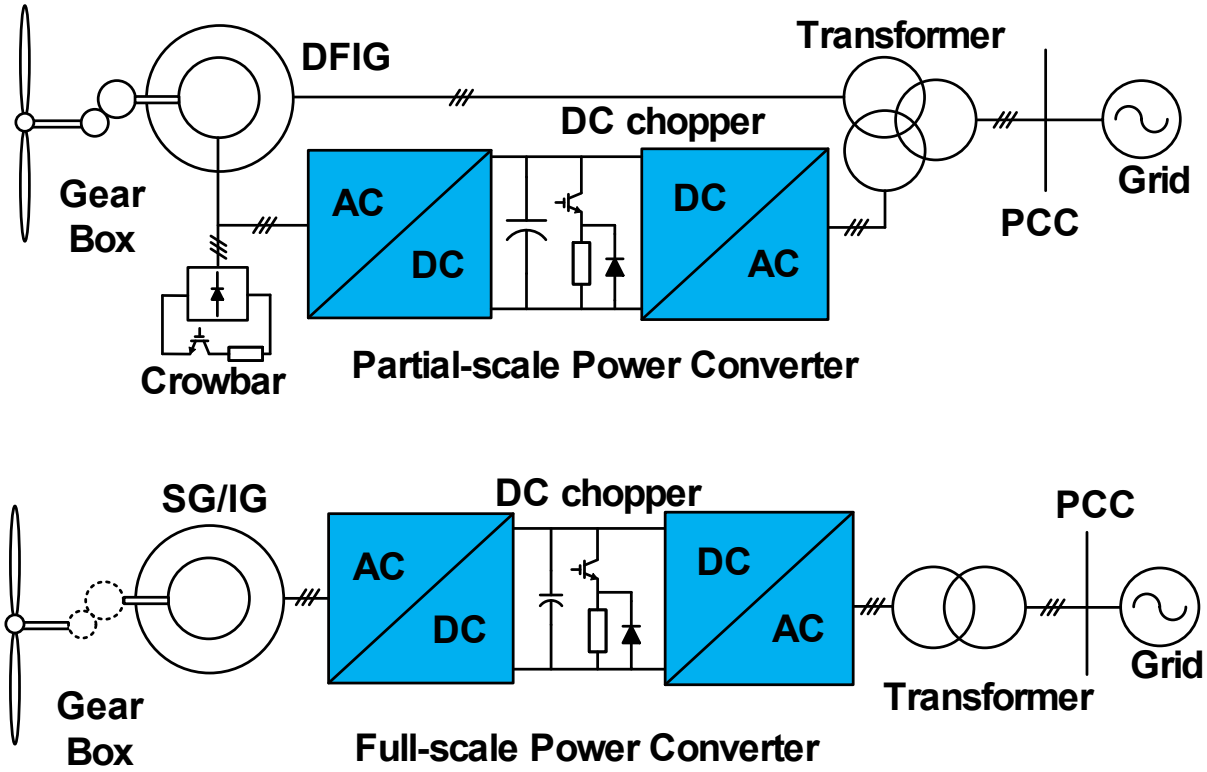

- DFIG system
  - Economical power converter
  - Crowbar
  - slip rings
- PMSG system
  - Gearless
  - Full controllability
  - Expensive power electronics

Control Targets of DFIG Power Converter

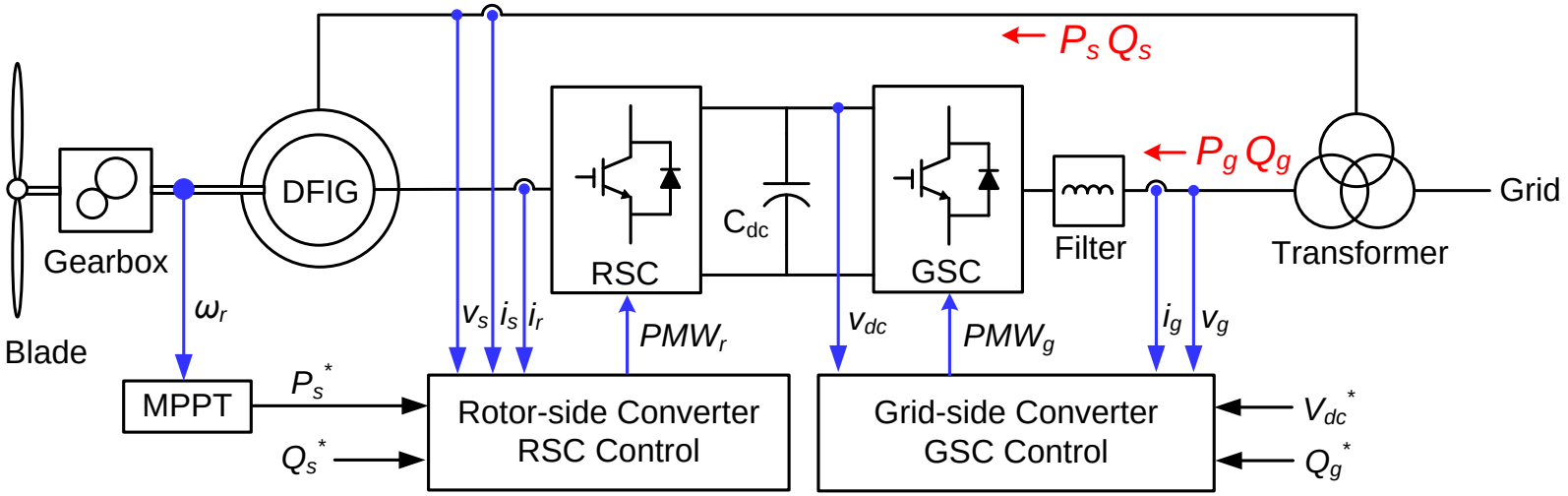

- **Rotor-side Converter (RSC):**
  - Control stator active power following MPPT
  - Supply stator reactive power as needed
- **Grid-side Converter (GSC):**
  - Keep DC-link voltage constant
  - Provide reactive power as required

Control Targets of PMSG Power Converter

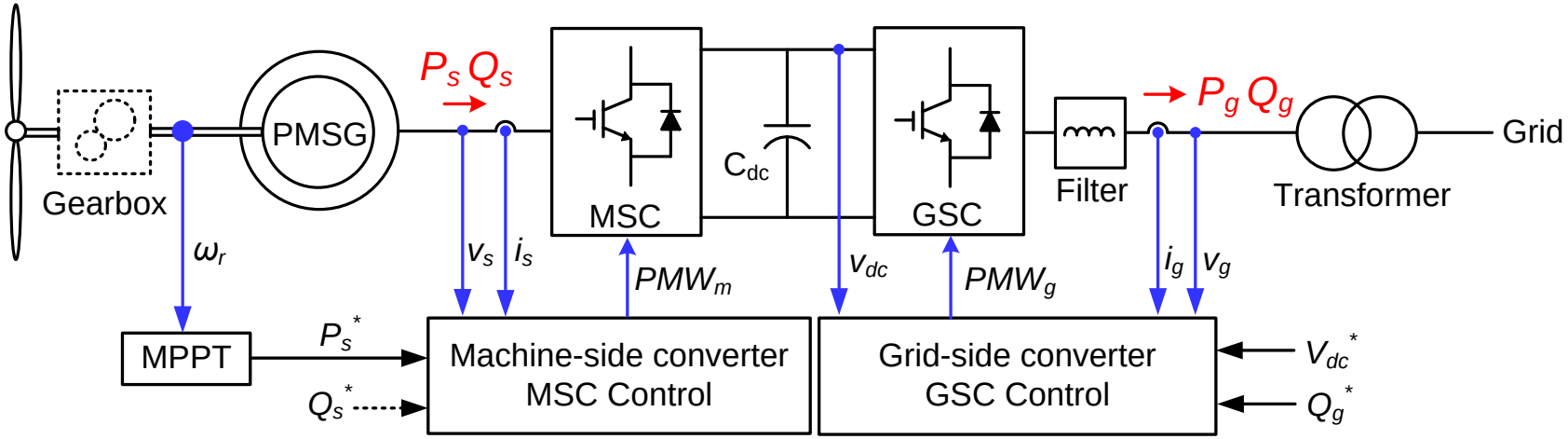

- **Machine-side Converter (MSC):**
  - Control stator active power following MPPT
  - Zero reactive power for min. loss dissipation
- **Grid-side Converter (GSC):**
  - Keep DC-link voltage constant
  - Provide reactive power as required

Modeling of GSC

Mathematical modeling under abc reference frame

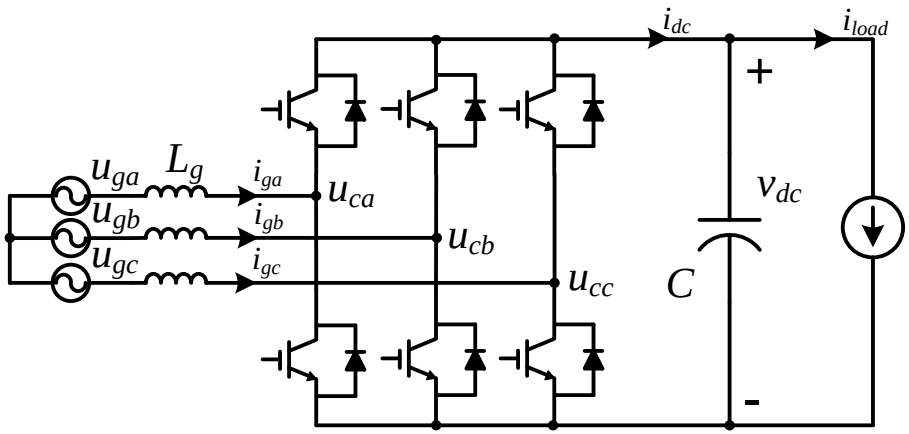

According to KVL in the ac-side and KCL in the dc-side:

$$\begin{cases} u_{ga} - L_g \dfrac{di_{ga}}{dt} - S_a v_{dc} = u_{gb} - L_g \dfrac{di_{gb}}{dt} - S_b v_{dc} = u_{gc} - L_g \dfrac{di_{gc}}{dt} - S_c v_{dc} \\ C \dfrac{dv_{dc}}{dt} = S_a i_{ga} + S_b i_{gb} + S_c i_{gc} - i_{load} \end{cases}$$

Modeling of GSC

Mathematical modeling under abc reference frame (Cont.)

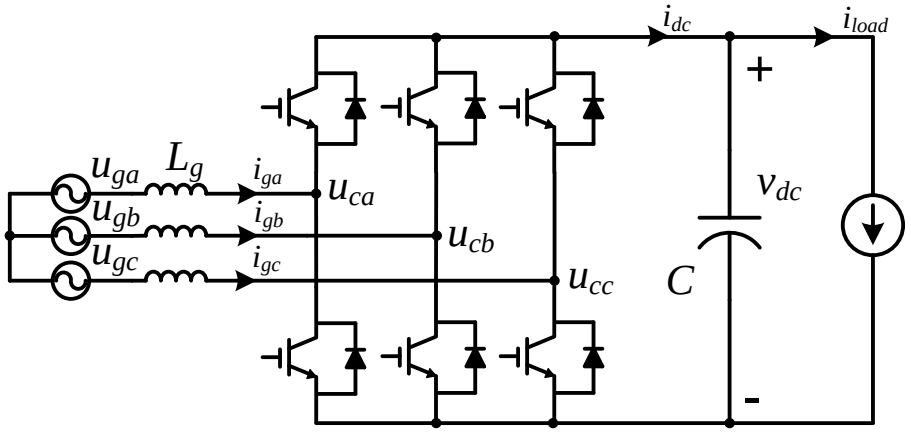

In a symmetrical three-phase system: $u_{ga}+u_{gb}+u_{gc}=0$, $i_{ga}+i_{gb}+i_{gc}=0$

$$\begin{cases} \begin{bmatrix} u_{ga} \\ u_{gb} \\ u_{gc} \end{bmatrix} = L_g \frac{d}{dt}\begin{bmatrix} i_{ga} \\ i_{gb} \\ i_{gc} \end{bmatrix} + \begin{bmatrix} S_a - \frac{S_a+S_b+S_c}{3} \\ S_b - \frac{S_a+S_b+S_c}{3} \\ S_c - \frac{S_a+S_b+S_c}{3} \end{bmatrix} v_{dc} \\ C\frac{d}{dt}v_{dc} = \begin{bmatrix} S_a & S_b & S_c \end{bmatrix}\begin{bmatrix} i_{ga} \\ i_{gb} \\ i_{gc} \end{bmatrix} - i_{load} \end{cases}$$

- Complicated and coupled
- Discontinuous and nonlinear
- Not compatible with classical controller design

Modeling of GSC

State-average modeling under abc reference frame

To ensure a continuous modelling, state-average approach is applied

$$\langle x \rangle_{T_s} = \frac{1}{T_s}\int_{t}^{t+T_s} x(\tau)d\tau$$

The switching function is substituted by duty cycle,

$$\begin{cases} \begin{bmatrix} \langle u_{ga} \rangle_{T_s} \\ \langle u_{gb} \rangle_{T_s} \\ \langle u_{gc} \rangle_{T_s} \end{bmatrix} = L_g \frac{d}{dt} \begin{bmatrix} \langle i_{ga} \rangle_{T_s} \\ \langle i_{gb} \rangle_{T_s} \\ \langle i_{gc} \rangle_{T_s} \end{bmatrix} + \begin{bmatrix} d_a - \dfrac{d_a + d_b + d_c}{3} \\ d_b - \dfrac{d_a + d_b + d_c}{3} \\ d_c - \dfrac{d_a + d_b + d_c}{3} \end{bmatrix} \langle v_{dc} \rangle_{T_s} \\ C\dfrac{d}{dt}\langle v_{dc} \rangle_{T_s} = \begin{bmatrix} d_a & d_b & d_c \end{bmatrix} \begin{bmatrix} \langle i_{ga} \rangle_{T_s} \\ \langle i_{gb} \rangle_{T_s} \\ \langle i_{gc} \rangle_{T_s} \end{bmatrix} - \langle i_{load} \rangle_{T_s} \end{cases}$$

- Continuous and linear
- Neglected switching ripple

Modeling of GSC

Coordinate transformation

- Clarke transformation (3s->2s)

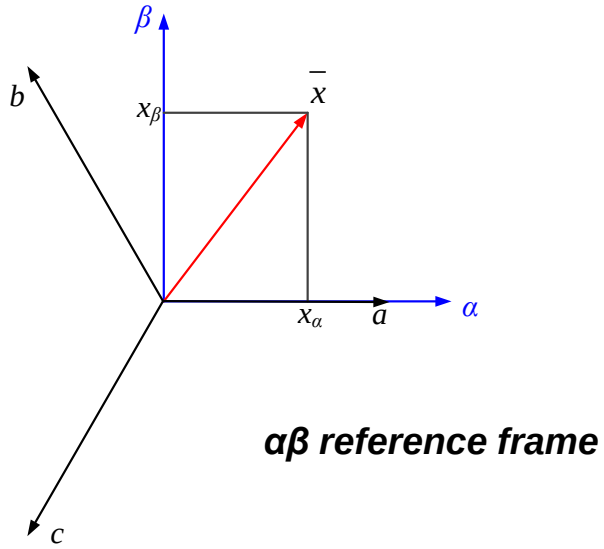

αβ reference frame

- Park transformation (2s->2r)

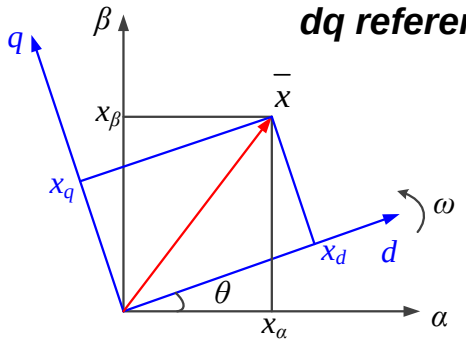

dq reference frame

$$C_{32} = \frac{2}{3}\begin{bmatrix} 1 & -\frac{1}{2} & -\frac{1}{2} \\ 0 & \frac{\sqrt{3}}{2} & -\frac{\sqrt{3}}{2} \end{bmatrix} \quad C_{23} = \begin{bmatrix} 1 & 0 \\ -\frac{1}{2} & \frac{\sqrt{3}}{2} \\ -\frac{1}{2} & -\frac{\sqrt{3}}{2} \end{bmatrix}$$

$$C_{2s/2r} = \begin{bmatrix} \cos\omega t & \sin\omega t \\ -\sin\omega t & \cos\omega t \end{bmatrix} \quad C_{2r/2s} = \begin{bmatrix} \cos\omega t & -\sin\omega t \\ \sin\omega t & \cos\omega t \end{bmatrix}$$

Modeling of GSC

Space vector

In a three-phase system, electrical values under abc frame can be expressed:

$$x_a = X\cos(\omega t);\quad x_b = X\cos(\omega t - 2\pi/3);\quad x_c = X\cos(\omega t + 2\pi/3)$$

To express three scalars in terms of one vector, the space vector is introduced:

$$\vec{x} = x_a + \gamma x_b + \gamma^2 x_c \qquad \text{where} \qquad \gamma = \exp(\mathrm{j}\frac{2\pi}{3})$$

Clark transformation:

$$\begin{bmatrix} x_\alpha \\ x_\beta \end{bmatrix} = C_{32}\begin{bmatrix} x_a \\ x_b \\ x_c \end{bmatrix} = \begin{bmatrix} \mathrm{X}\cos(\omega t) \\ \mathrm{X}\sin(\omega t) \end{bmatrix}$$

$$\overline{X} = x_\alpha + jx_\beta = X\exp(\mathrm{j}\omega t)$$

Park transformation:

$$\begin{bmatrix} x_d \\ x_q \end{bmatrix} = C_{2s/2r}\begin{bmatrix} x_\alpha \\ x_\beta \end{bmatrix} = \begin{bmatrix} \mathrm{X} \\ 0 \end{bmatrix}$$

- Three-phase system is simplified to two-phase system
- AC values become DC values

Modeling of GSC

Large-signal modeling under dq reference frame

$$\begin{cases} \begin{bmatrix} \langle u_{ga} \rangle_{T_s} \\ \langle u_{gb} \rangle_{T_s} \\ \langle u_{gc} \rangle_{T_s} \end{bmatrix} = L_g \frac{d}{dt} \begin{bmatrix} \langle i_{ga} \rangle_{T_s} \\ \langle i_{gb} \rangle_{T_s} \\ \langle i_{gc} \rangle_{T_s} \end{bmatrix} + \begin{bmatrix} d_a - \frac{d_a + d_b + d_c}{3} \\ d_b - \frac{d_a + d_b + d_c}{3} \\ d_c - \frac{d_a + d_b + d_c}{3} \end{bmatrix} \langle v_{dc} \rangle_{T_s} \\ C \frac{d}{dt} \langle v_{dc} \rangle_{T_s} = \begin{bmatrix} d_a & d_b & d_c \end{bmatrix} \begin{bmatrix} \langle i_{ga} \rangle_{T_s} \\ \langle i_{gb} \rangle_{T_s} \\ \langle i_{gc} \rangle_{T_s} \end{bmatrix} - \langle i_{load} \rangle_{T_s} \end{cases}$$

$$\begin{cases} \begin{bmatrix} \langle u_{g\alpha} \rangle_{T_s} \\ \langle u_{g\beta} \rangle_{T_s} \end{bmatrix} = L_g \frac{d}{dt} \begin{bmatrix} \langle i_{g\alpha} \rangle_{T_s} \\ \langle i_{g\beta} \rangle_{T_s} \end{bmatrix} + \begin{bmatrix} d_\alpha \\ d_\beta \end{bmatrix} \langle v_{dc} \rangle_{T_s} \\ C \frac{d}{dt} \langle v_{dc} \rangle_{T_s} = \frac{3}{2} \begin{bmatrix} d_\alpha & d_\beta \end{bmatrix} \begin{bmatrix} \langle i_{g\alpha} \rangle_{T_s} \\ \langle i_{g\beta} \rangle_{T_s} \end{bmatrix} - \langle i_{load} \rangle_{T_s} \end{cases}$$

- Coupling components is introduced
- Continuous and simplified modeling

$$\begin{cases} \begin{bmatrix} \langle u_{gd} \rangle_{T_s} \\ \langle u_{gq} \rangle_{T_s} \end{bmatrix} = L_g \frac{d}{dt} \begin{bmatrix} \langle i_{gd} \rangle_{T_s} \\ \langle i_{gq} \rangle_{T_s} \end{bmatrix} + L \begin{bmatrix} 0 & -\omega \\ \omega & 0 \end{bmatrix} \begin{bmatrix} \langle i_{gd} \rangle_{T_s} \\ \langle i_{gq} \rangle_{T_s} \end{bmatrix} + \begin{bmatrix} d_d \\ d_q \end{bmatrix} \langle v_{dc} \rangle_{T_s} \\ C \frac{d}{dt} \langle v_{dc} \rangle_{T_s} = \frac{3}{2} \begin{bmatrix} d_d \\ d_q \end{bmatrix}^T \begin{bmatrix} \langle i_{gd} \rangle_{T_s} \\ \langle i_{gq} \rangle_{T_s} \end{bmatrix} - \langle i_{load} \rangle_{T_s} \end{cases}$$

Modeling of GSC

Small-signal modeling under dq reference frame

By adding the disturbance around the static operation point

$$\langle x \rangle_{T_s} = X + x$$

- Equation at static operation point:

$$\begin{cases} U_{gd} = -\omega L_g I_{gq} + D_d V_{dc} \\ U_{gq} = \omega L_g I_{gd} + D_q V_{dc} \\ I_{load} = \frac{3}{2}(D_d I_{gd} + D_q I_{gq}) \end{cases}$$

- Equation for disturbance:

$$\begin{cases} u_{gd} = L_g \frac{d i_{gd}}{dt} - \omega L_g i_{gq} + D_d v_{dc} + V_{dc} d_d \\ u_{gq} = L_g \frac{d i_{gq}}{dt} + \omega L_g i_{gd} + D_q v_{dc} + V_{dc} d_q \\ C \frac{d}{dt} v_{dc} = \frac{3}{2}(D_d i_{gd} + I_{gd} d_d + D_q i_{gq} + I_{gq} d_q) - i_{load} \end{cases}$$

- ❖ Linear characteristics are suitable for classical control theory
- ❖ Transfer function can be obtained

Control of GSC (PI)

Overall control structure of GSC

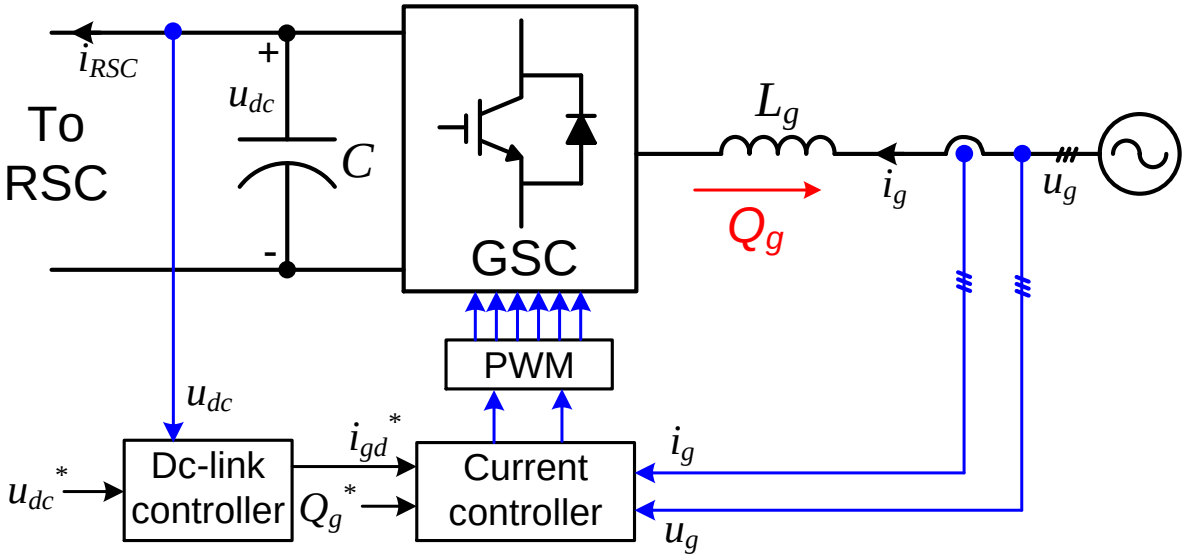

- Inner current loop
- Outer dc-link voltage loop

Control of GSC (PI)

Plant of grid current and decoupling control

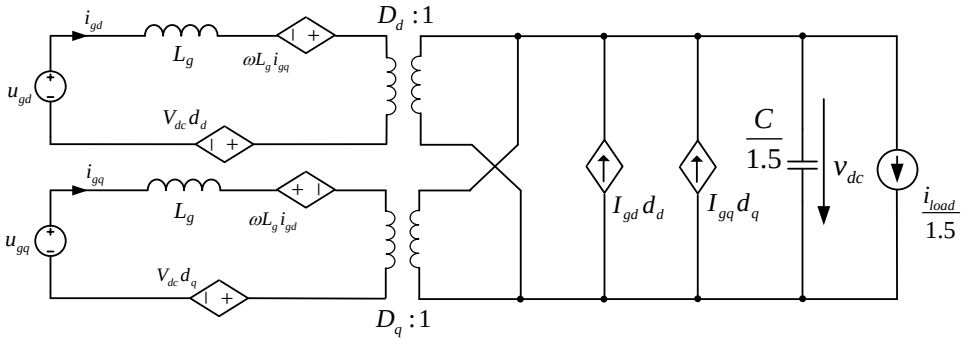

$$\frac{d}{dt}\begin{bmatrix} i_{gd} \\ i_{gq} \end{bmatrix} = -\begin{bmatrix} 0 & -\omega \\ \omega & 0 \end{bmatrix}\begin{bmatrix} i_{gd} \\ i_{gq} \end{bmatrix} - \frac{1}{L_g}\begin{bmatrix} d_d \\ d_q \end{bmatrix} V_{dc}$$

$$\frac{d}{dt}\begin{bmatrix} i_{gd} \\ i_{gq} \end{bmatrix} = -\frac{1}{L_g}\begin{bmatrix} d_d \\ d_q \end{bmatrix} V_{dc}$$

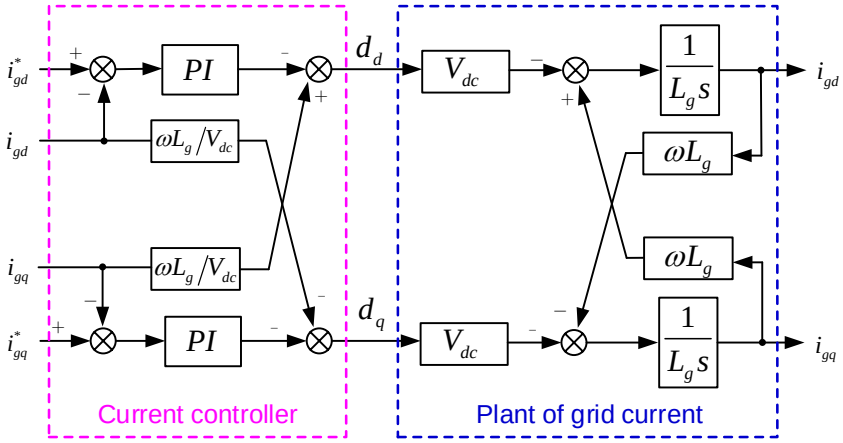

Control of GSC (PI)

PWM delay

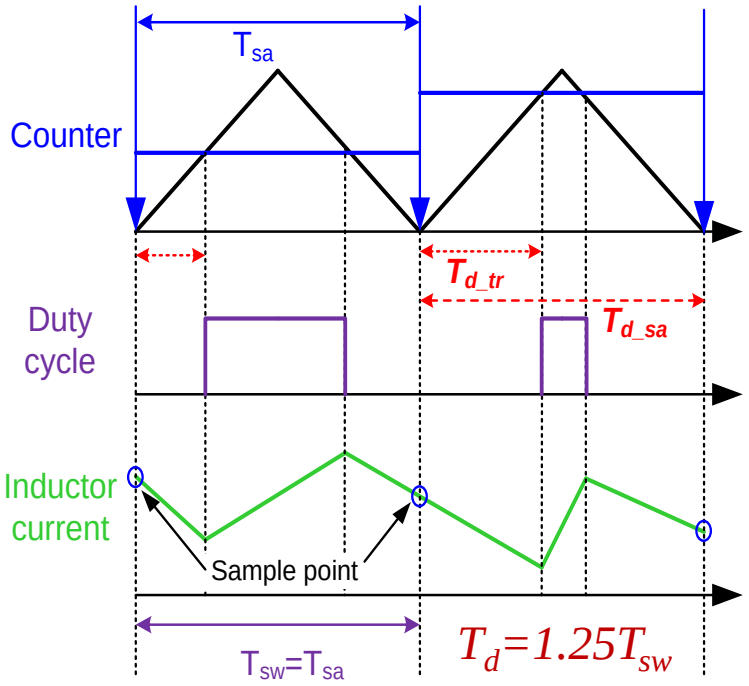

Symmetrical PWM

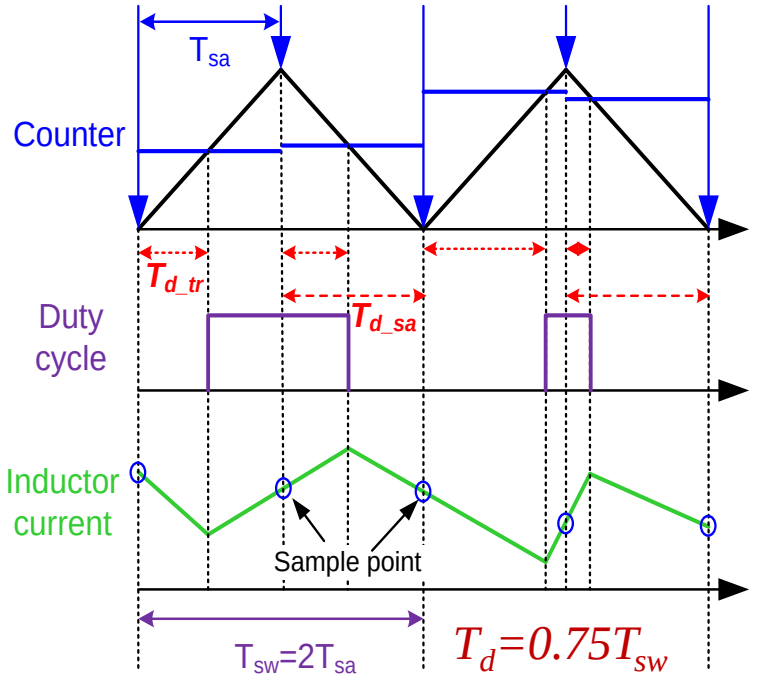

Asymmetrical PWM

Delay unit can roughly be considered as inertia unit: $G_{PWM}(s) = \frac{1}{T_d s + 1}$

Control of GSC (PI)

Block diagram of current loop control

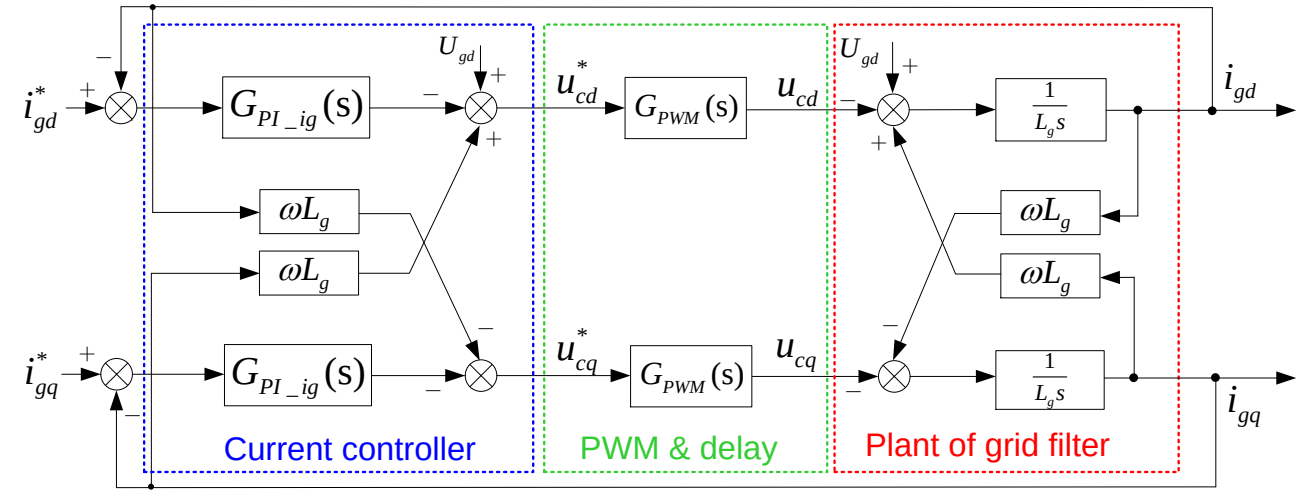

$$G_{PI\_ig}(s) = K_{p\_ig} + \frac{K_{i\_ig}}{s} \qquad G_{PWM}(s) = \frac{1}{T_d s + 1} \qquad G_{pl\_ig}(s) = \frac{1}{L_g s}$$

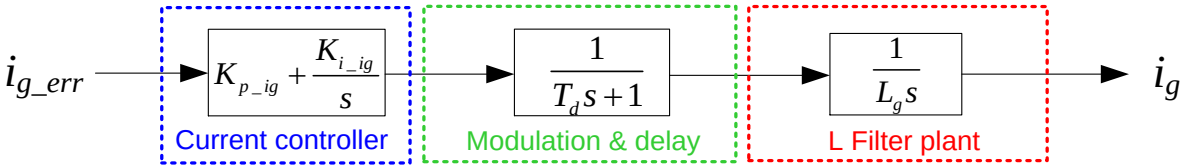

- Open-loop transfer function of grid current:

$$G_{ol\_ig}(s) = G_{PI\_ig}(s) G_{PWM}(s) G_{pl\_ig}(s)$$

Control of GSC (PI)

System parameters and design of PI controller

	2 MW	7.5 kW
Grid peak phase voltage U_g (V)	563	311
Dc-link voltage V_{dc} (V)	1050	650
Boost inductor L_g (mH)	0.5	18
Sampling freqency f_{sa} (kHz)	2	10
Switching freqency f_{sw} (kHz)	2	5
Delay time in PWM T_d (μs)	625	250
Proportional coefficient of PI controller K_{p_ig}	0.3	40
Integral coefficient of PI controller K_{i_ig}	15	120

- Design criteria of PI controller:
  - Bandwidth: 1/20~1/10 switching frequency
  - Phase margin: higher than 45°

Control of GSC (PI)

Bode plots of 2 MW system

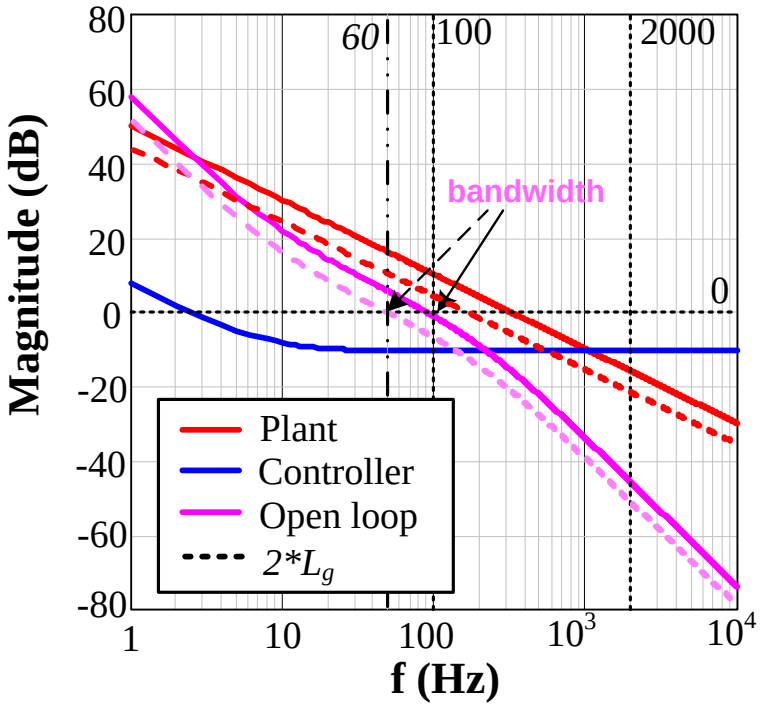

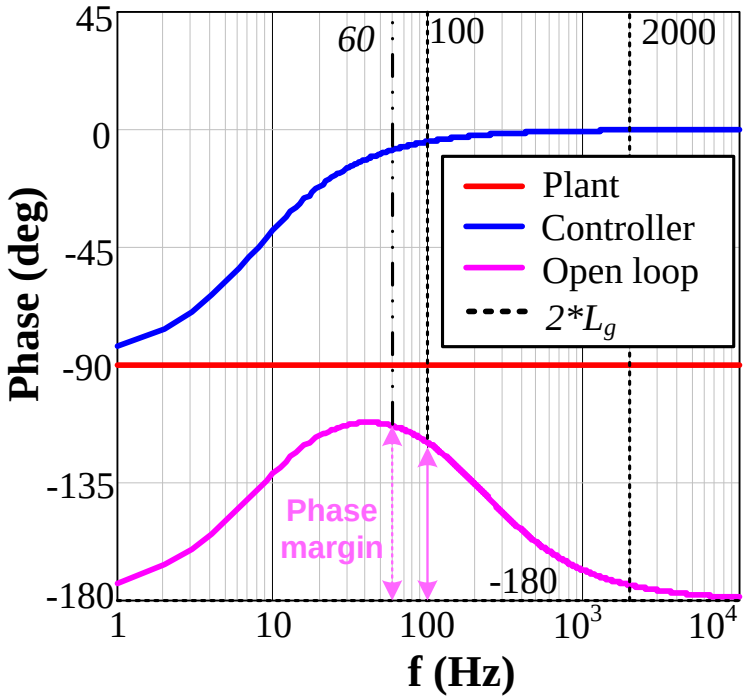

- Bandwidth (100 Hz) vs. switching freq. (2 kHz)
- Phase margin: 60.2° (>45°)
- Robustness check with varied inductance

Control of GSC (PI)

Bode plots of 7.5 kW system

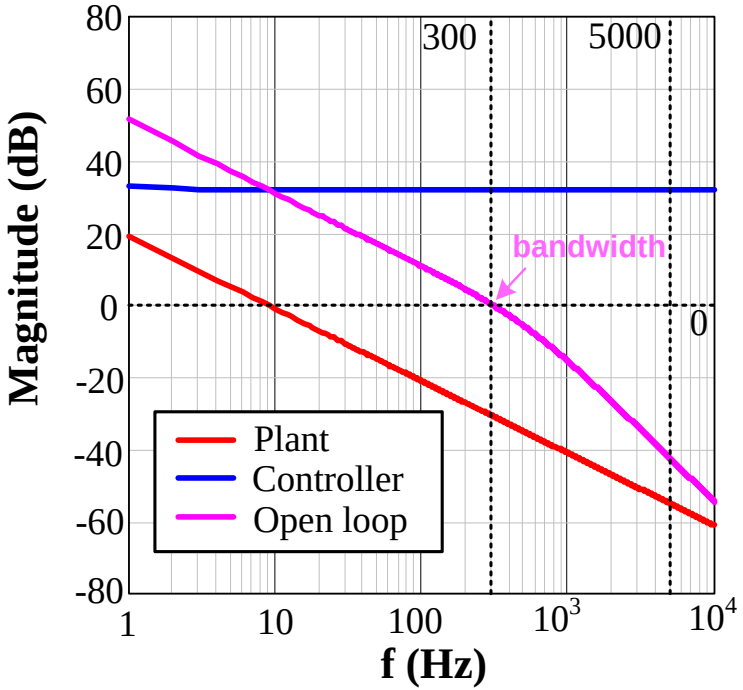

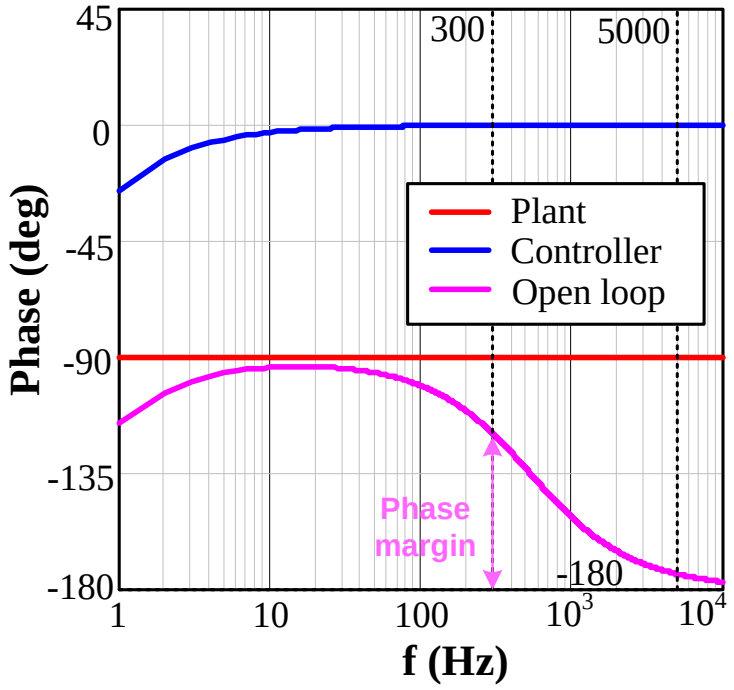

- Bandwidth (300 Hz) vs. switching freq. (5 kHz)
- Phase margin: 60.4° (>45°)

Control of GSC (PI)

Plant of dc-link capacitor

$$\frac{d}{dt}v_{dc} = \frac{3}{2C}\begin{bmatrix} d_d & d_q \end{bmatrix}\begin{bmatrix} I_{gd} \\ I_{gq} \end{bmatrix} + \frac{3}{2C}\begin{bmatrix} D_d & D_q \end{bmatrix}\begin{bmatrix} i_{gd} \\ i_{gq} \end{bmatrix} \quad \Rightarrow \quad \frac{v_{dc}(s)}{i_d(s)} = \frac{3D_d}{2Cs} = \frac{3U_g}{2V_{dc}Cs}$$

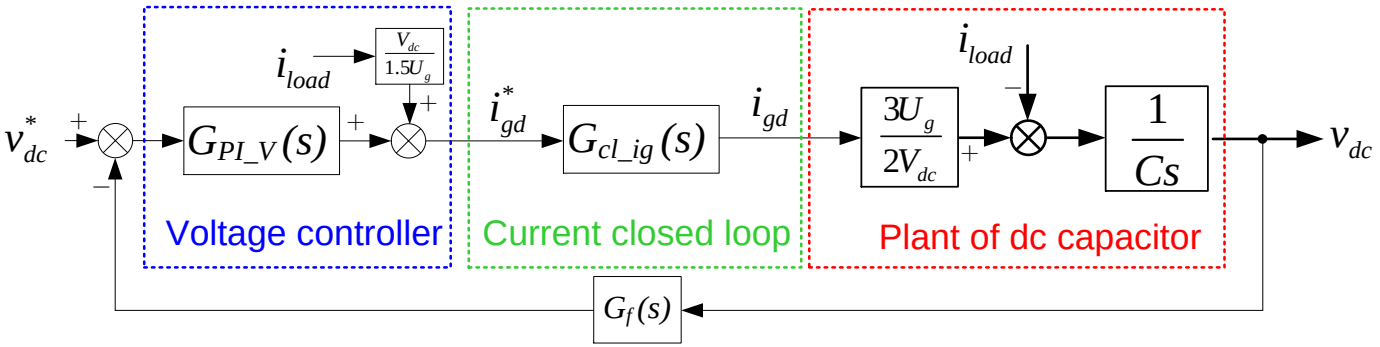

Control of GSC (PI)

Block diagram

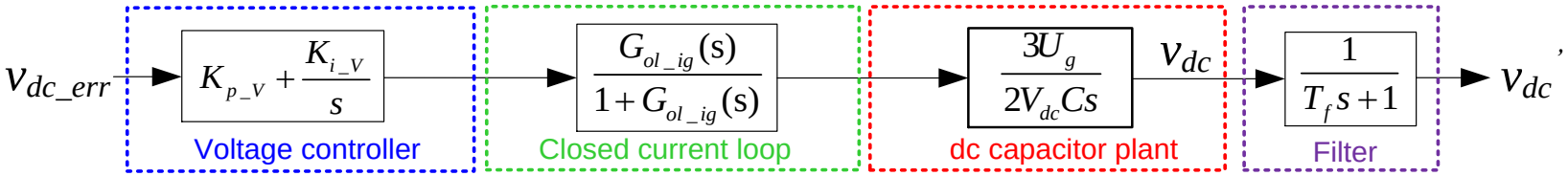

$$G_{PI\_V}(s) = K_{p\_V} + \frac{K_{i\_V}}{s} \qquad G_{cl\_ig}(s) = \frac{G_{ol\_ig}(s)}{1+G_{ol\_ig}(s)} \qquad G_{pl\_V}(s) = \frac{3U_g}{2V_{dc}Cs} \qquad G_f(s) = \frac{1}{T_f s+1}$$

Control of GSC (PI)

System parameters

	2 MW	7.5 kW
Dc-link capacitor C (μF)	20,000	600
Filter time constant T_f (ms)	0.001	10
Proportional coefficient of PI controller K_{p_V}	2	0.1
Integral coefficient of PI controller K_{i_V}	10	0.5

- Design criteria of PI controller:
  - Bandwidth: 1/50~1/10 of inner current loop
  - Phase margin: higher than 45°

Control of GSC (PI)

Bode plot (2 MW)

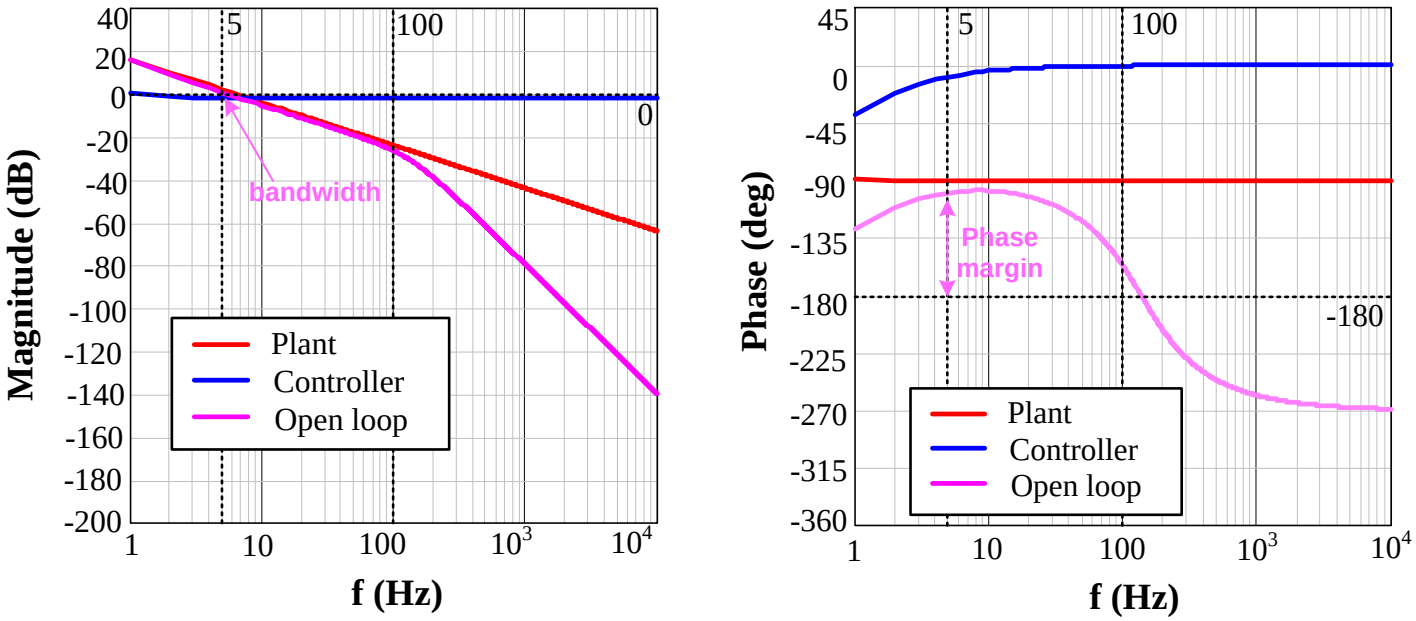

- Outer loop bandwidth (5 Hz) vs. Inner loop bandwidth (100 Hz)
- Phase margin: 80.2° (>45°)

Control of GSC (PI)

Bode plot (7.5 kW)

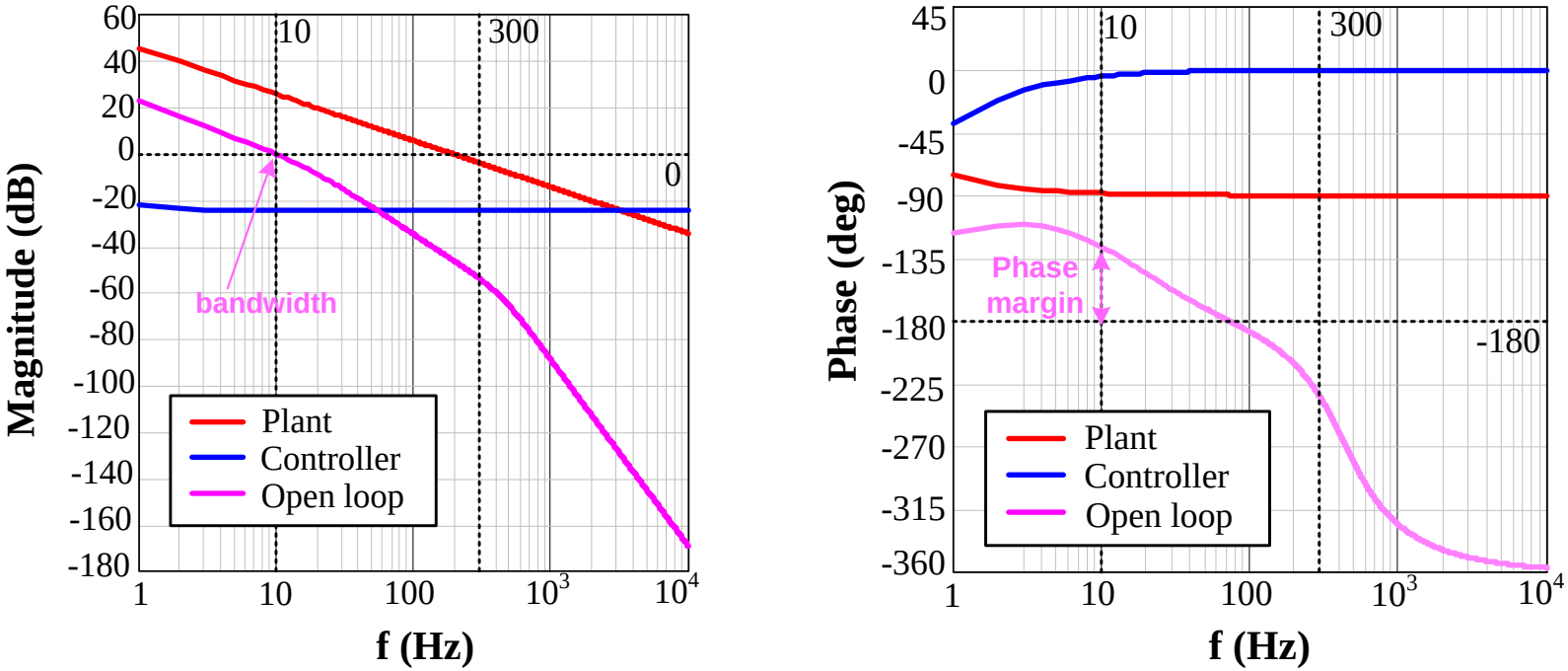

- Outer loop bandwidth (10 Hz) vs. Inner loop bandwidth (300 Hz)
- Phase margin: 53.2° (>45°)

Control of GSC (PI)

Control Scheme

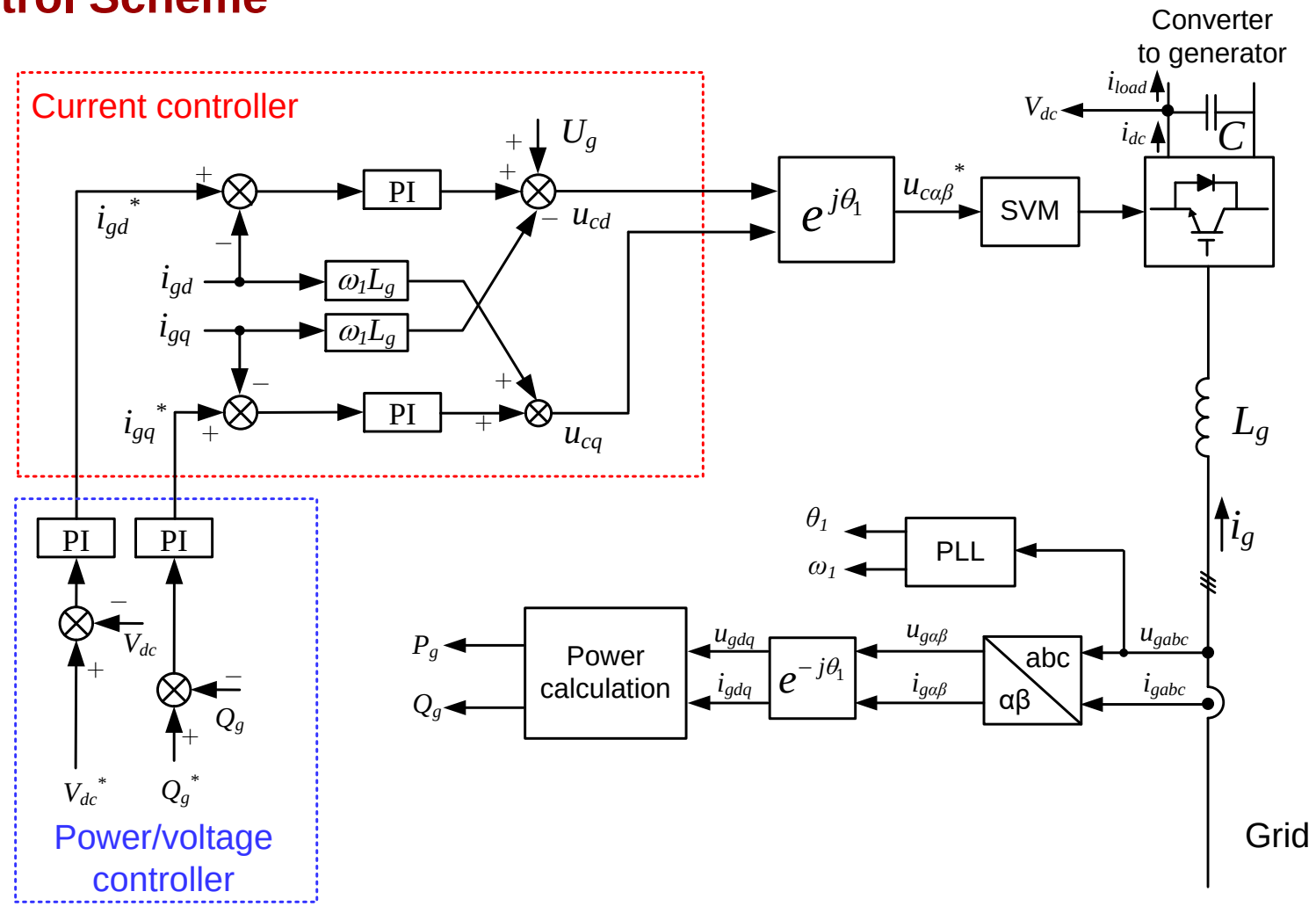

Control of GSC (PI)

Simulation results at 2 MW system

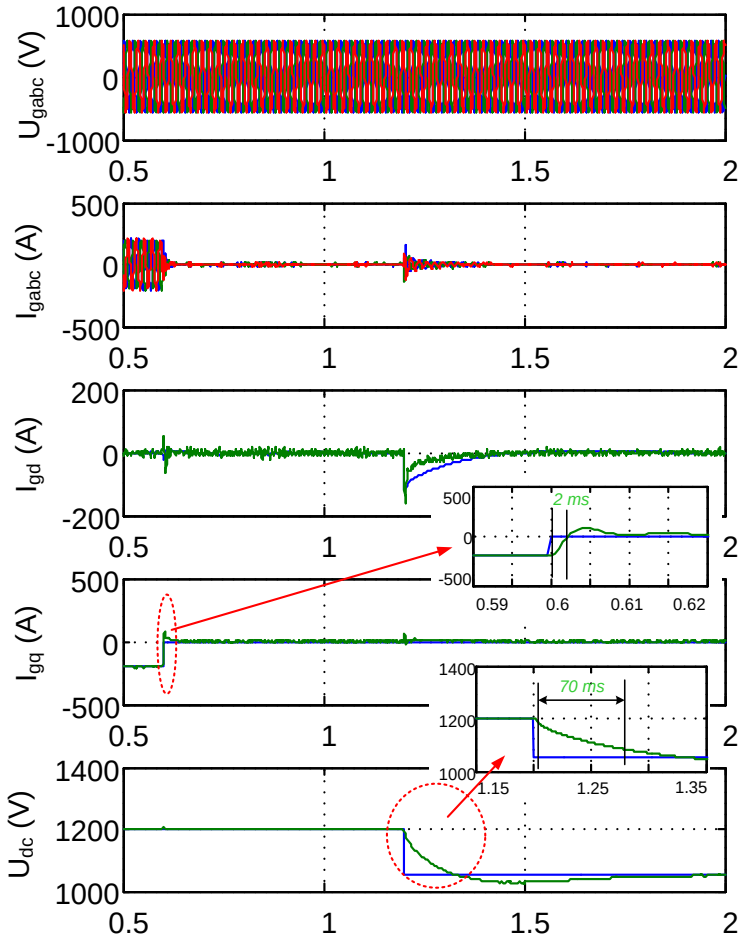

Step response of inner loop and outer loop

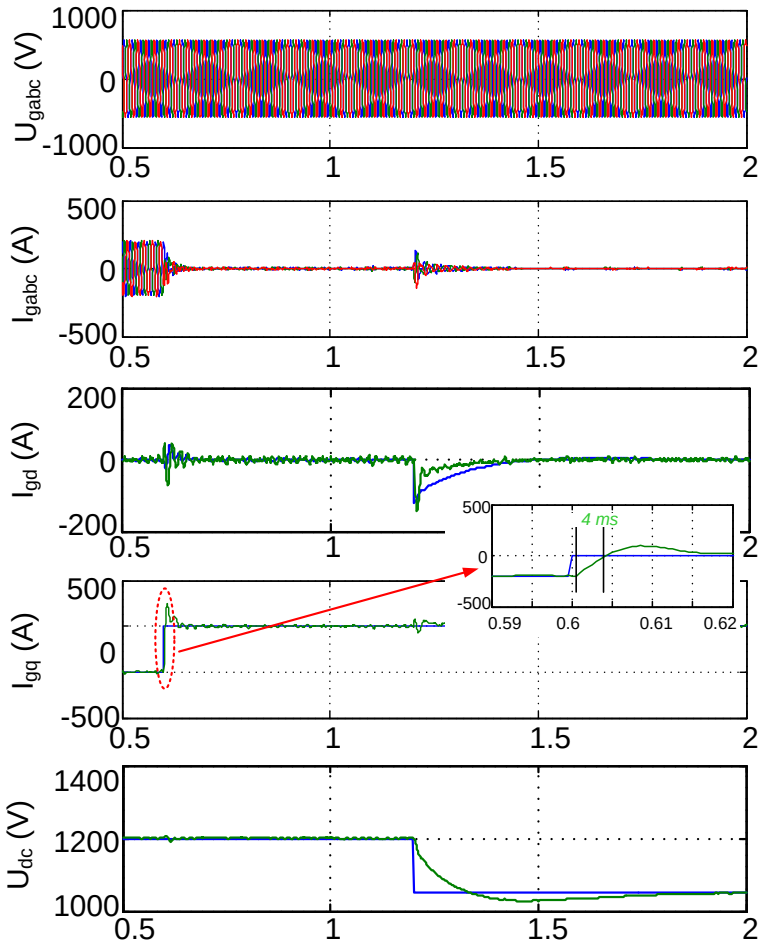

Step response with 2*grid filter

Control of GSC (PI)

Experimental configuration

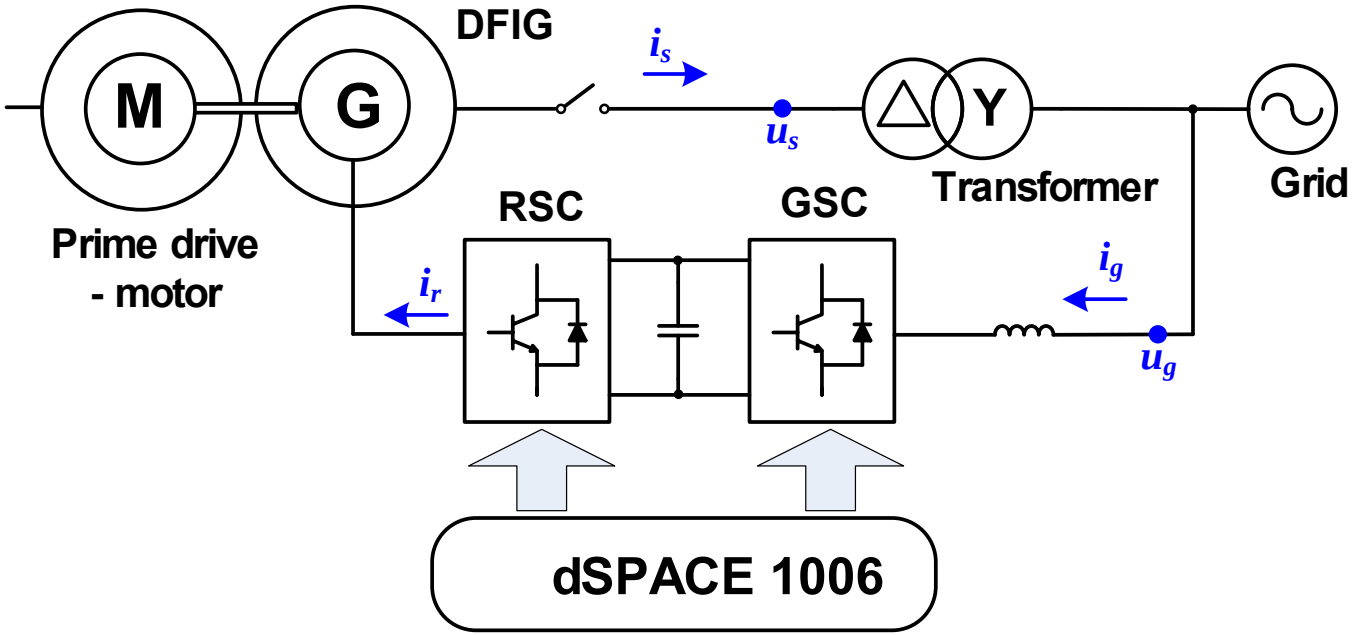

Control of GSC (PI)

Experimental validation

$$f_{BW} \cdot t_r = 0.35$$

Grid-tied converter	Switching frequency		5 kHz
	Inner loop	Bandwidth	300 Hz
		Expected rise time	1.17 ms
	Outer loop	Bandwidth	10 Hz
		Expected rise time	35 ms

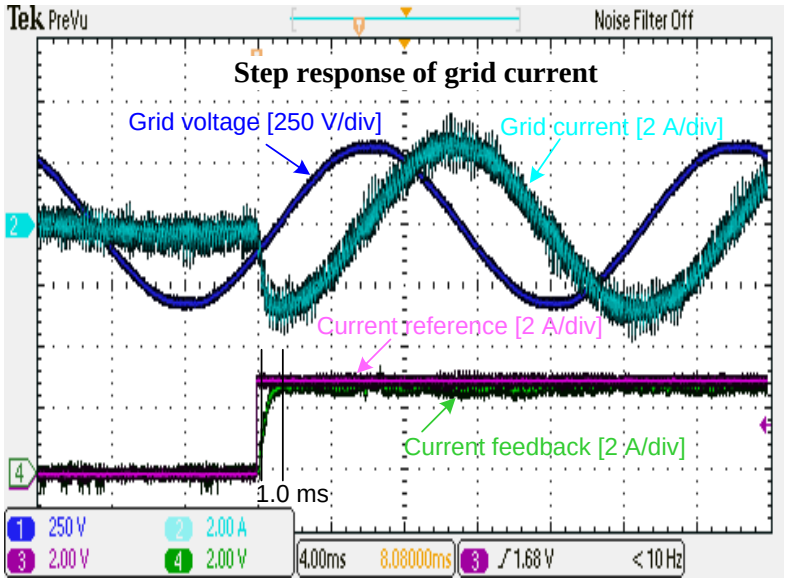

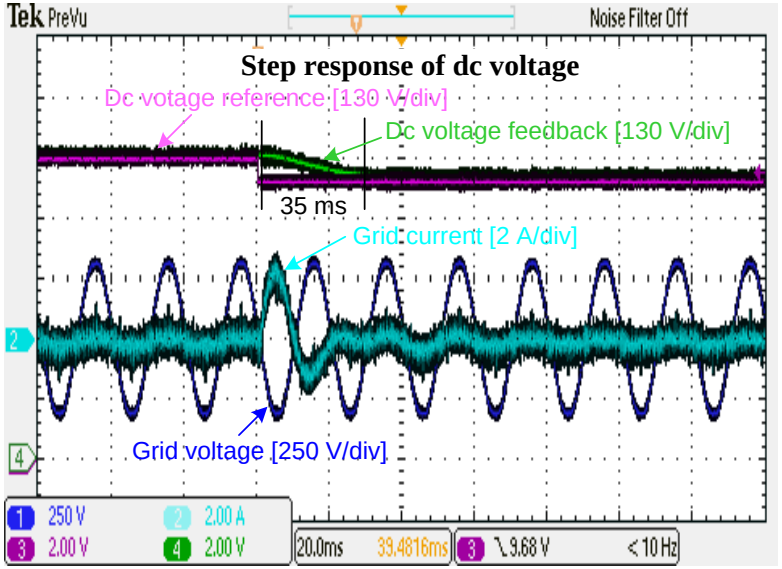

Control of GSC (PR)

Introduction of PR controller

- Ideal Proportional-Resonant (PR) controller:

$$C_{PR\_ideal}(s) = k_p + \frac{k_i}{s - j\omega} + \frac{k_i}{s + j\omega} = k_p + \frac{2k_i s}{s^2 + \omega^2}$$

- Practical PR controller:

$$C_{PR}(s) = k_p + \frac{k_r \omega_c s}{s^2 + \omega_c s + \omega_0^2}$$

K_p – proportional gain

K_r – resonant gain

W_0 – grid frequency

W_c – resonant bandwidth

Control of GSC (PR)

Open-loop transfer function

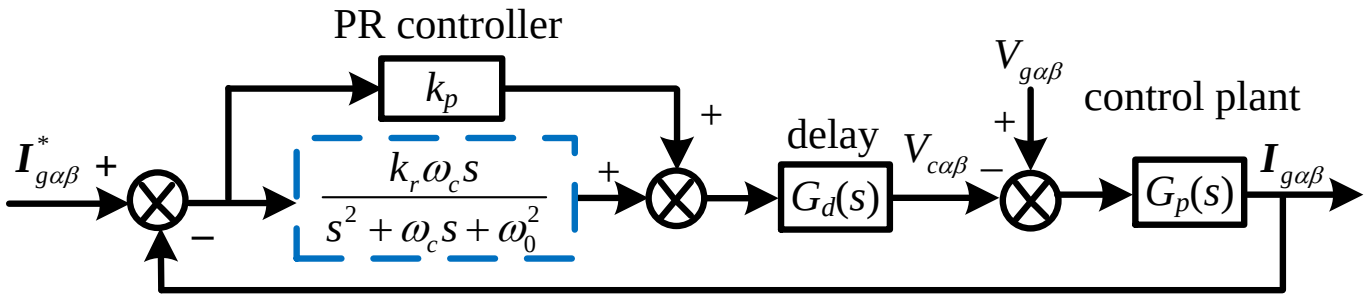

$$C_{PR}(s) = k_p + \frac{k_r\omega_c s}{s^2 + \omega_c s + \omega_0^2} \qquad G_d(s) = e^{-sT_d} \qquad G_p(s) = 1/sL_g$$

- Open-loop transfer function: $G_{ol}(s) = C_{PR}(s)G_d(s)G_p(s)$

Control of GSC (PR)

Theoretical design

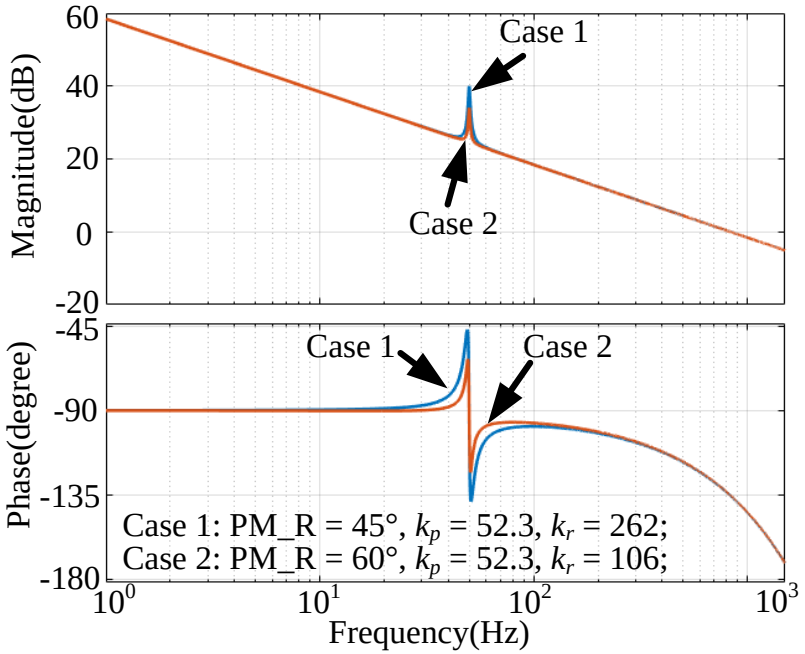

Cut-off freq.: PM_P = 45°

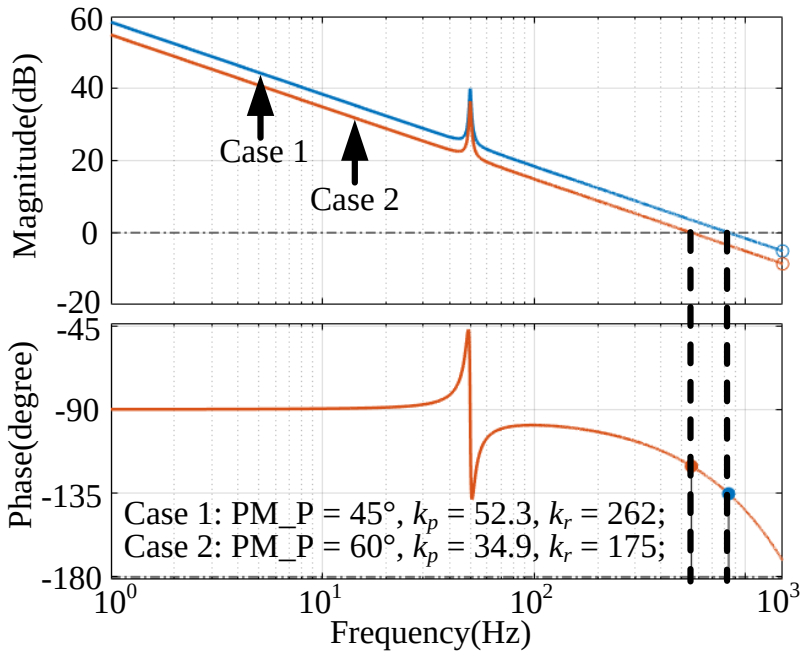

Resonant freq.: PM_R = 45°

- Sufficient phase margin at cut-off frequency
- Sufficient phase margin at resonant frequency

Control of GSC (PR)

Simulation validation

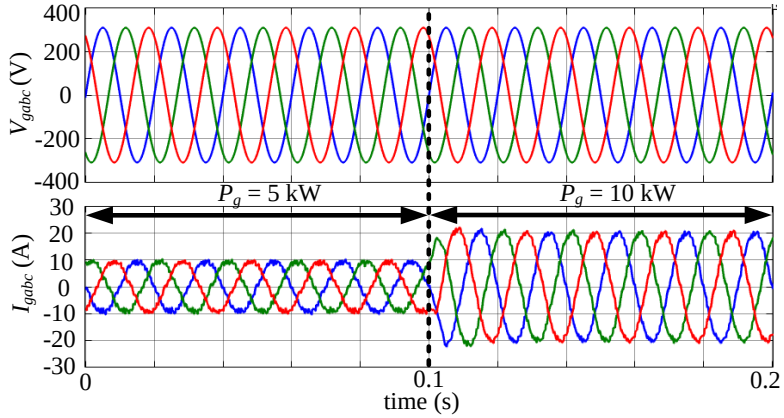

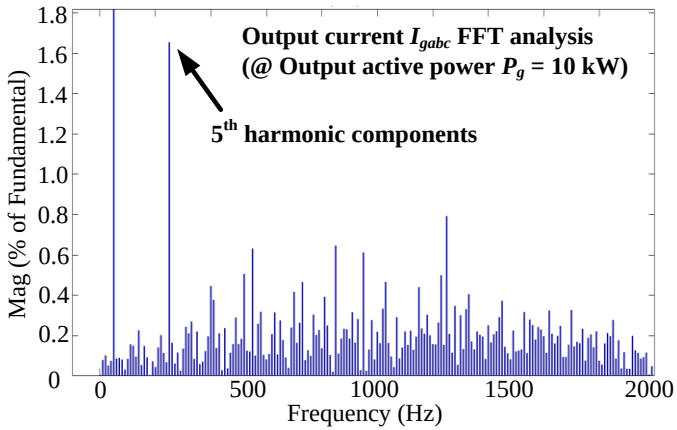

PM_P = PM_R = 45°, kp = 52.3, kr = 262

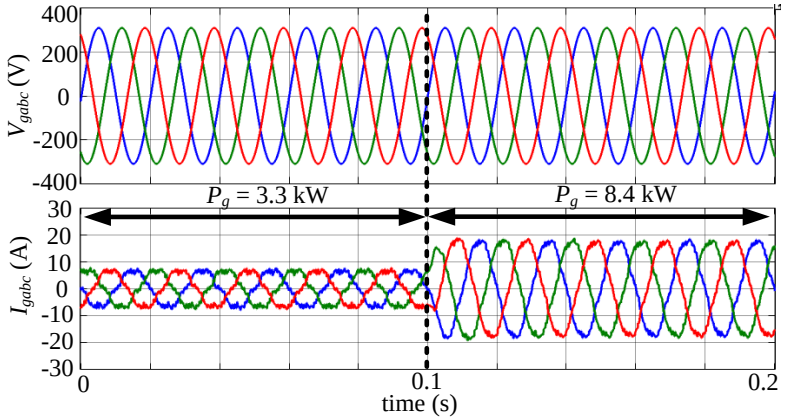

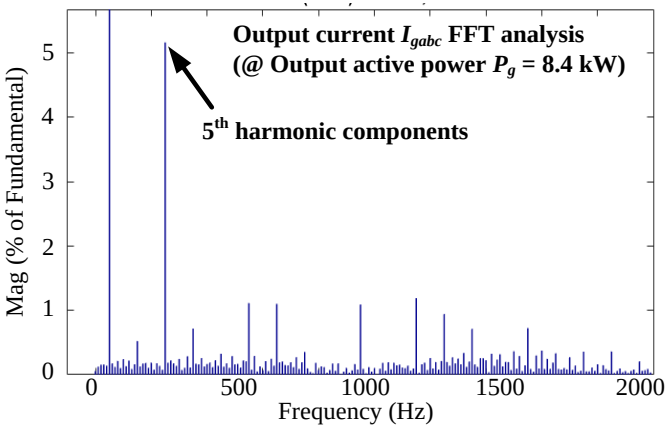

PM_P = PM_R = 60°, kp = 34.9, kr = 70.7

Modeling of DFIG Machine-side Converter

DFIG model under dq reference frame

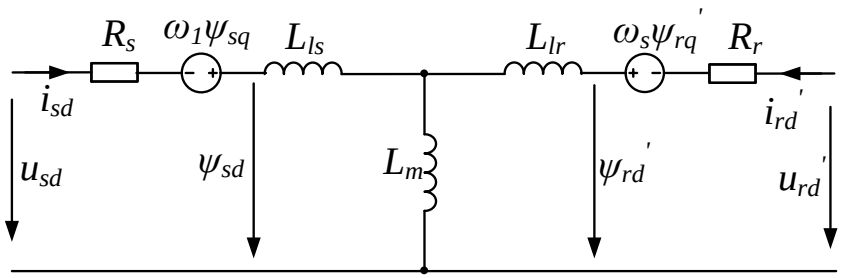

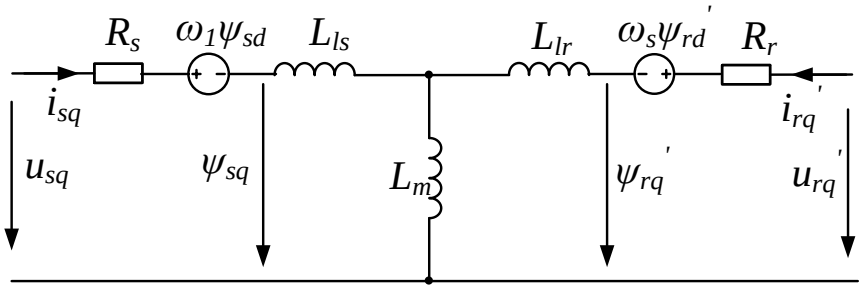

Voltage equation:

$$\begin{cases} u_{sd} = R_s i_{sd} + \dfrac{d}{dt}\psi_{sd} - \omega_1\psi_{sq} \\ u_{sq} = R_s i_{sq} + \dfrac{d}{dt}\psi_{sq} + \omega_1\psi_{sd} \\ u_{rd}' = R_r i_{rd}' + \dfrac{d}{dt}\psi_{rd}' - \omega_s\psi_{rq}' \\ u_{rq}' = R_r i_{rq}' + \dfrac{d}{dt}\psi_{rq}' + \omega_s\psi_{rd}' \end{cases}$$

Flux equation:

$$\begin{cases} \psi_{sd} = L_s i_{sd} + L_m i_{rd}' \\ \psi_{sq} = L_s i_{sq} + L_m i_{rq}' \\ \psi_{rd}' = L_m i_{sd} + L_r i_{rd}' \\ \psi_{rq}' = L_m i_{sq} + L_r i_{rq}' \end{cases}$$

Modeling of DFIG Machine-side Converter

DFIG model under dq reference frame (Cont.)

- According to stator Voltage Oriented Control (VOC),

$$\begin{cases} u_{sd} = U_s \\ u_{sq} = 0 \end{cases}$$

- During steady-state, neglecting stator resistance,

$$\begin{cases} \psi_{sd} = 0 \\ \psi_{sq} = -\dfrac{U_s}{\omega_1} \end{cases}$$

- Stator current can be expressed in terms of rotor current,

$$\begin{cases} i_{sd} = -\dfrac{L_m}{L_s} i'_{rd} \\ i_{sq} = -\dfrac{U_s}{\omega_1 L_s} - \dfrac{L_m}{L_s} i'_{rq} \end{cases}$$

Modeling of DFIG Machine-side Converter

DFIG model under dq reference frame (Cont.)

- Rotor flux can be expressed by rotor current,

$$\begin{cases} \psi_{rd}^{'} = \sigma L_r i_{rd}^{'} \\ \psi_{rq}^{'} = -\dfrac{U_s L_m}{\omega_1 L_s} + \sigma L_r i_{rq}^{'} \end{cases}$$

- Relationship between rotor voltage and rotor current,

$$\begin{cases} u_{rd}^{'} = R_r i_{rd}^{'} + \sigma L_r \dfrac{d}{dt} i_{rd}^{'} + s_l \dfrac{L_m}{L_s} U_s - \sigma L_r \omega_s i_{rq}^{'} \\ u_{rq}^{'} = R_r i_{rq}^{'} + \sigma L_r \dfrac{d}{dt} i_{rq}^{'} + \sigma L_r \omega_s i_{rd}^{'} \end{cases}$$

- Moreover, the stator-side active power and reactive power can be expressed by,

$$\begin{cases} P_s = \dfrac{3}{2} U_s i_{sd} = -\dfrac{3}{2} \dfrac{L_m U_s}{L_s} i_{rd}^{'} \\ Q_s = -\dfrac{3}{2} U_s i_{sq} = \dfrac{3}{2} \left(\dfrac{U_s^{\,2}}{\omega_1 L_s} + \dfrac{L_m U_s}{L_s} i_{rq}^{'} \right) \end{cases}$$

Modeling of DFIG Machine-side Converter

Plant model of DFIG

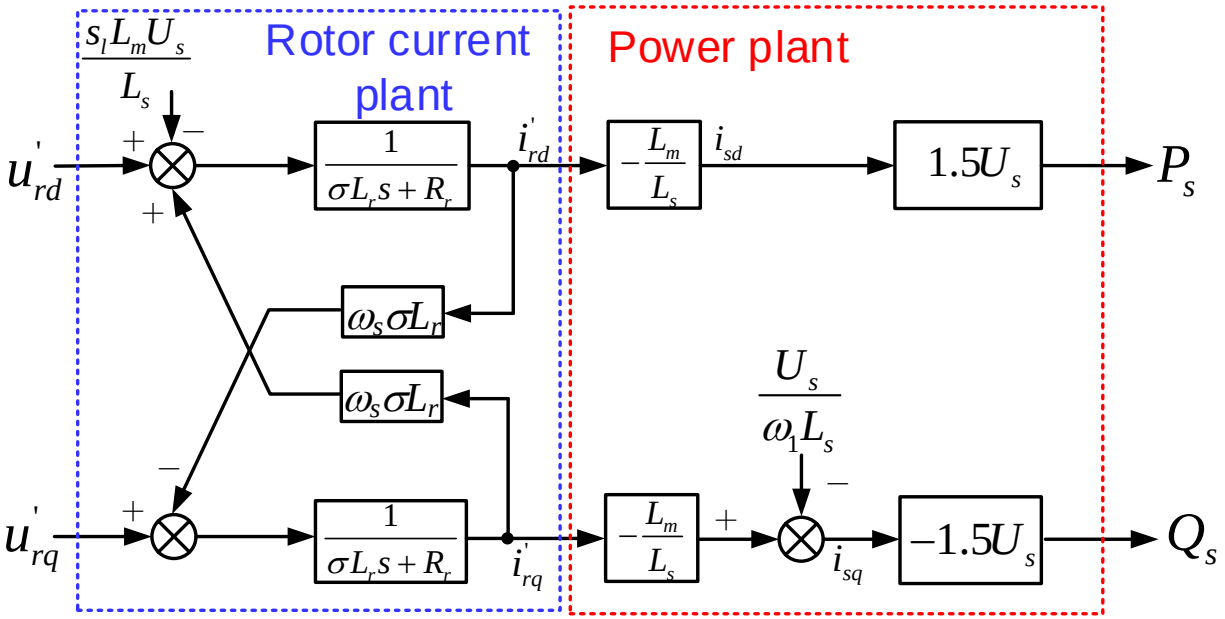

- Equivalent model is simplified with dq-reference frame model
- Variables under d-axis and q-axis are coupled with each other

Vector Control of DFIG Machine-side Converter

Control block diagram

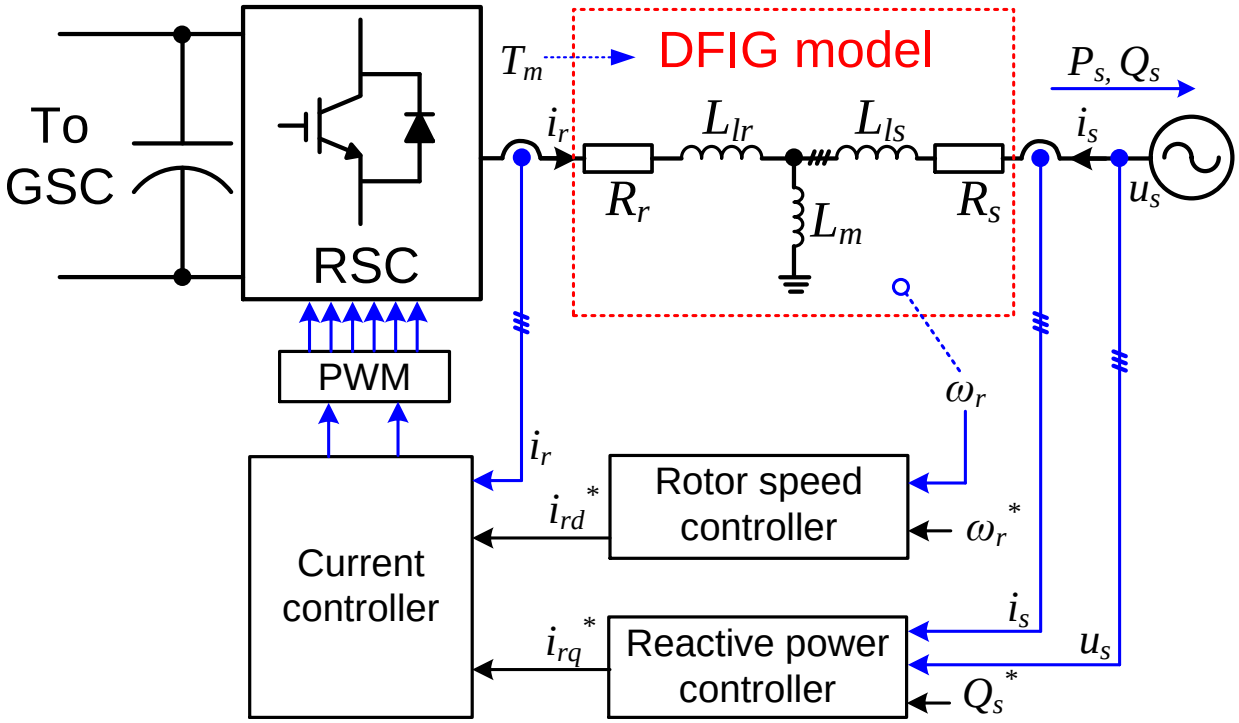

- Dual-loop control: Inner rotor current loop; Outer speed/power loop

Control of DFIG Machine-side Converter

Decouple control of inner rotor current

- DFIG is model with stator variables referred to stator-side,

$$\begin{cases} u_r = \dfrac{1}{k_{sr}} u_r' \\ i_r = k_{sr} i_r' \end{cases}$$

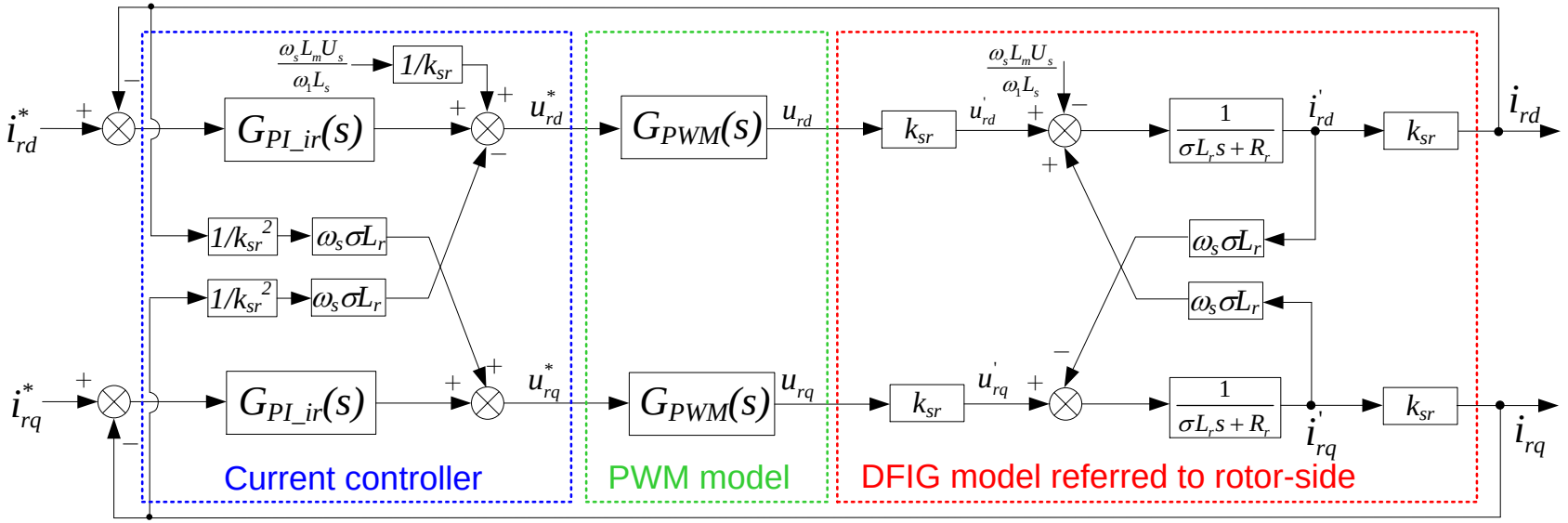

$$G_{PI\_ir}(s) = K_{p\_ir} + \frac{K_{i\_ir}}{s}$$

$$G_{pl\_ir}(s) = \frac{k_{sr}^2}{R_r + \sigma L_r s}$$

Control of DFIG Machine-side Converter

Transfer function of open-loop rotor current

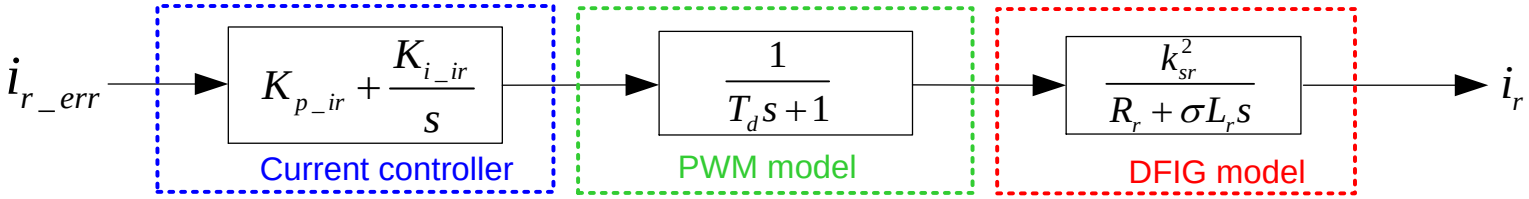

$$G_{ol\_ir}(s) = G_{PI\_ir}(s) G_{PWM}(s) G_{pl\_ir}(s)$$

	2 MW	7.5 kW
Stator peak phase voltage U_s (V)	563	311
Stator resistance R_s (mΩ)	1.69	440
Stator inductance L_s (mH)	2.95	82.74
Rotor resistance R_r (mΩ)	1.52	640
Rotor inductance L_r (mH)	2.97	84.46
Magnetizing inductance L_m (mH)	2.91	79.30
Leakage coefficient σ	0.03	0.10
Winding ratio between stator and rotor k_{sr}	0.369	0.336
Sampling freqency f_{sa} (kHz)	2	10
Switching freqency f_{sw} (kHz)	2	5
Delay time introduced by PWM T_d (μs)	625	250
Proportional coeffcient of current controller K_{p_ir}	0.5	200
Integral coefficient of current controller K_{i_ir}	7.5	1000

Control of DFIG Machine-side Converter

Bode plot of open-loop rotor current (2 MW)

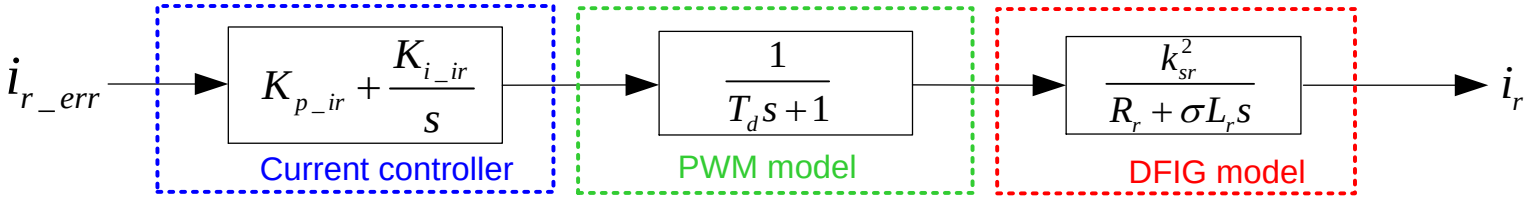

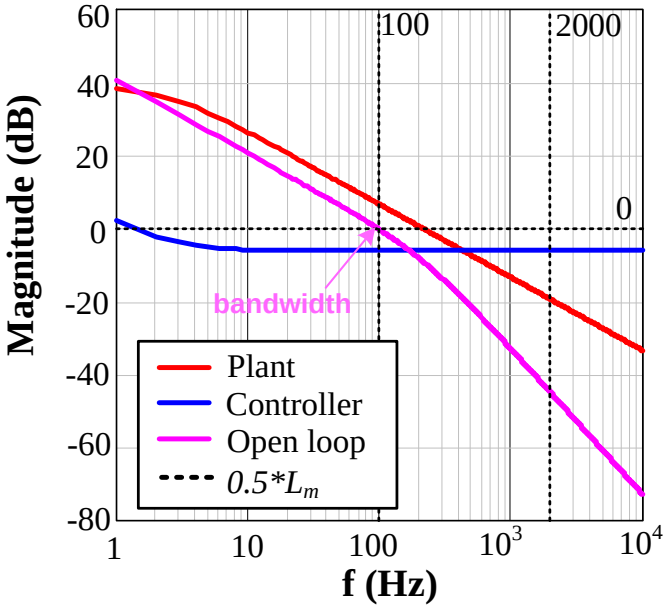

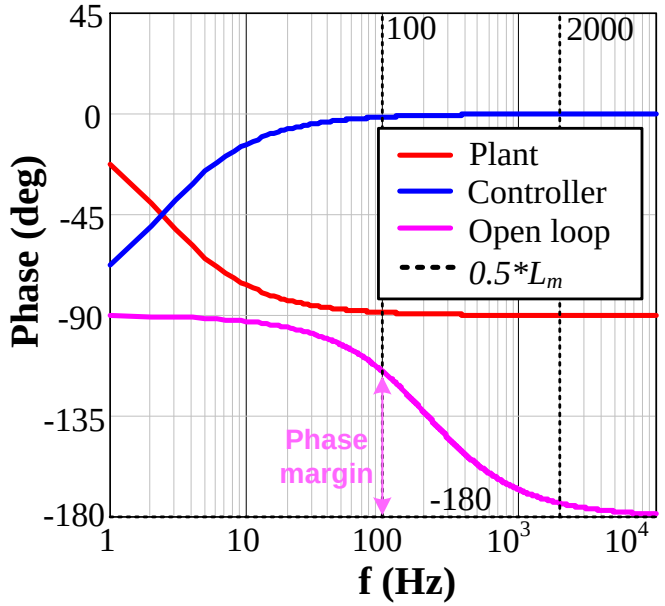

- Bandwidth (100 Hz) vs. switching freq. (2 kHz)
- Phase margin: 64.8° (>45°)

Control of DFIG Machine-side Converter

Bode plot of open-loop rotor current (7.5 kW)

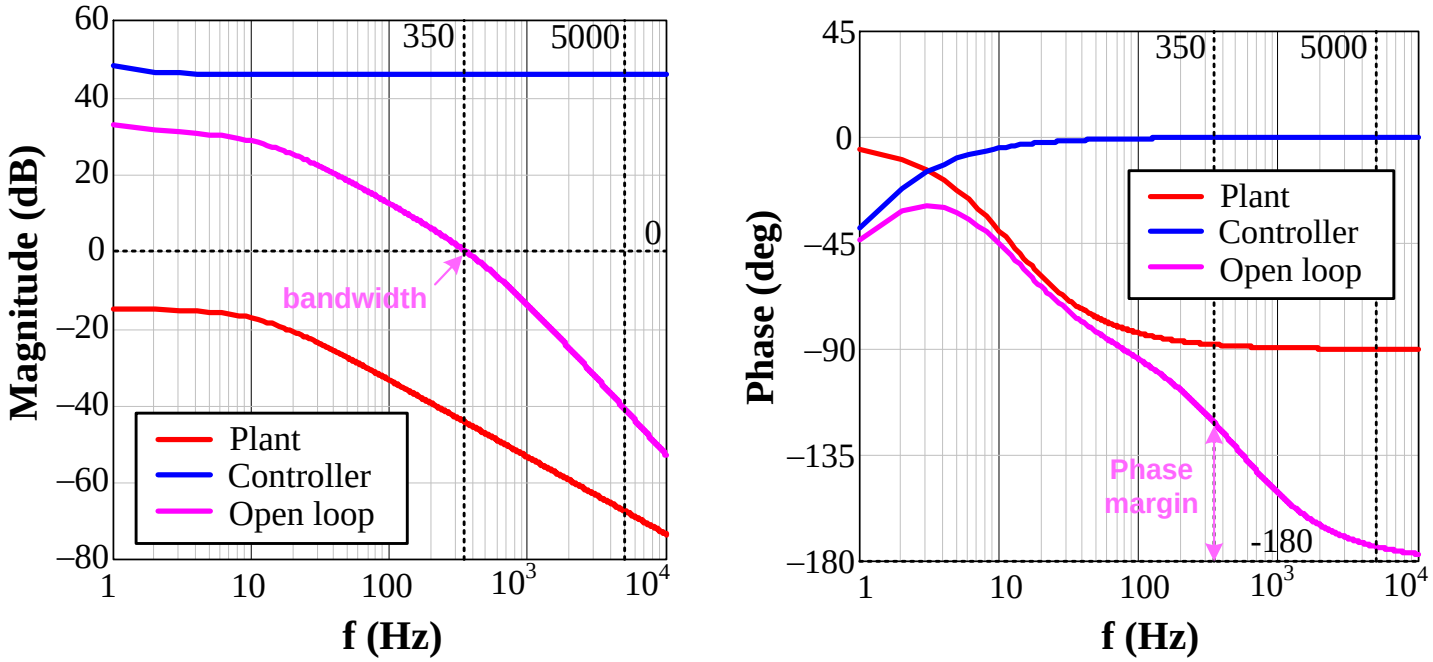

- Bandwidth (350 Hz) vs. switching freq. (5 kHz)
- Phase margin: 58.4° (>45°)

Control of DFIG Machine-side Converter

Control block diagram of power outer loop

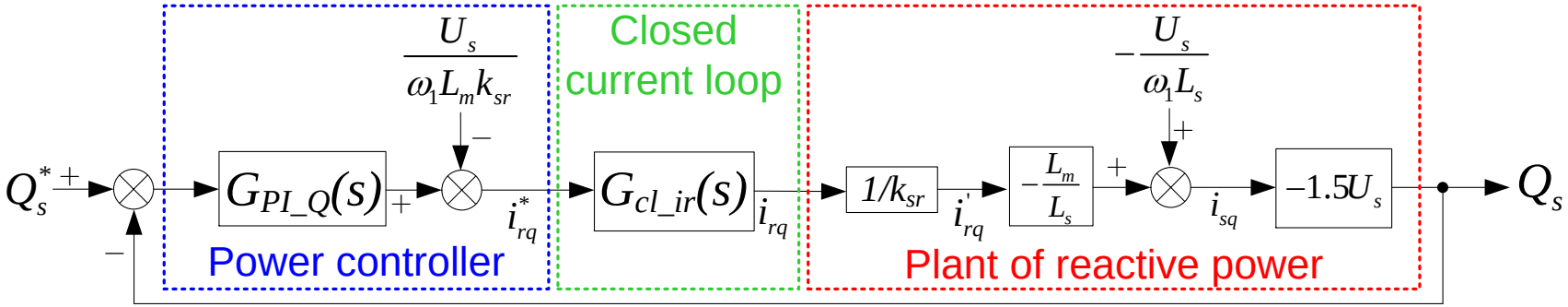

$$G_{PI\_Q}(s) = K_{p\_Q} + \frac{K_{i\_Q}}{s} \qquad G_{cl\_ir}(s) = \frac{G_{ol\_ir}(s)}{1 + G_{ol\_ir}(s)} \qquad G_{pl\_Q}(s) = \frac{1.5U_s L_m}{k_{sr} L_s}$$

Control of DFIG Machine-side Converter

Blot plot of power outer loop (2 MW)

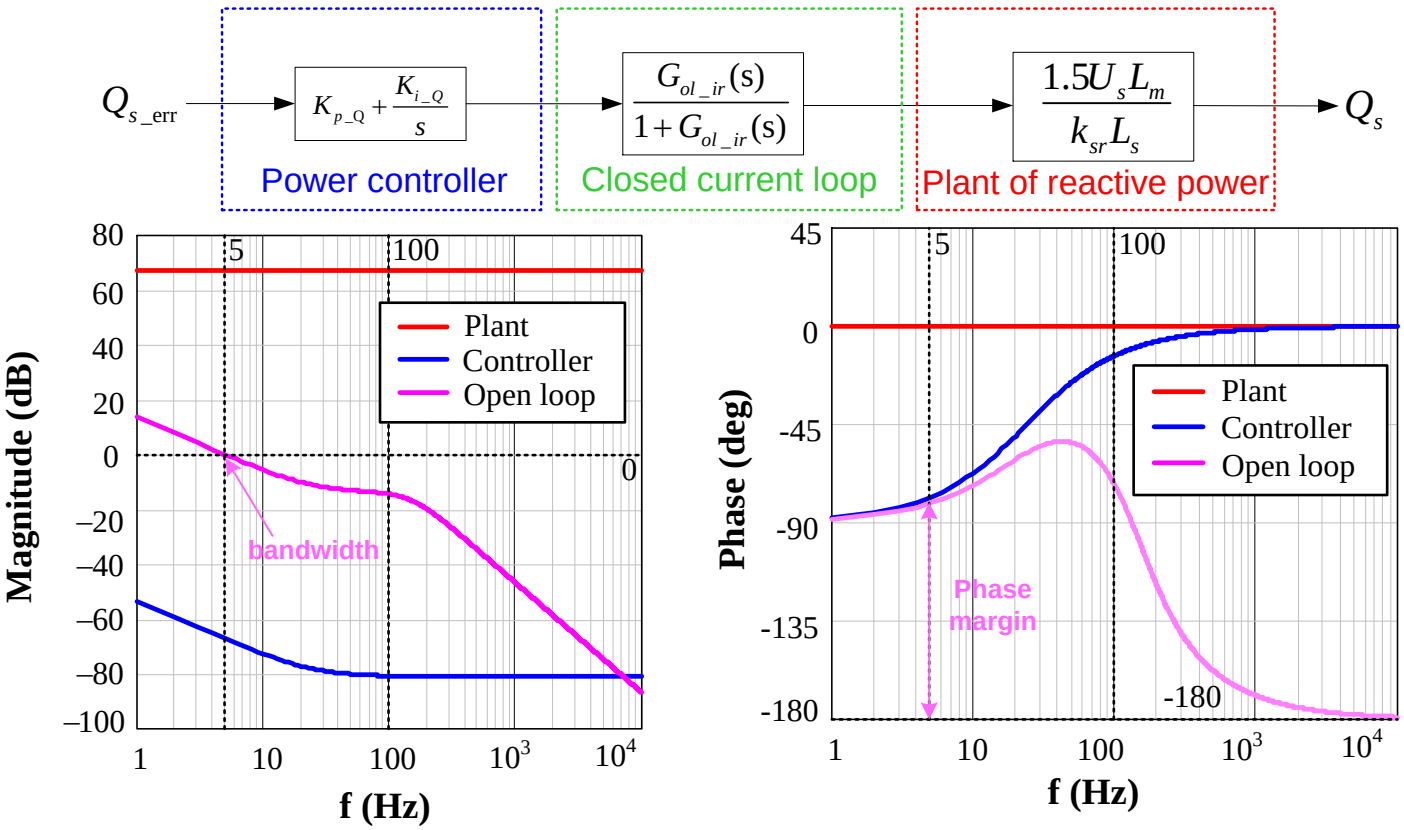

- Q Bandwidth (5 Hz) vs. inner loop (100 Hz)
- Phase margin: 99.1° (>45°)

Control of DFIG Machine-side Converter

Blot plot of power outer loop (7.5 kW)

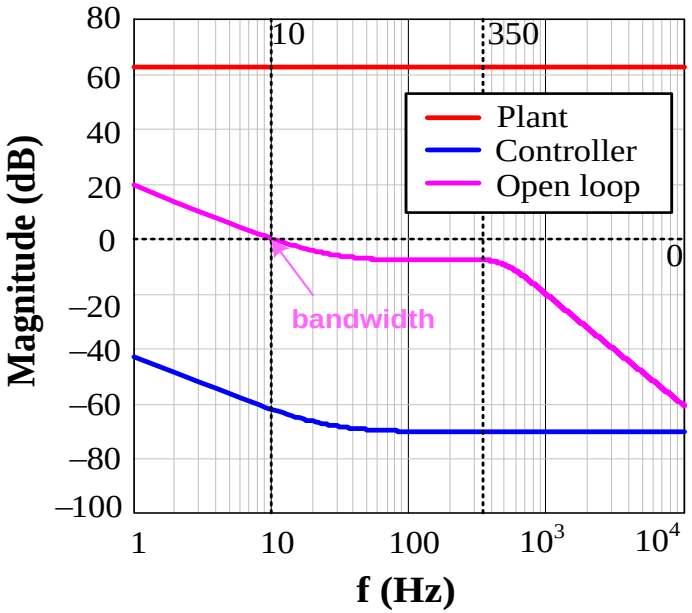

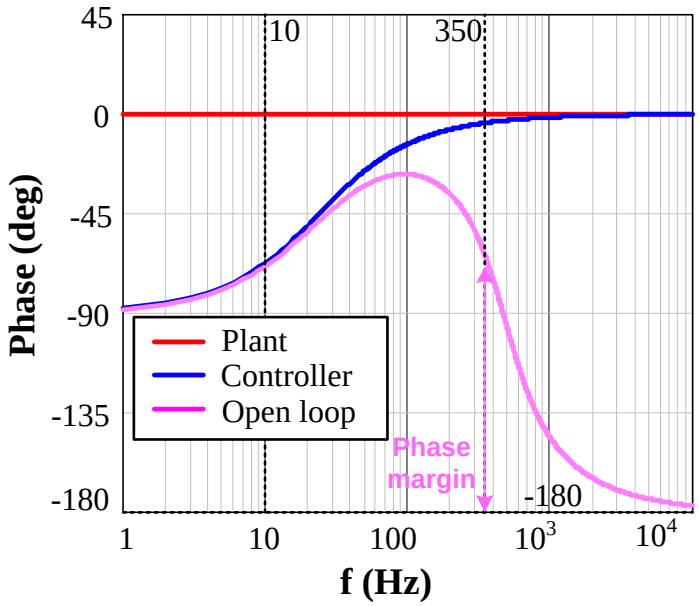

- Q Bandwidth (5 Hz) vs. inner loop (100 Hz)
- Phase margin: 111.3° (>45°)

Control of DFIG Machine-side Converter

Control Scheme

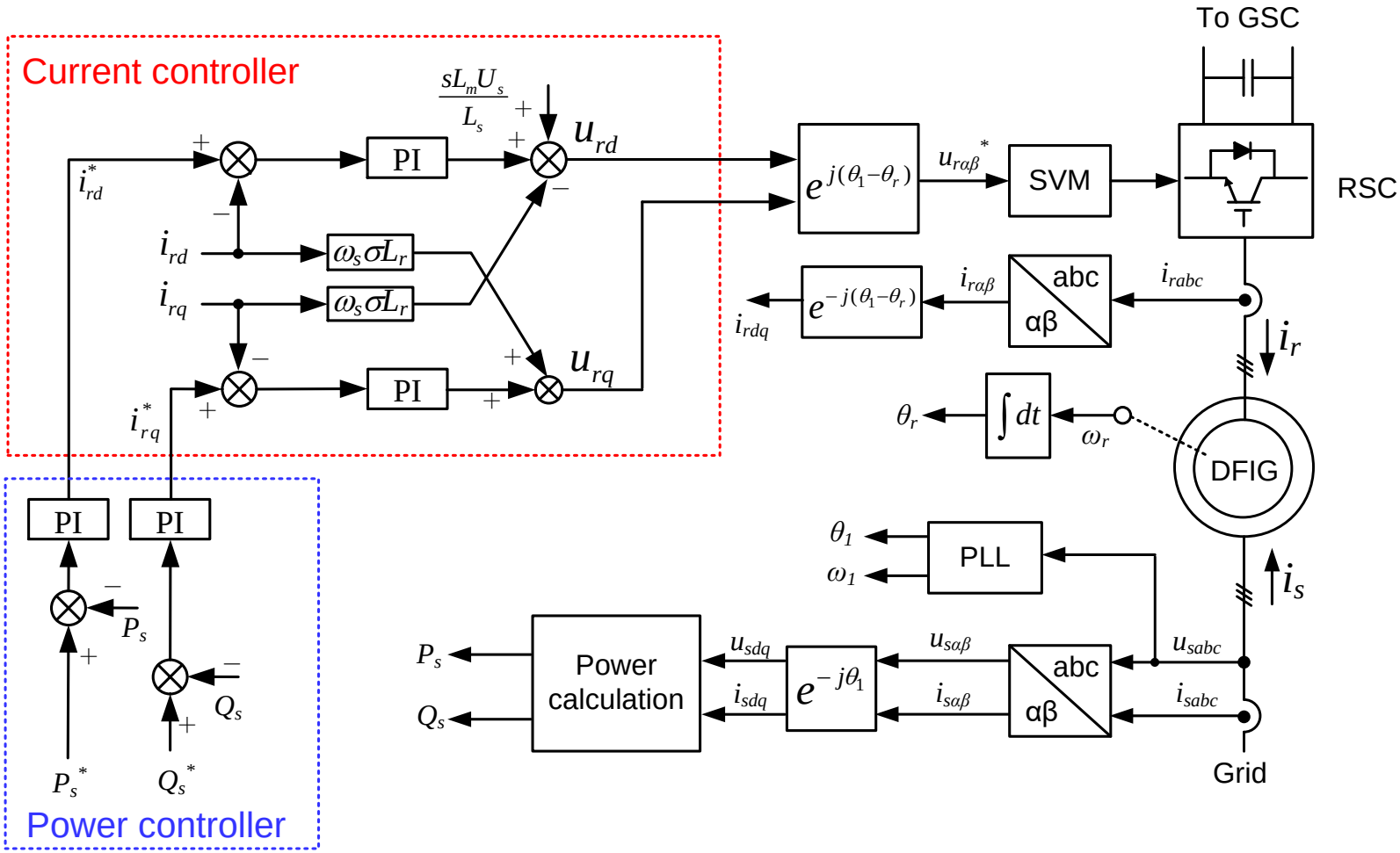

Control of DFIG Machine-side Converter

Simulation validation at 2 MW DFIG

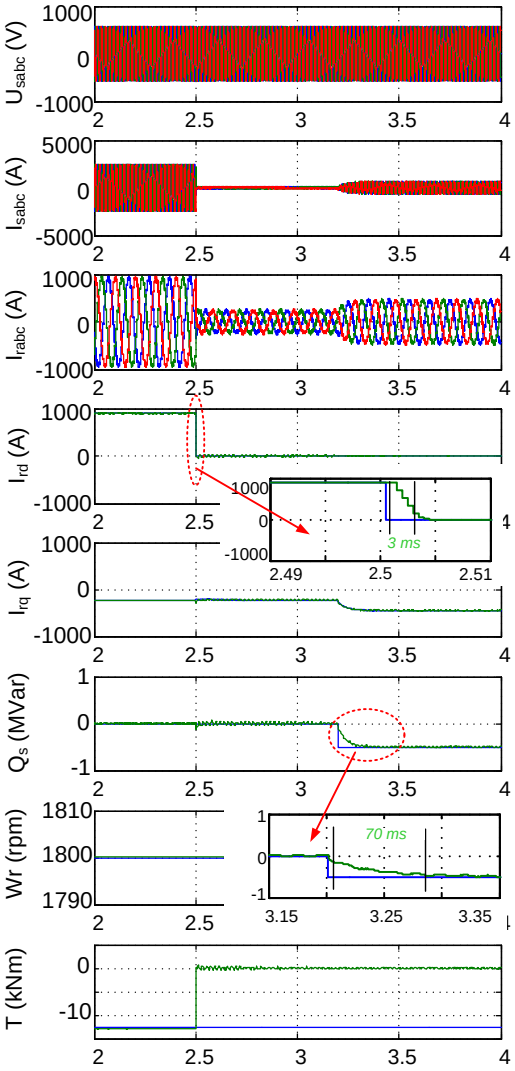

Step response of inner loop and outer loop

Control of DFIG Machine-side Converter

Experimental verification at 7.5 kW DFIG

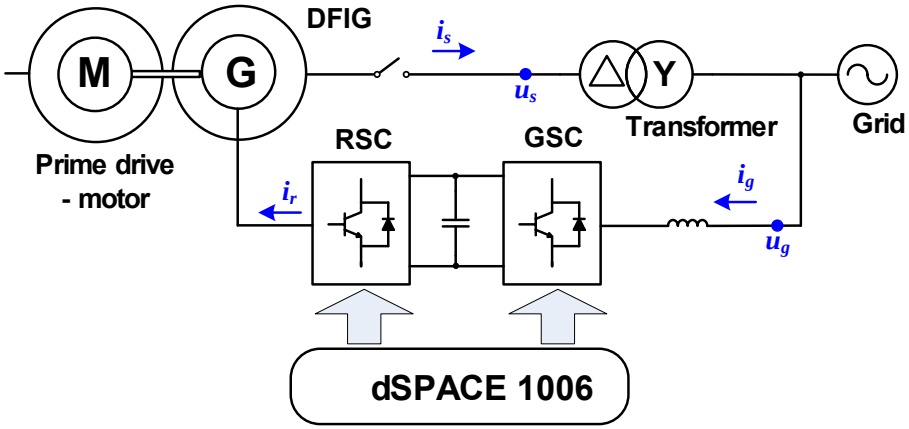

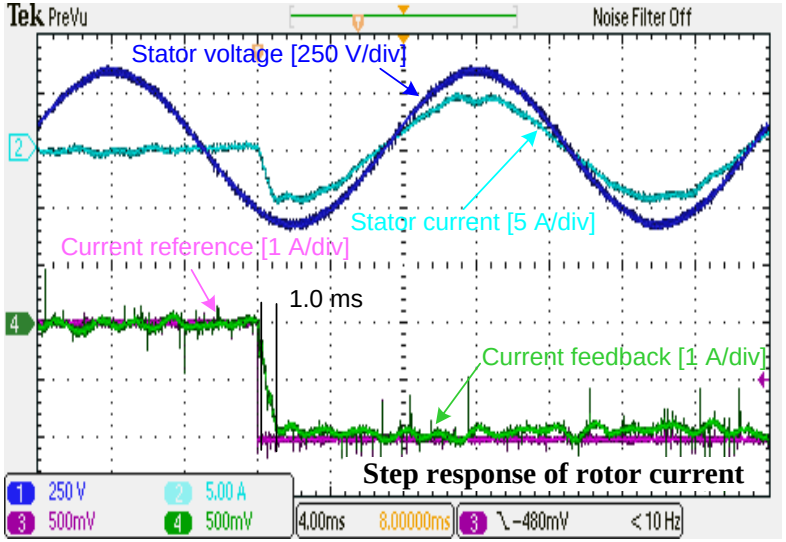

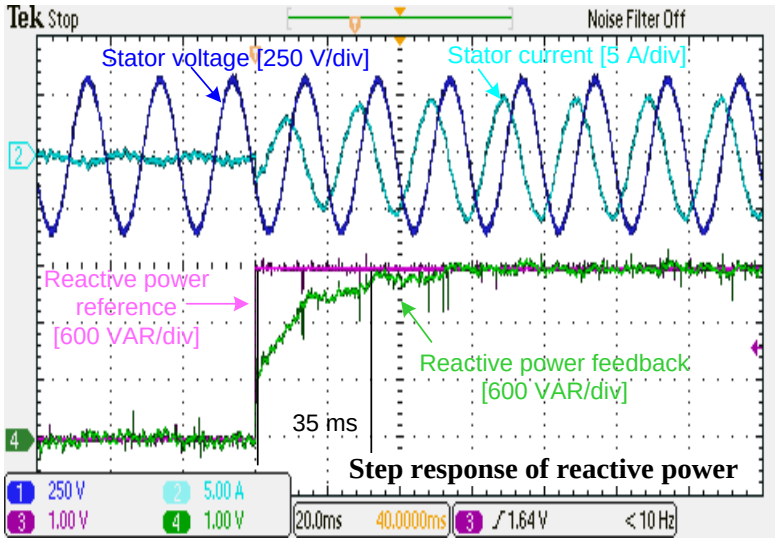

Control of DFIG Machine-side Converter

RSC mathematical modeling adopting Direct Power Control (DPC)

$$U_{rddpc} = V_{rddpc} + E_{rddpc} = -C_{power}(P_s^* - P_s) - \omega_s\left(\frac{Q_s}{k_\sigma U_{sd}} - \frac{L_r U_{sd}}{L_m \omega_1}\right) = -C_{PI}(P_s^* - P_s) - \omega_s\left(\frac{Q_s}{k_\sigma U_{sd}} - \frac{L_r U_{sd}}{L_m \omega_1}\right)$$

$$U_{rqdpc} = V_{rqdpc} + E_{rqdpc} = C_{power}(Q_s^* - Q_s) - \omega_s \frac{P_s}{k_\sigma U_{sd}} = C_{PI}(Q_s^* - Q_s) - \omega_s \frac{P_s}{k_\sigma U_{sd}}$$

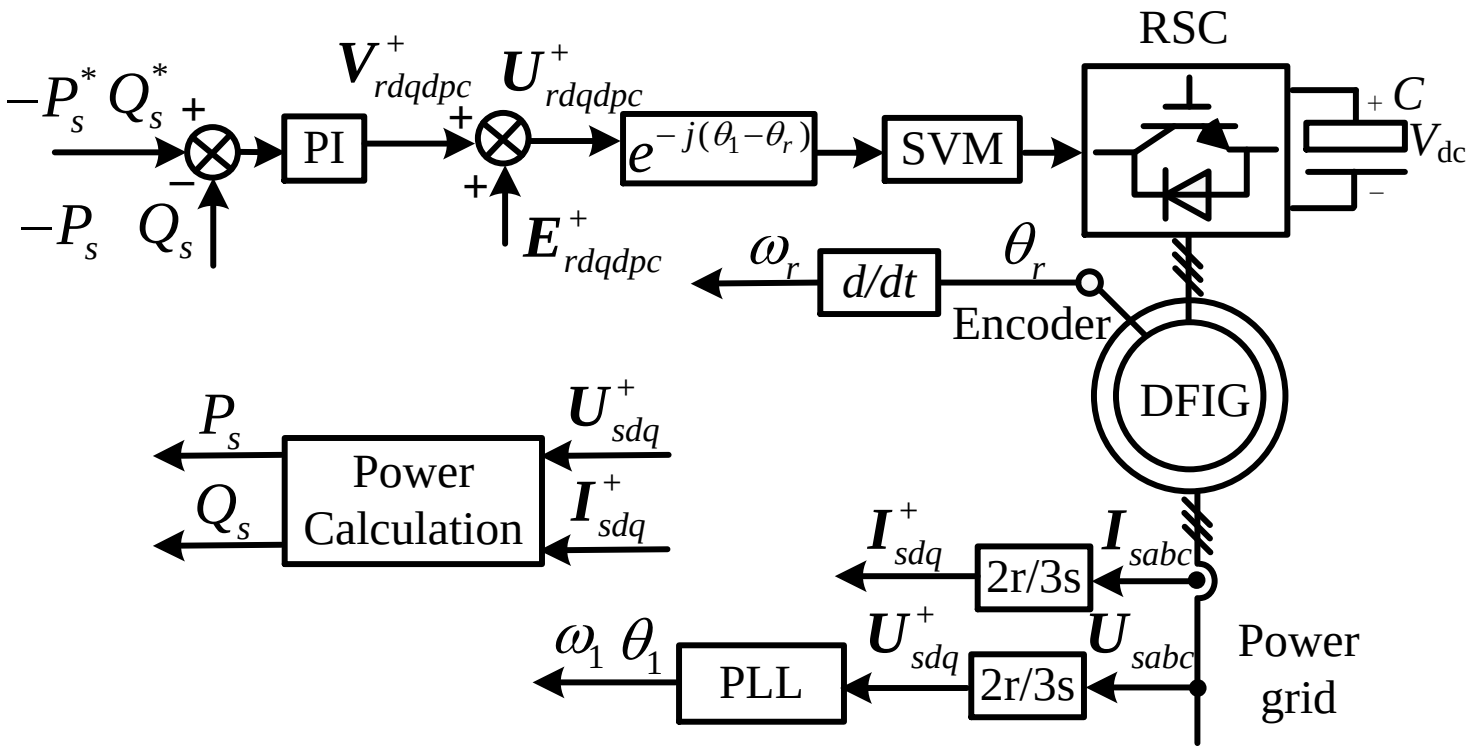

Control of DFIG Machine-side Converter

GSC mathematical modeling adopting DPC

$$U_{cddpc} = V_{gddpc} + E_{gddpc} = -G_{PQ}(s)\left(P_g^* - P_g\right) - \frac{2}{3}\frac{\omega_1 L_g}{u_{gd}} Q_g + u_{gd} = -C_{PI}(s)\left(P_g^* - P_g\right) - \frac{2}{3}\frac{\omega_1 L_g}{u_{gd}} Q_g + u_{gd}$$

$$U_{cqdpc} = V_{gqdpc} + E_{gqdpc} = G_{PQ}(s)\left(Q_g^* - Q_g\right) - \frac{2}{3}\frac{\omega_1 L_g}{u_{gd}} P_g = C_{PI}(s)\left(Q_g^* - Q_g\right) - \frac{2}{3}\frac{\omega_1 L_g}{u_{gd}} P_g$$

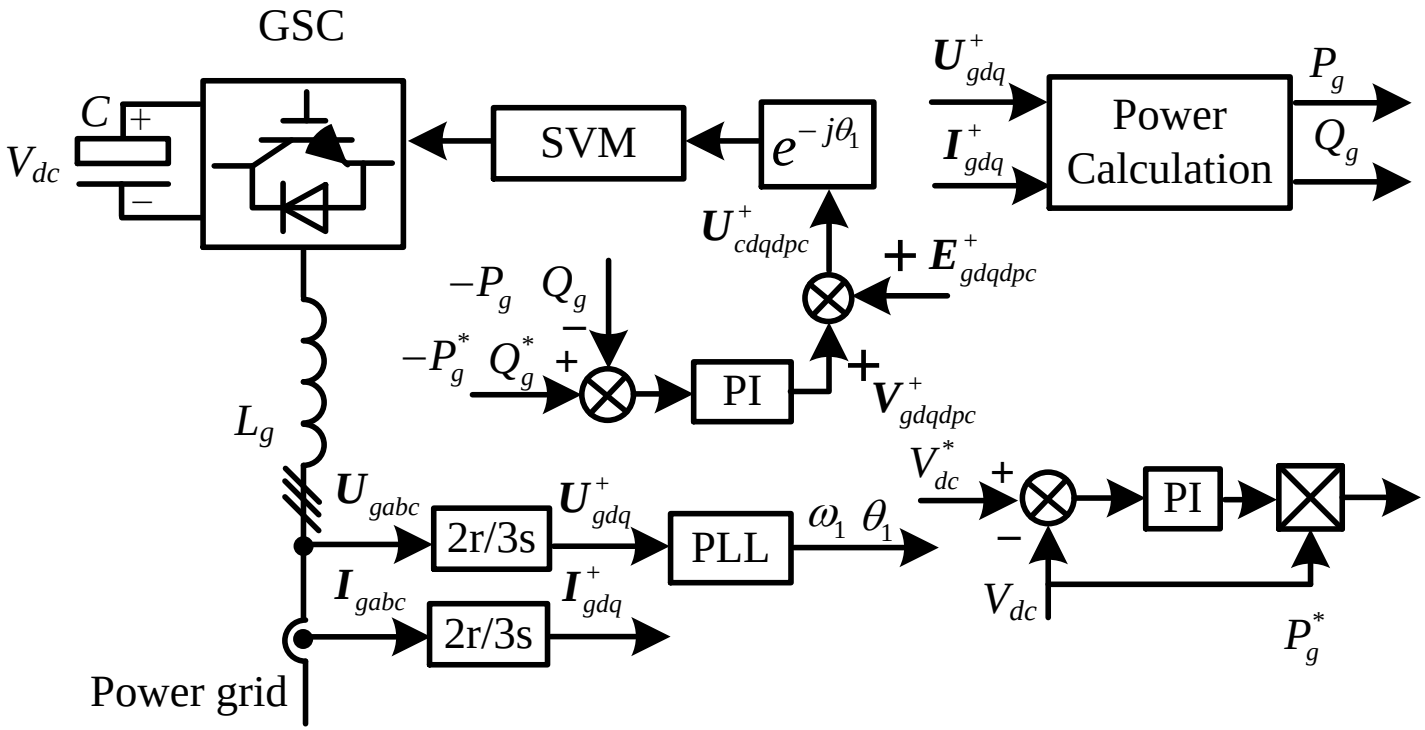

Control of DFIG Machine-side Converter

Simulation results

Grid/Stator peak phase voltage (V)	563
Rotor-side converter	
Proportional coefficient of power controller K_{p_PsQs}	1.2
Integral coefficient of power controller K_{i_PsQs}	15
Grid-side converter	
Proportional coefficient of power controller K_{p_PgQg}	2.0
Integral coefficient of power controller K_{i_PgQg}	15
Proportional coefficient of voltage controller K_{p_vdc}	12
Integral coefficient of voltage controller K_{i_vdc}	75

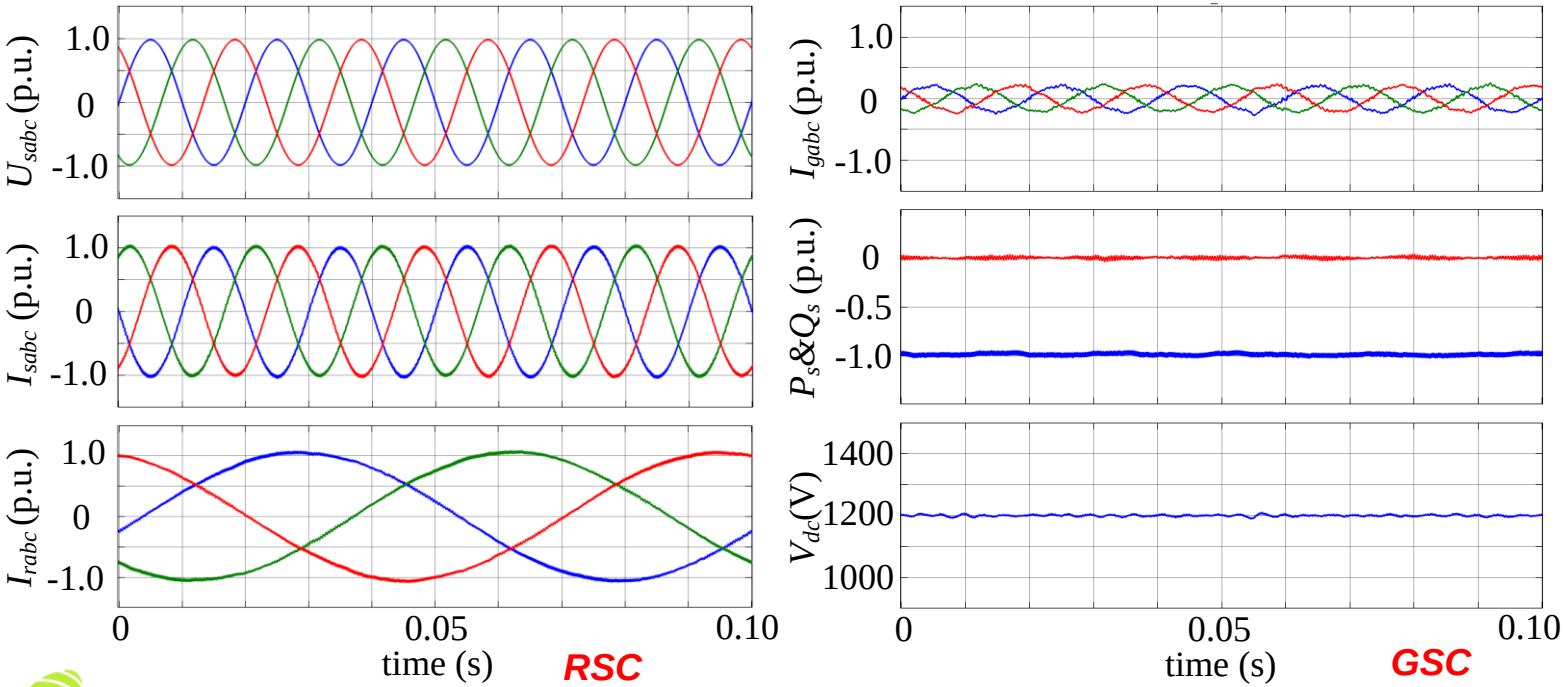

Modeling of PMSG Machine-side Converter

PMSG system with back-to-back power converter

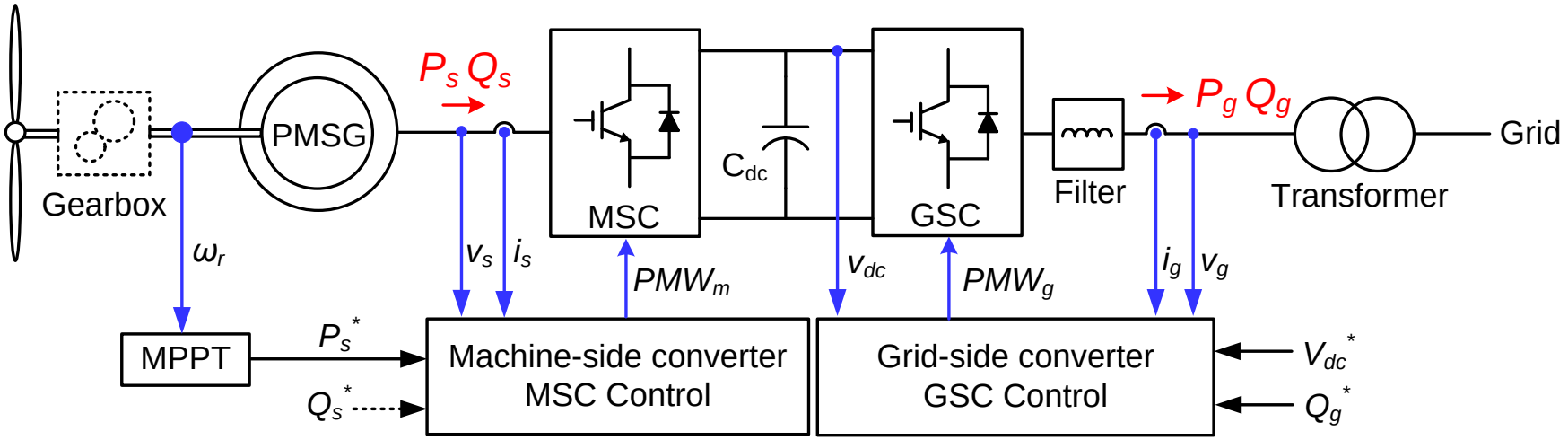

Modeling of PMSG Machine-side Converter

Steady-state equivalent circuit

Voltage equation under dq frame:

$$u_{sd} = R_s i_{sd} + L_s \frac{di_{sd}}{dt} - \omega_e L_s i_{sq}$$

$$u_{sq} = R_s i_{sq} + L_s \frac{di_{sq}}{dt} + \omega_e L_s i_{sd} + \omega_e \psi_m$$

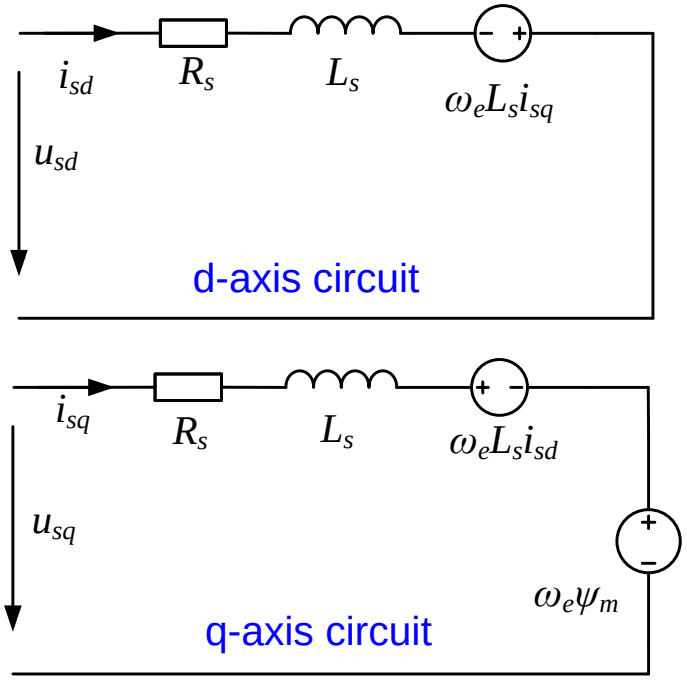

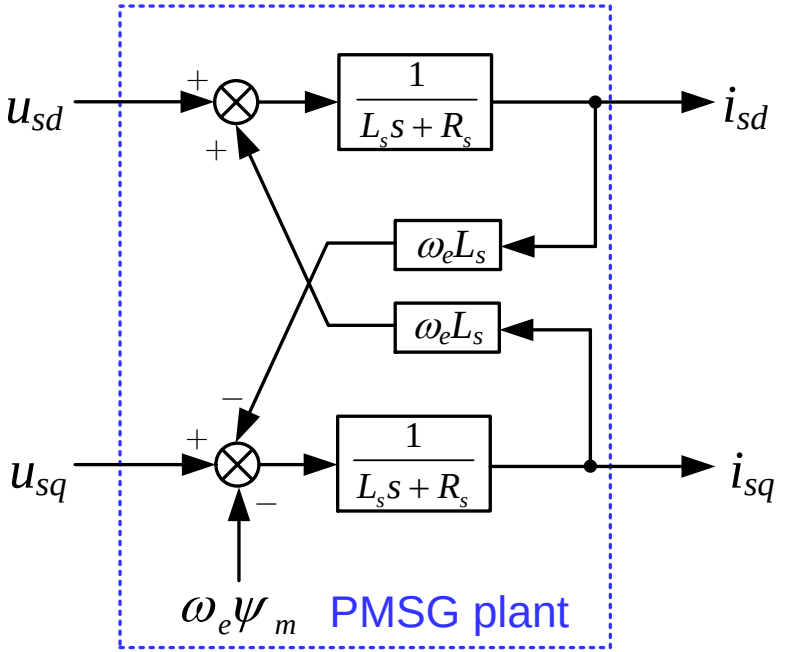

Control of PMSG Machine-side Converter

Control scheme

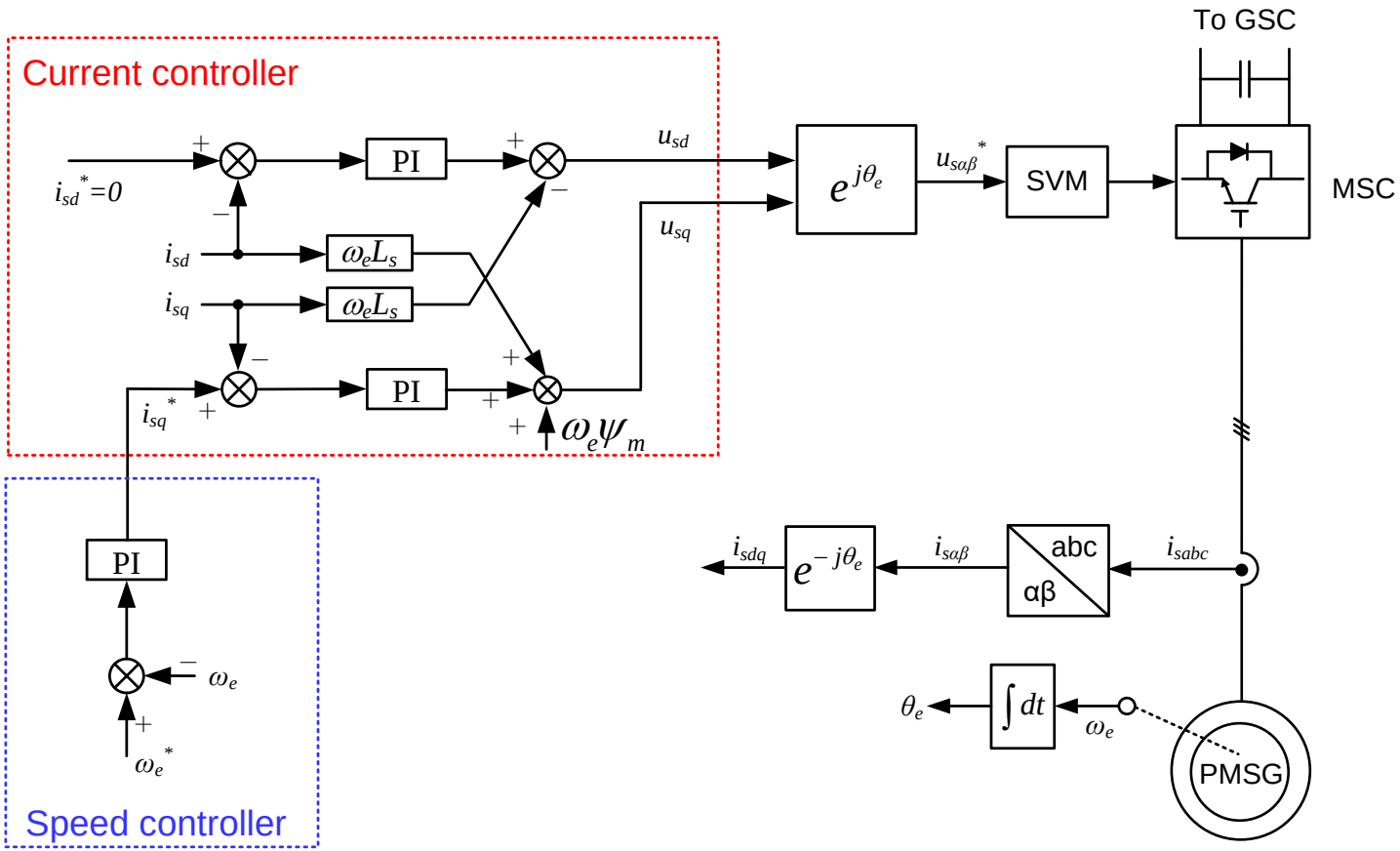

Control of PMSG Machine-side Converter

Parameters of 2 MW PMSG

MSC specification

Rated wind speed v_{w_rate} [m/s]	12
Rated turbine speed n_{rot_rate} [rpm]	19
Number of pole pairs p	102
Rated shaft speed n_s [rpm]	19
Magnetizing inductance L_m [mH]	0.276
Rated fundamental frequency f_e [Hz]	32.3
Rated output voltage [V_{rms}]	554
Rated current [A_{rms}]	2085
Proportional coefficient of speed controller K_{p_ω}	50
Integral coefficient of speed controller K_{i_ω}	1000
Proportional coefficient of current controller K_{p_is}	0.5
Integral coefficient of current controller K_{i_is}	50

GSC specification

DC-link voltage U_{dc} [V_{dc}]	1050
Switching frequency f_s [kHz]	2
Filter inductance [mH]	0.15
Rated output voltage [V_{rms}]	704
Rated current [A_{rms}]	1641
Proportional coefficient of voltage controller K_{p_vdc}	50
Integral coefficient of voltage controller K_{i_dvc}	1500
Proportional coefficient of current controller K_{p_ig}	0.3
Integral coefficient of current controller K_{i_ig}	30

Control of PMSG Machine-side Converter

Simulation validation

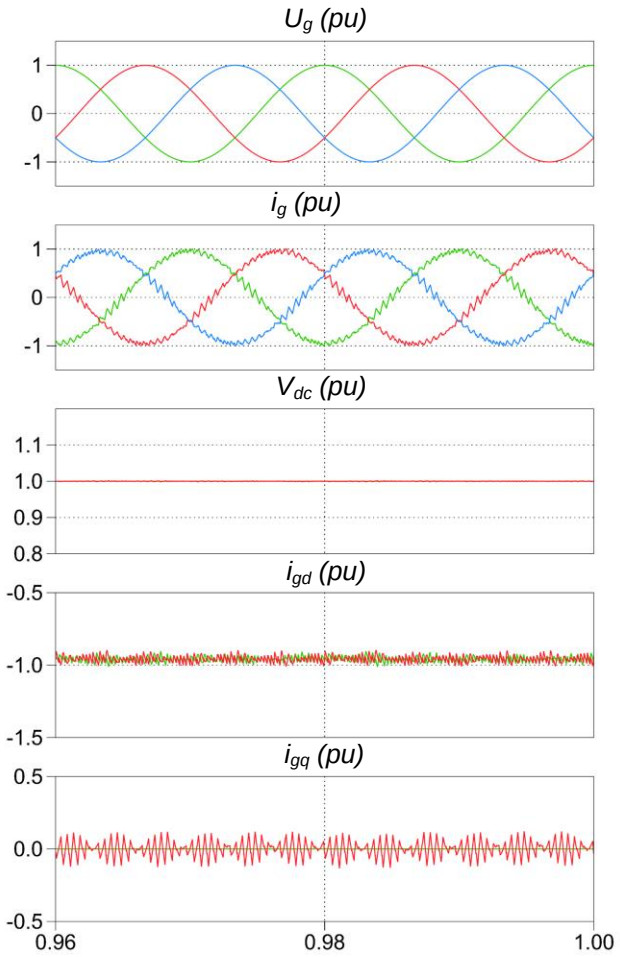

GSC steady-state

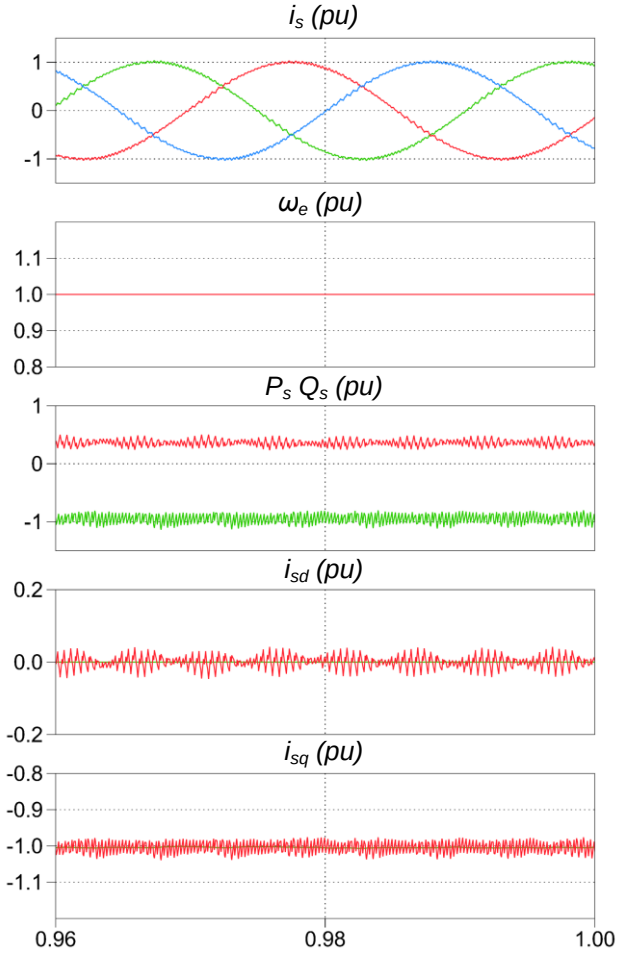

MSC steady-state

Summary

- **Control targets** of DFIG and PMSG back-to-back power converters

- Grid-side converter:
  - Modeling and control of **inner grid-current** and **outer dc-link voltage**
  - **PI controller** under dq frame
  - **PR controller** under αβ frame

- Machine-side converter:
  - DFIG system:
    - **PI controller design** of inner rotor-current and outer stator power
    - Modeling and controller design of **Direct Power Control (DPC)**
  - PMSG system:
    - **Control and simulation validation** of machine-side converter

Outline

1. State-of-art of wind turbine system
   - Configuration evolution
   - Grid codes requirement
   - General control structure

2. Modeling and control of wind turbine system
   - Topology of DFIG and PMSG
   - Modeling and control of grid-side converter
   - Modelling of control of machine-side converter (DFIG and PMSG)

3. Abnormal operation of wind turbine system
   - Classification of grid faults
   - DFIG operation under symmetrical/asymmetrical grid faults
   - PMSG operation under symmetrical/asymmetrical grid faults

Classification of Grid Faults

Definition of grid fault

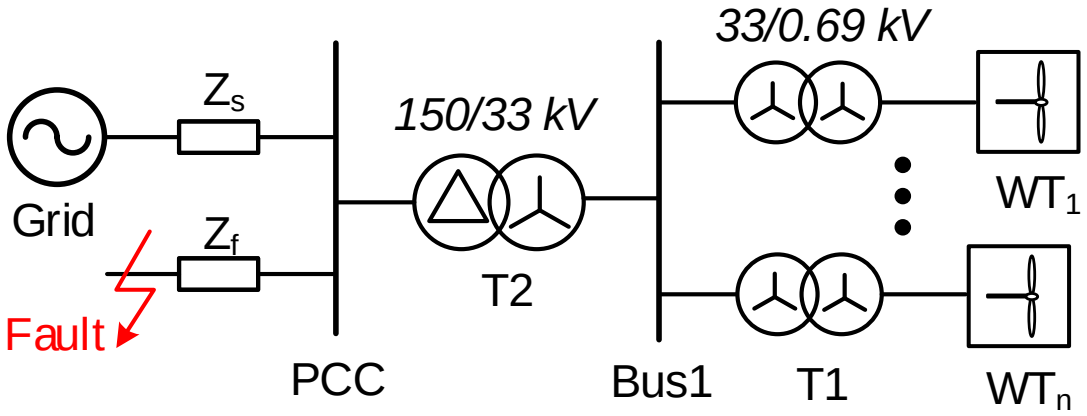

- Y/D transformer: transmission-level (PCC) and collector grid (Bus1)
- Dip level P_{dip}:

$$p_{dip} = \frac{Z_s}{Z_f + Z_s}$$

Classification of Grid Faults

Propagation of grid faults

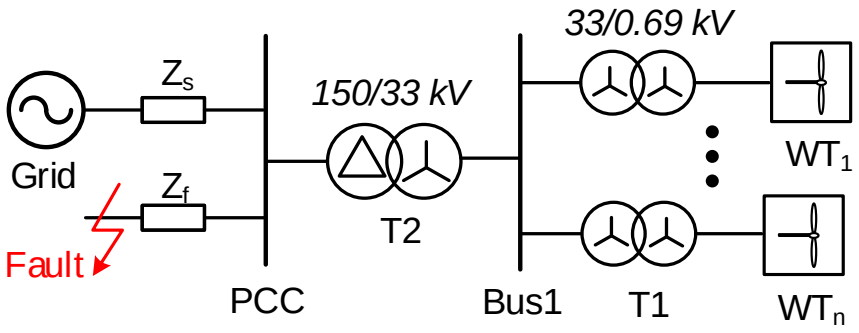

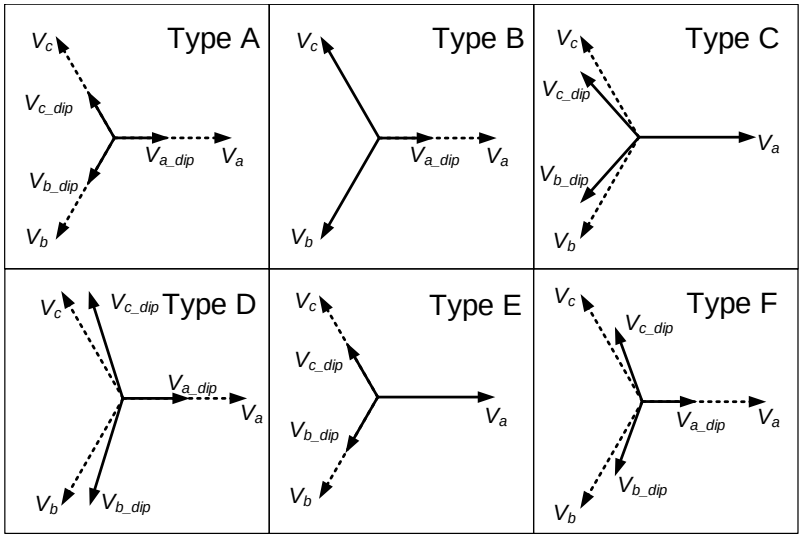

- Symmetrical fault: 3Φ-g
- Asymmetrical faults: Φ-g; 2Φ; 2Φ-g

Fault types		3Φ-g	Φ-g	2Φ	2Φ-g
PCC	Dip level	p_{dip}	p_{dip}	p_{dip}	p_{dip}
	Classification	A	B	C	E
	Pos., neg. and zero components	1- p_{dip}; 0; 0	1- $p_{dip}/3$; -$p_{dip}/3$; -$p_{dip}/3$	1- $p_{dip}/2$; $p_{dip}/2$; 0	1- 2 $p_{dip}/3$; $p_{dip}/3$; $p_{dip}/3$
Bus1	Classification	A	C	D	F
	Pos., neg. and zero components	1- p_{dip}; 0; 0	1- $p_{dip}/3$; $p_{dip}/3$; 0	1- $p_{dip}/2$; -$p_{dip}/2$; 0	1- 2 $p_{dip}/3$; -$p_{dip}/3$; 0

Classification of Grid Faults

Grid codes requirement on Low-Voltage Ride-Through

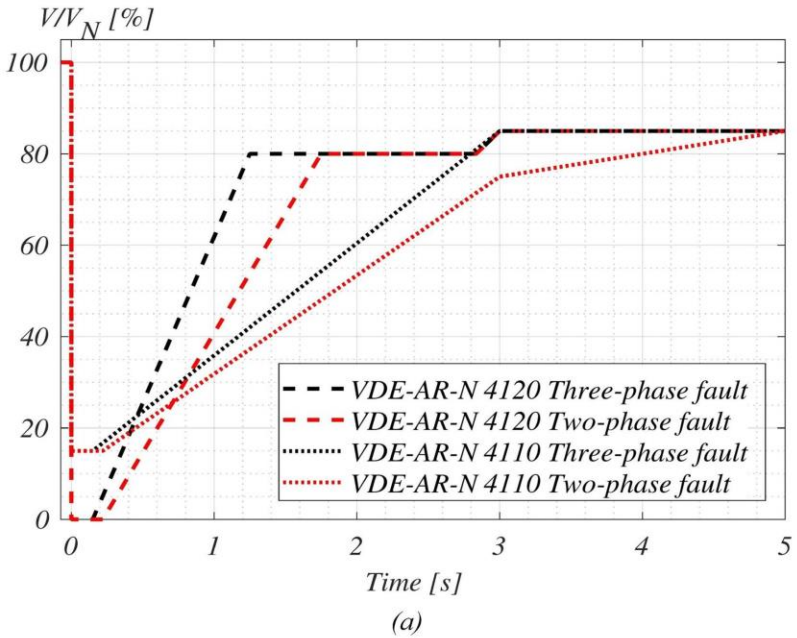

(a)

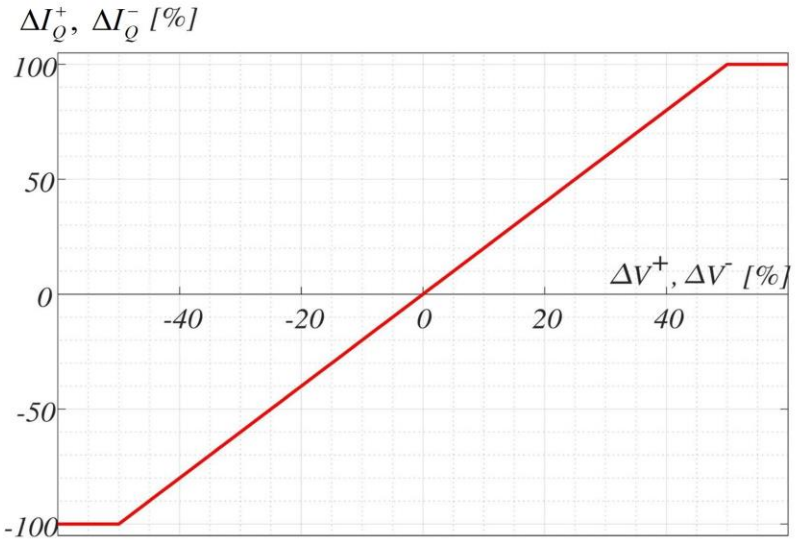

(b)

- Various withstand periods with different types of grid faults
- Reactive current to support voltage recovery

DFIG Operation under Grid Faults

Existing challenges during grid fault

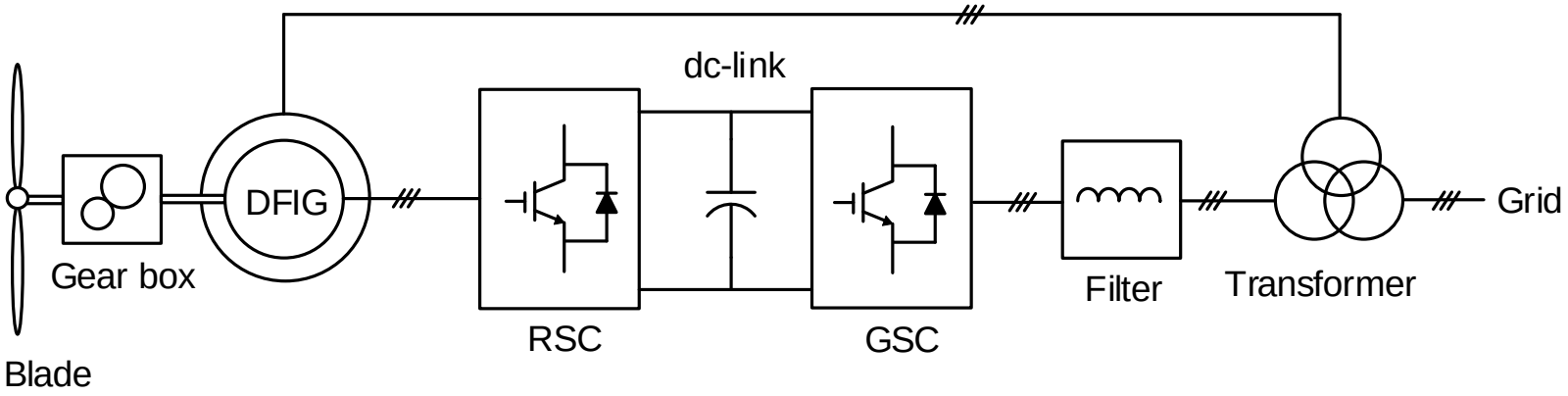

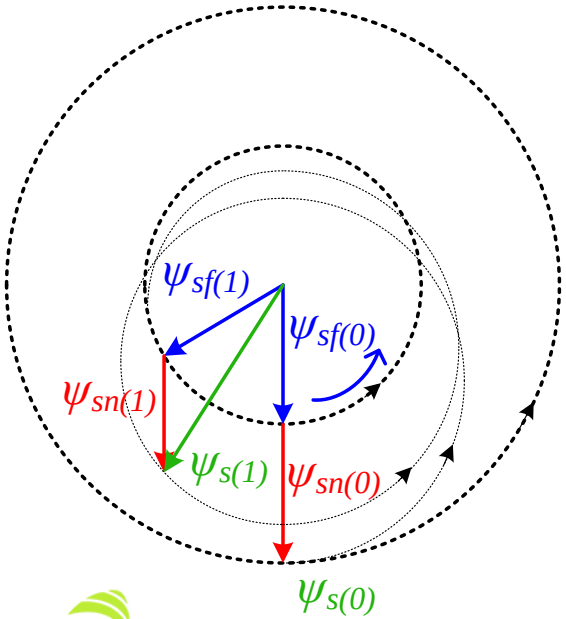

- Stator flux cannot be changed abruptly
- Rotor voltage is related to stator flux and rotor current:

$$\overline{u_r^r} = \frac{L_m}{L_s}\frac{d}{dt}\overline{\varphi_s^r} + (R_r + \sigma L_r \frac{d}{dt})\overline{i_r^r}$$

- Stator flux under rotor reference frame:

$$\overline{\varphi_s^r} = \frac{U_s}{j\omega} e^{j(\omega-\omega_r)t}$$

DFIG Operation under Grid Faults

Dynamic DFIG models during grid fault

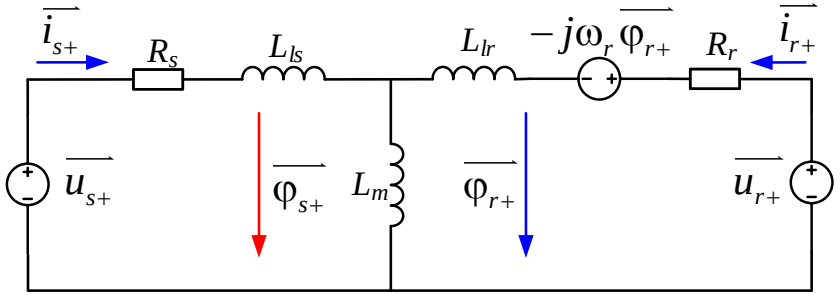

Positive machine

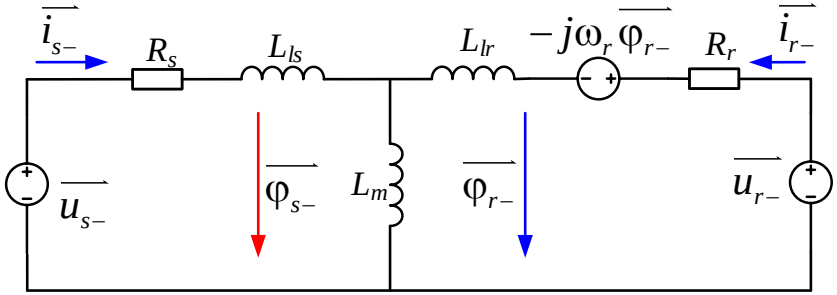

Negative machine

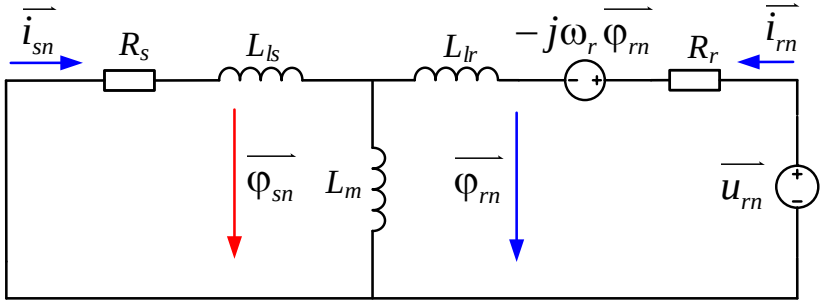

Natural machine

$$\overrightarrow{\varphi_s^r} = \frac{U_s}{j\omega} e^{j(\omega-\omega_r)t}$$

$$e_{r+} = \frac{L_m}{L_s} \mathrm{s} \cdot U_{s+}$$

$$e_{r-} = \frac{L_m}{L_s} (2-\mathrm{s}) \cdot U_{s-}$$

$$e_{rn} = \frac{L_m}{L_s} (1-\mathrm{s}) \cdot U_{sn}$$

DFIG Operation under Grid Faults

Max. and min. natural flux under various grid faults

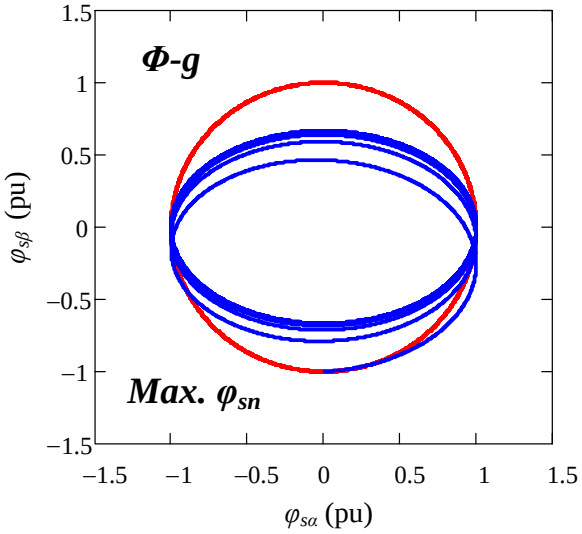

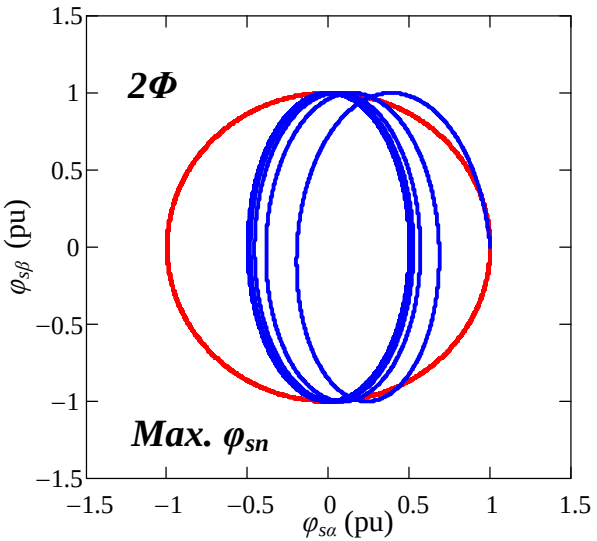

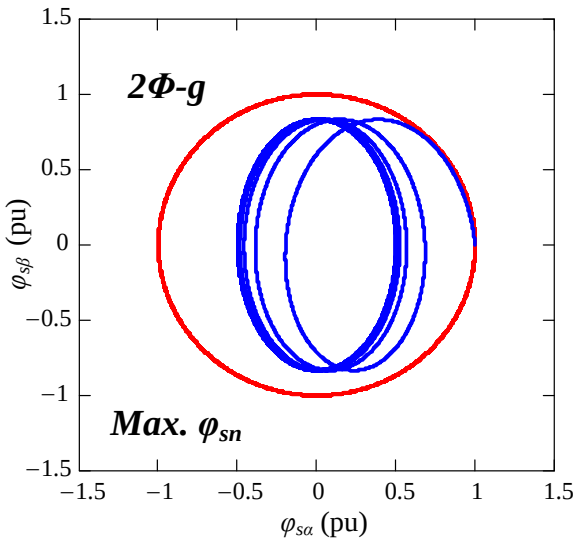

Fault types	3Φ-g	Φ-g	2Φ	2Φ-g
Max. natural flux (pu)	p_{dip}	$p_{dip}/3$	p_{dip}	p_{dip}
Min. natural flux (pu)	p_{dip}	0	0	$p_{dip}/3$

DFIG Operation under Grid Faults

State-of-art solutions

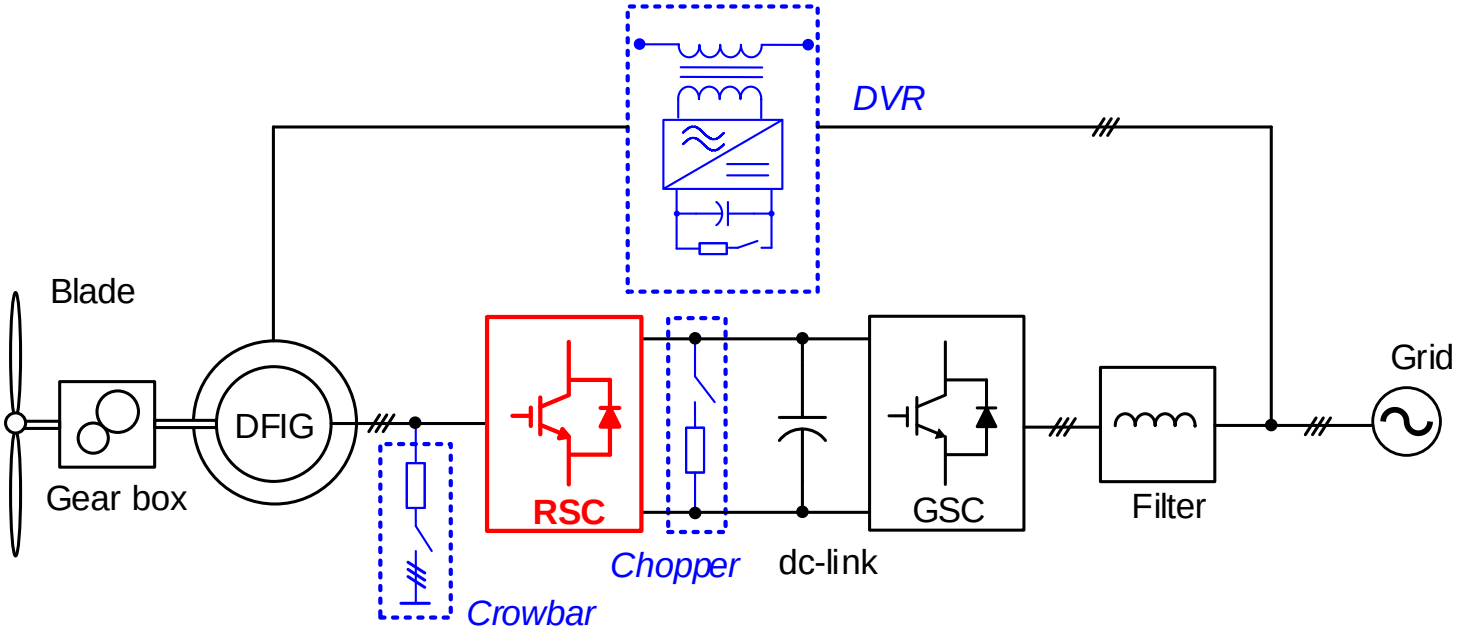

- Hardware solutions:
  - DVR: maintain a constant stator voltage during grid faults
  - Crowbar & dc-chopper: acceleration of natural flux damping
- Software solutions:
  - Demagnetizing control

DFIG Operation under Grid Faults

Concept of demagnetizing control

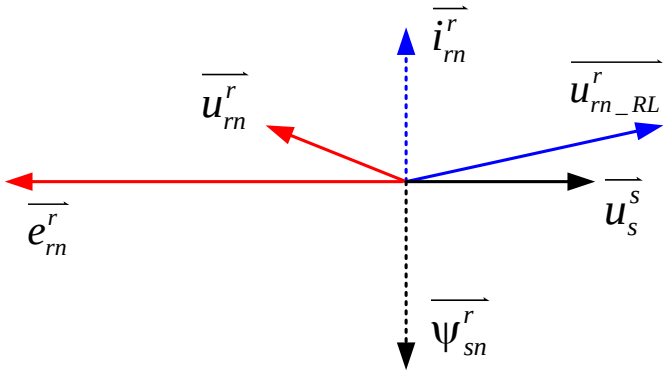

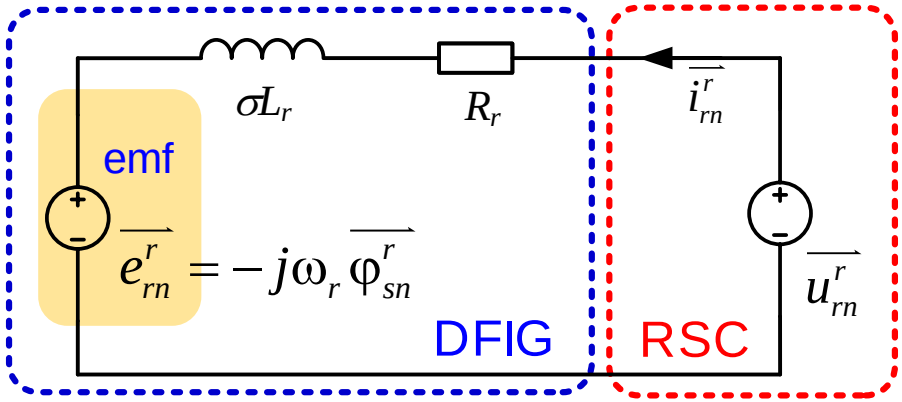

- Rotor current is controlled in opposite of the natural flux
- Most effective way to overcome transient natural flux
- Counteraction of rotor emf

DFIG Operation under Grid Faults

Safe Operation Area (SOA) during symmetrical faults

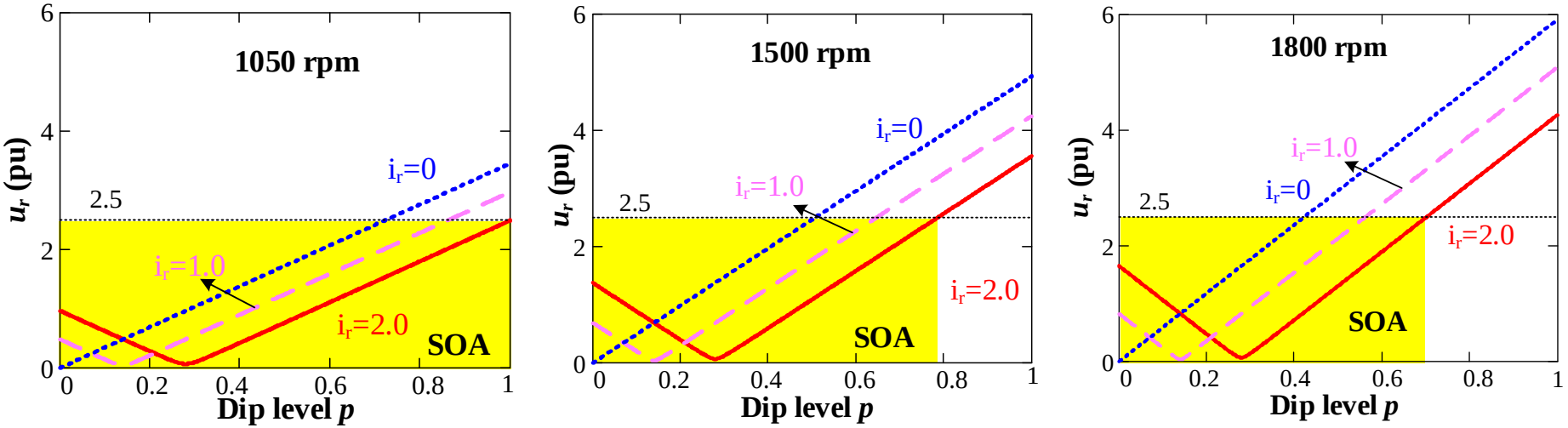

- Maximum of 2 pu demagnetizing current can be provided
- Higher rotor speed causes higher rotor emf
- A higher amount of demagnetizing current facilitates a higher ride-through capability

DFIG Operation under Grid Faults

Control scheme during symmetrical faults

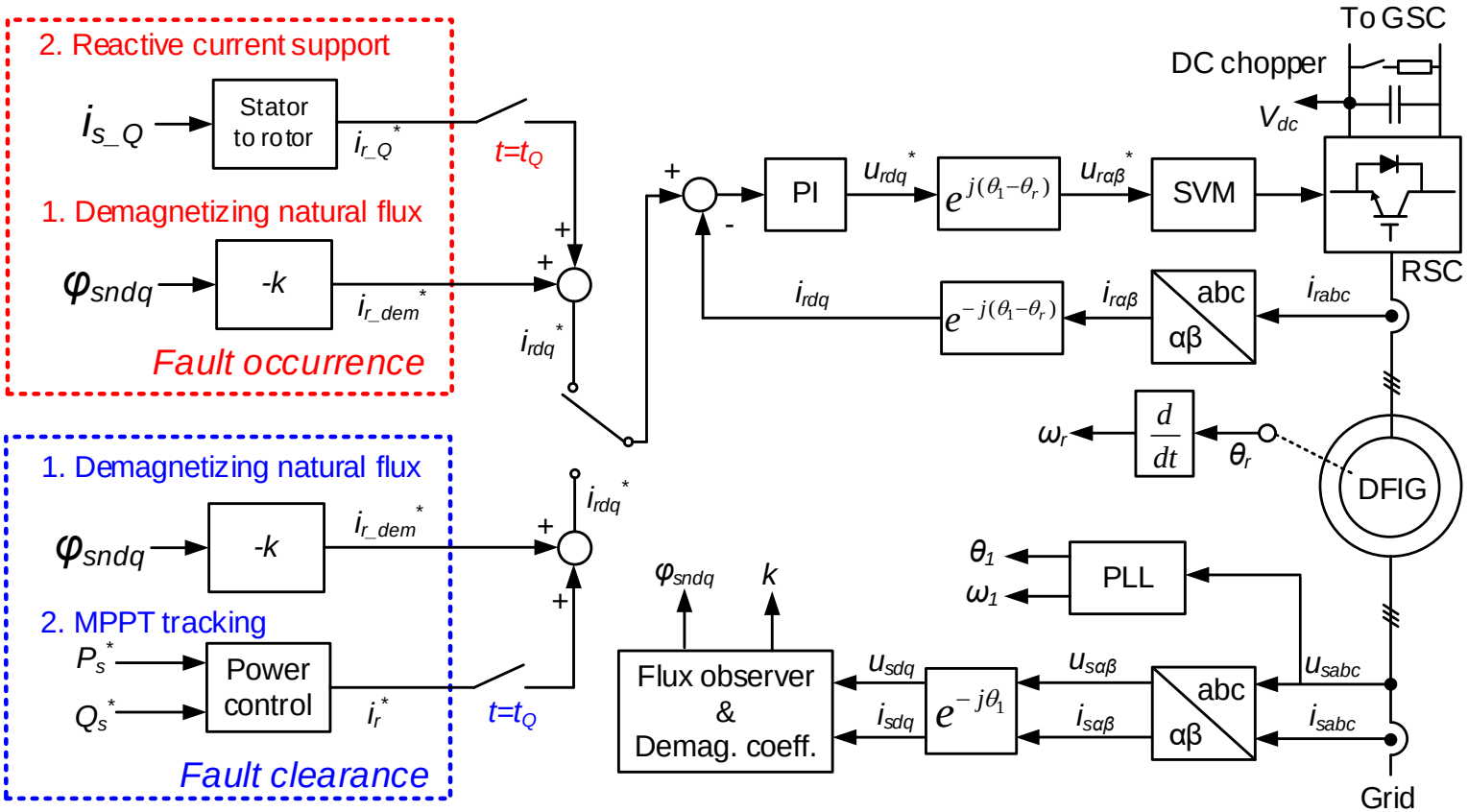

DFIG Operation under Grid Faults

Symmetrical faults at 1800 rpm

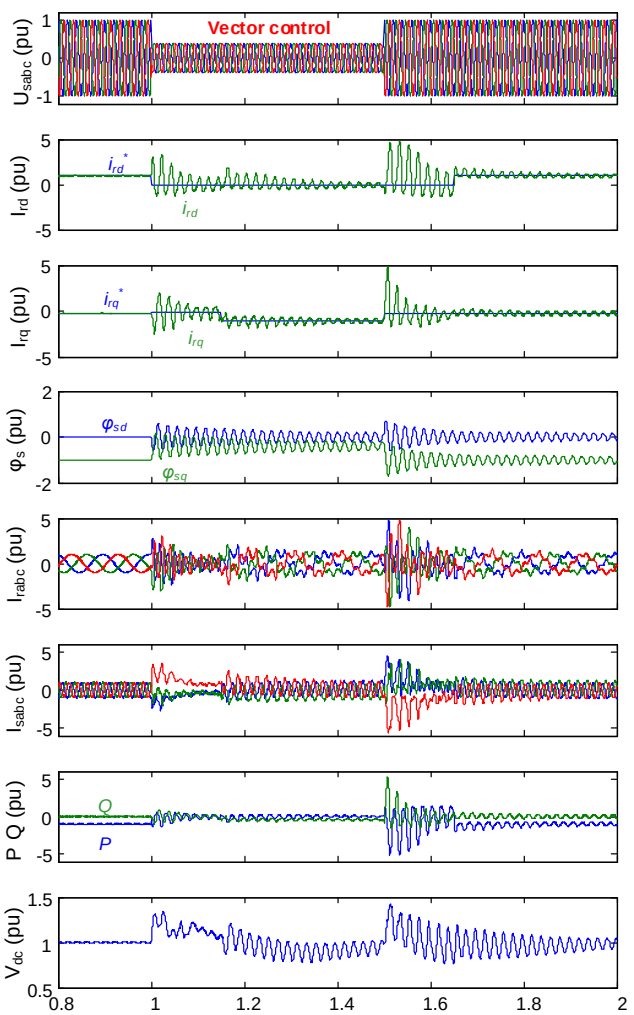

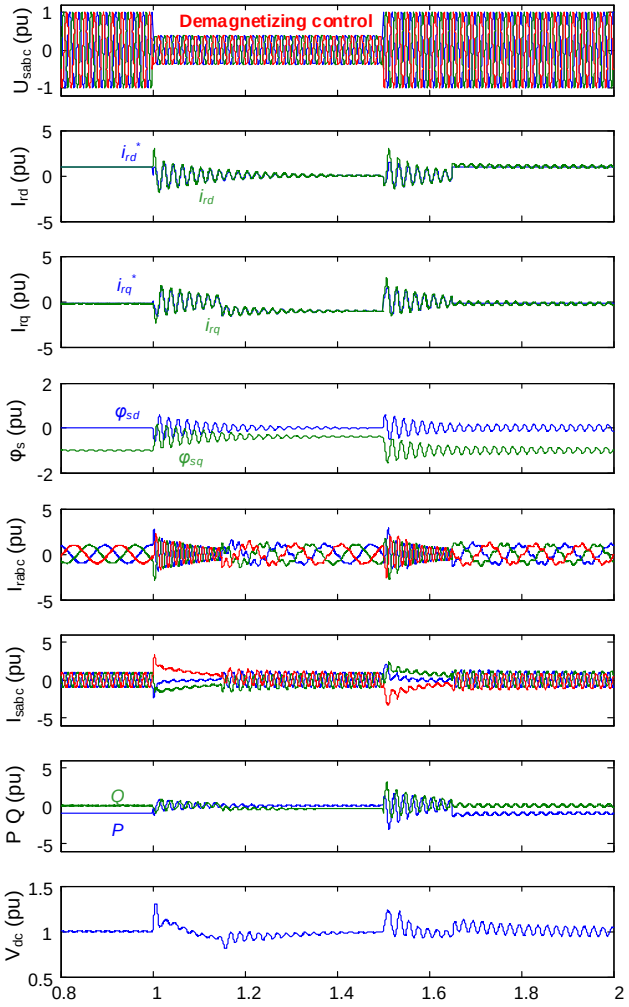

DFIG Operation under Grid Faults

Capability at various asymmetrical faults

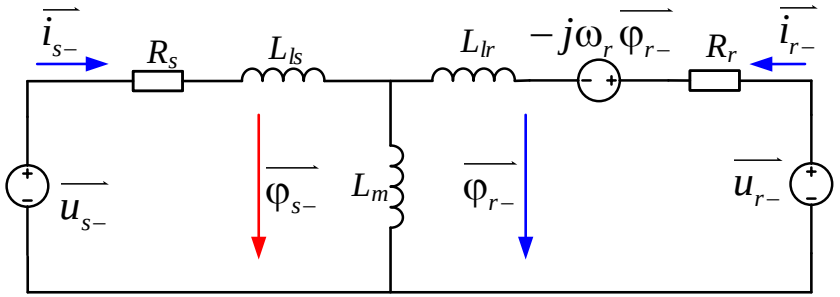

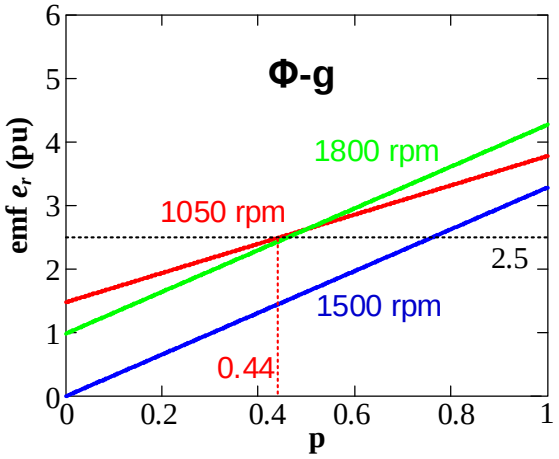

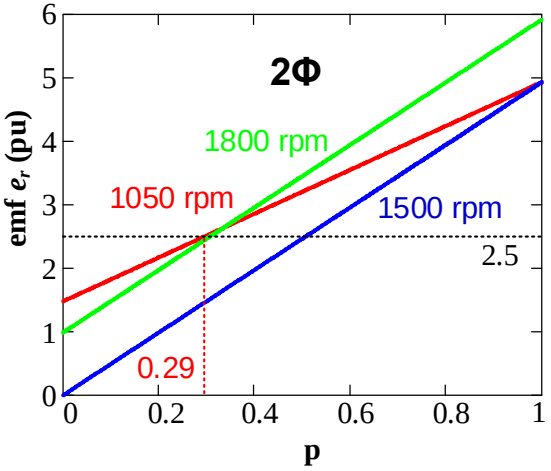

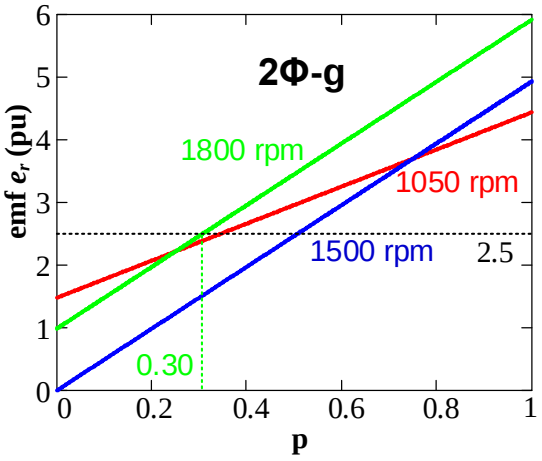

DFIG Operation under Grid Faults

Control objectives during asymmetrical faults

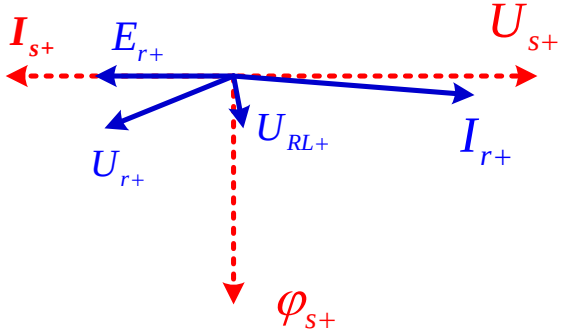

Positive component

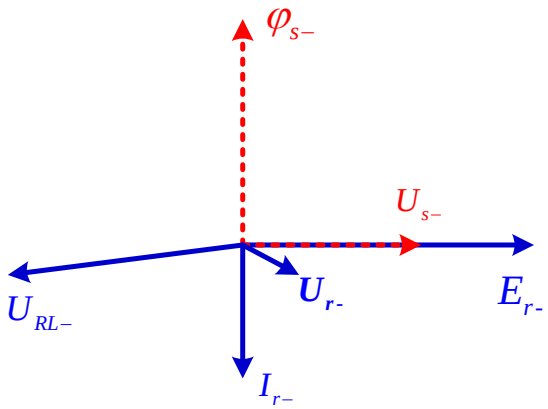

Negative component

- Normal condition: rotor current is almost in reverse with stator current
- Asymmetrical fault: rotor current is in the opposite of negative stator flux

DFIG Operation under Grid Faults

Improved capability using demagnetizing rotor current

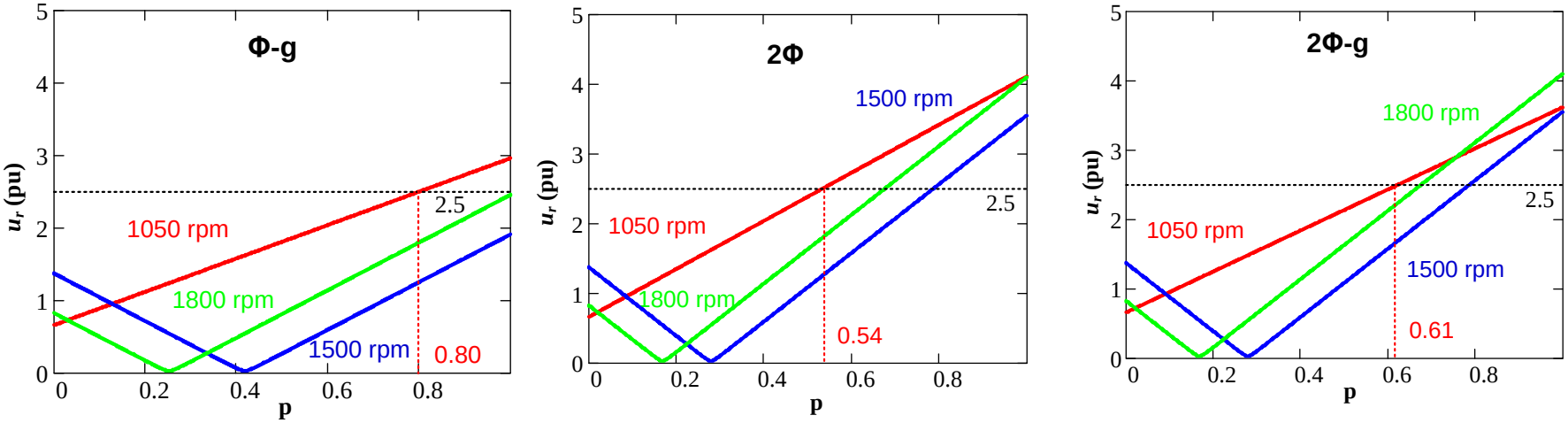

- Φ-g fault: withstand up to 0.80 dip level, compared to 0.44 dip level of traditional control
- 2Φ-g fault: withstand dip level from 0.29 to 0.54
- 2Φ fault: withstand dip level from 0.30 to 0.61

DFIG Operation under Grid Faults

Control scheme during asymmetrical faults

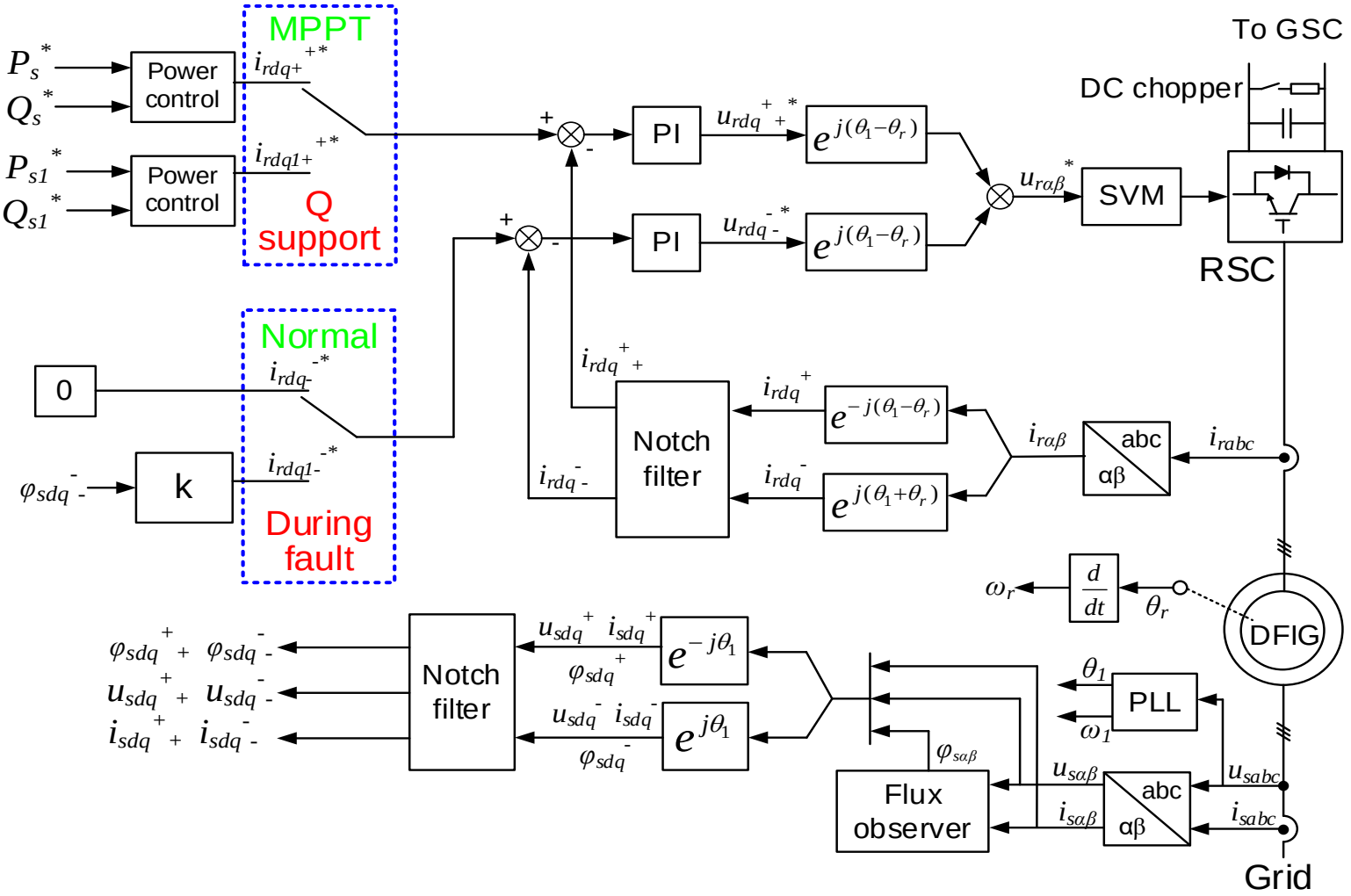

DFIG Operation under Grid Faults

Simulation results at Φ-g fault

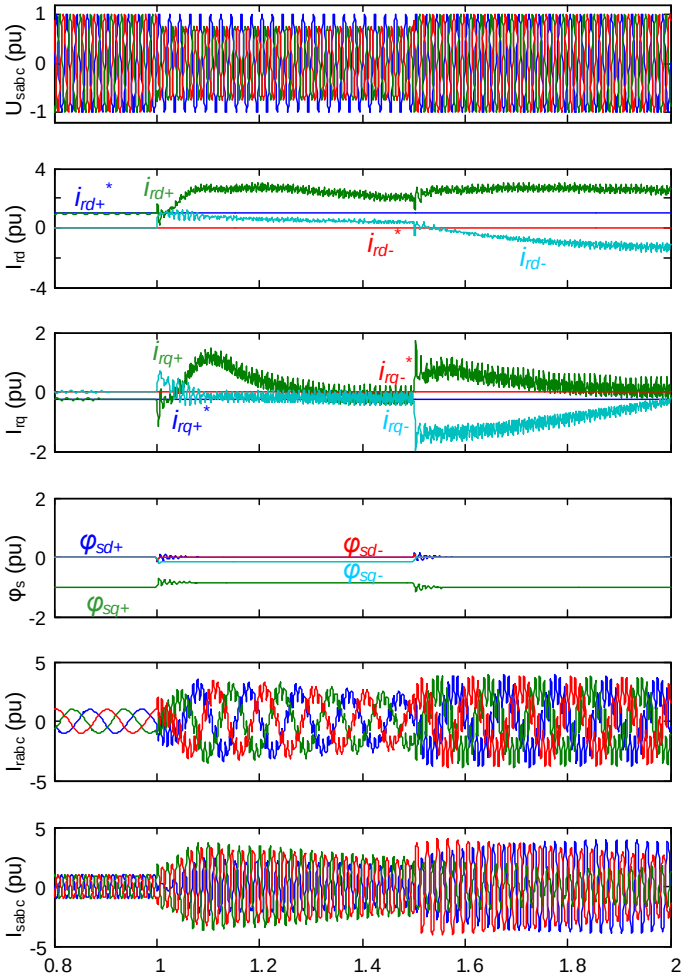

Traditional vector control

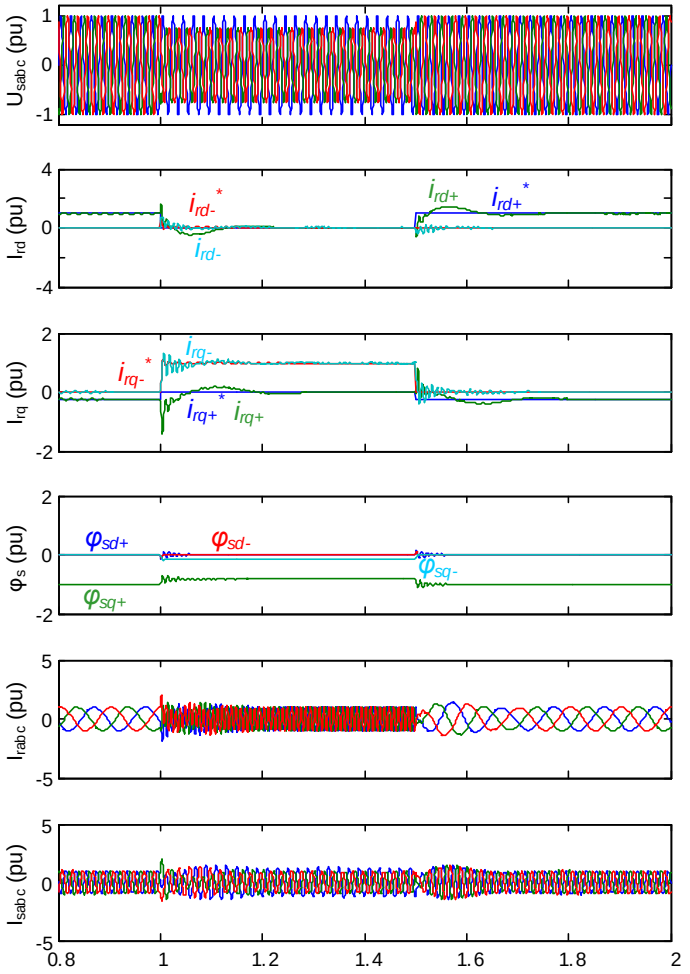

Proposed demagnetizing control

PMSG Operation under Grid Faults

PMSG system subjects to grid fault

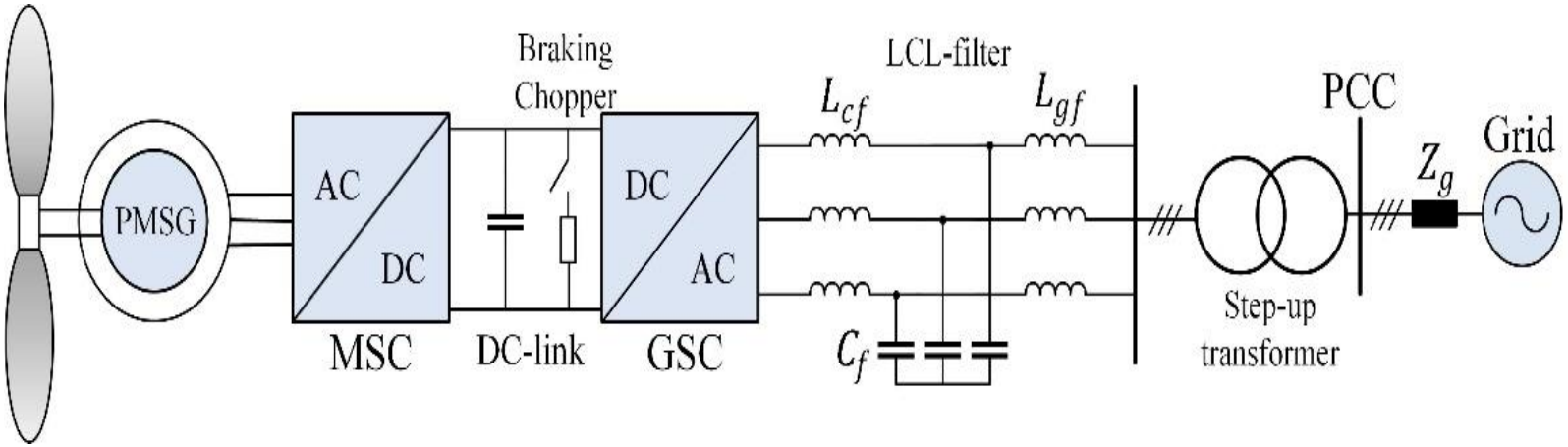

- Full-scale power converter fully decouples generator and power grid
- Grid-side converter is responsible for grid faults

PMSG Operation under Grid Faults

Control structure during symmetrical fault

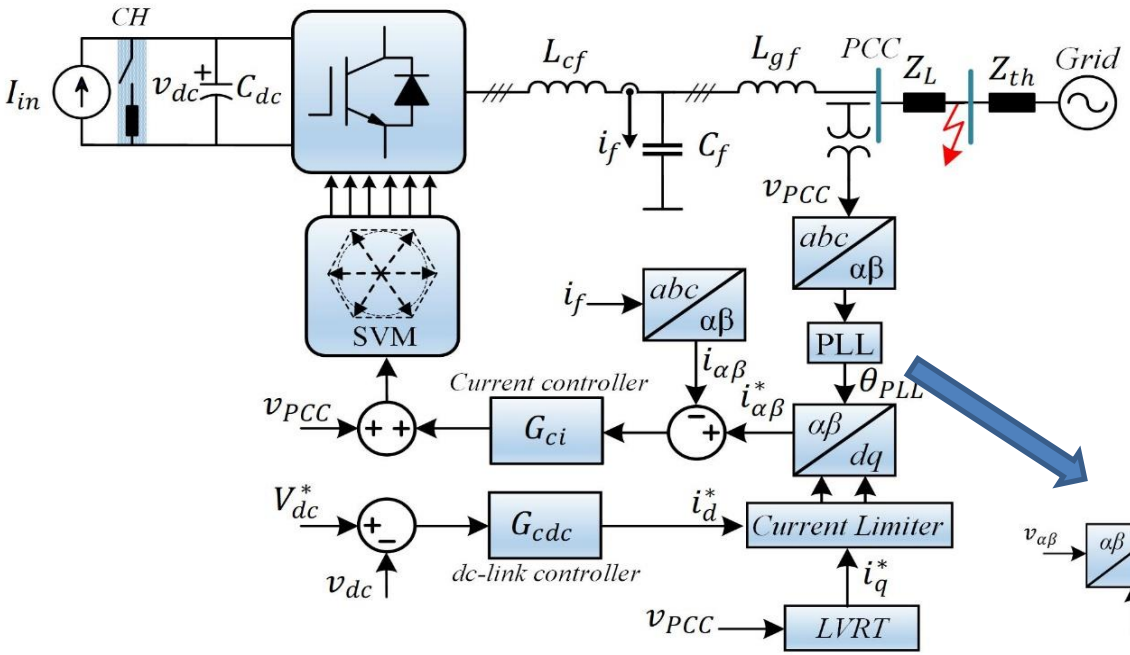

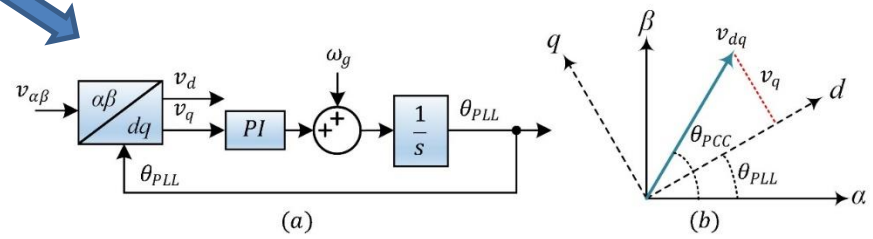

❖ Transfer function of SRF-PLL:

$$\frac{\theta_{PCC}(s)}{\theta_{PLL}(s)} = \frac{T(s)}{1+T(s)} = \frac{V_{PCC}K_p s + V_{PCC}K_i}{s^2 + V_{PCC}K_p s + V_{PCC}K_i},$$

❖ Control plant: $$G_{if}(s) = \left.\frac{i_f(s)}{v_{inv}(s)}\right|_{V_g=0} = \frac{s^2+\omega_{LC}^2}{L_{cf}s(s^2+\omega_r^2)},$$

❖ PR controller: $$G_{PR} = K_p + \frac{K_r s}{s^2+\omega_0^2},$$

❖ Current open-loop function:

$$G_{ol,c}(s) = G_{PR}(s)e^{-T_d s}G_{if}(s),$$

PMSG Operation under Grid Faults

7.5 kW PMSG system parameters

Symbol	Description	Physical Value
S_b	Rated power	7.5 kVA
V_N	Nominal grid voltage	400 V
f_n	Nominal frequency	50 Hz
V_{dc}^*	dc-link voltage reference	730 V
Q_{ext}^*	External reactive power reference	0
C_{dc}	dc-link capacitance	0.5 mF
L_{cf}	Converter-side inductor	0.071 pu
L_{gf}	Grid-side inductor	0.043 pu
C_f	Filter capacitor	0.068 pu
f_{sw}	Switching frequency	10 kHz
f_s	Sampling frequency	10 kHz
Z_L	Line reactance	0.1 pu
Z_g	Grid impedance	0.1 pu
SCR	Short-circuit ratio	5
I_{lim}	Maximum temporary converter current	1.2 pu
$K_{p,ic}$	Proportional gain PR controller	12
$K_{r,ic}$	Resonant gain of PR controller	2000

PMSG Operation under Grid Faults

Simulation results

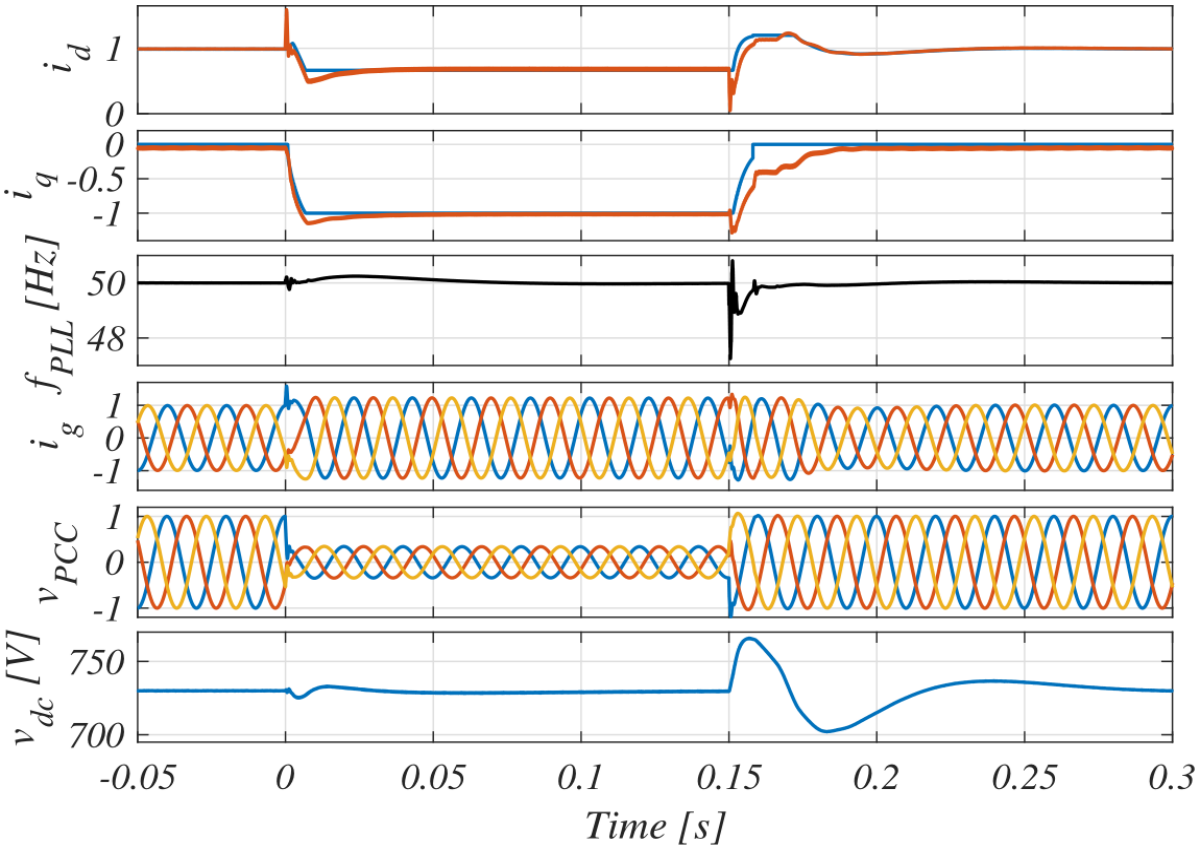

PMSG Operation under Grid Faults

Zero-voltage ride-through capability

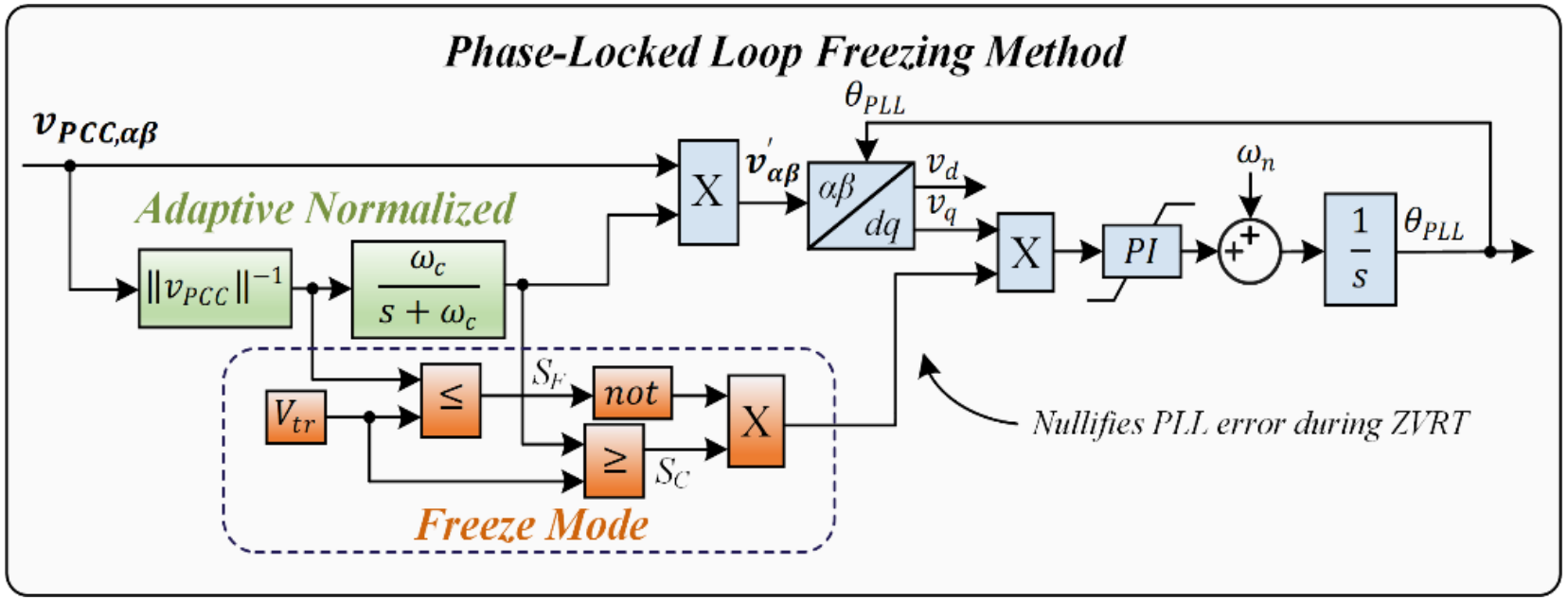

- Adaptive voltage normalization for independent voltage amplitude
- During fault: keeping pre-fault frequency and phase-angle
- Fault clearance: PLL is switched back to normal operation

PMSG Operation under Grid Faults

Simulation results at zero-voltage fault

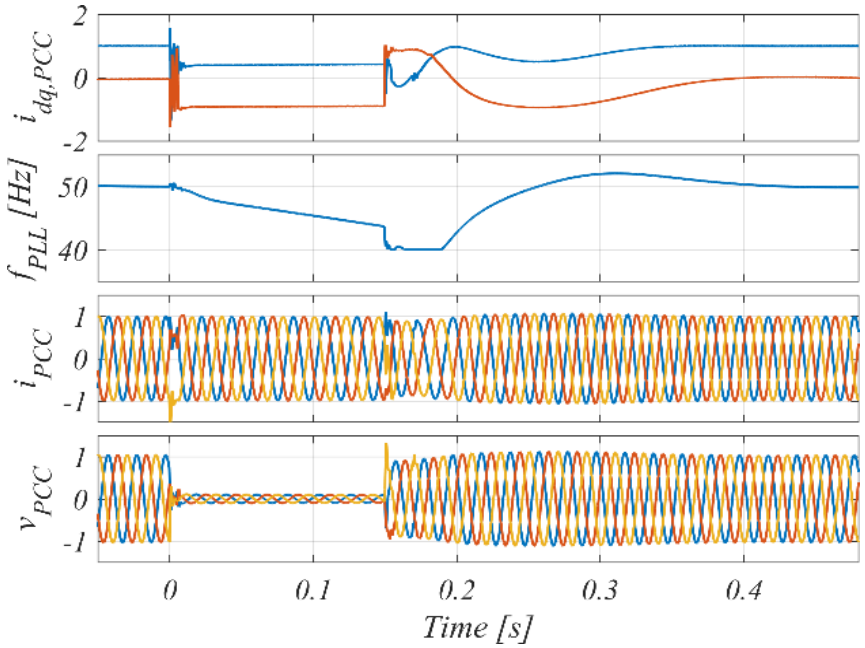

Adaptive PLL without freezing method

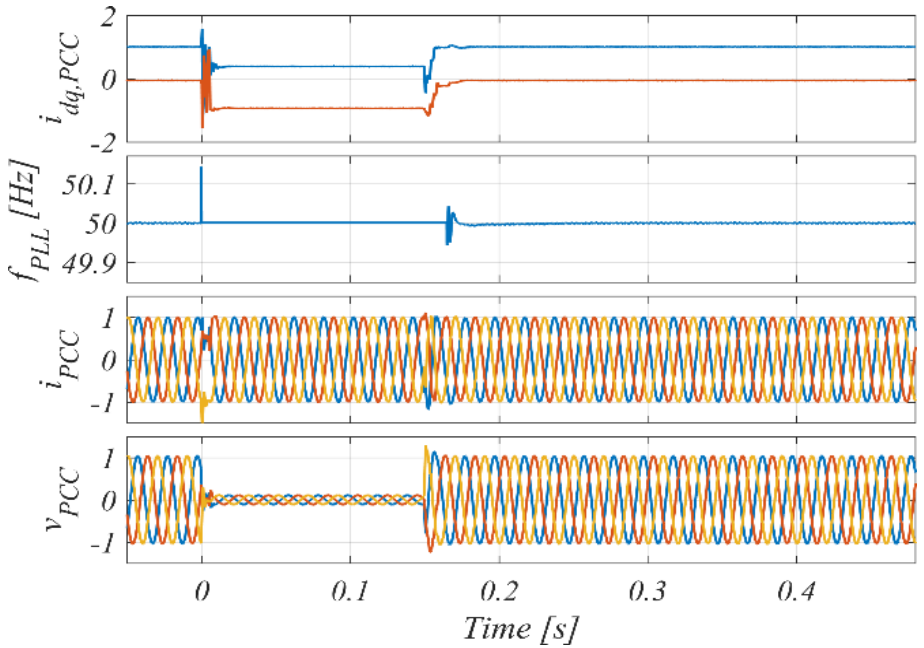

Adaptive PLL with freezing method

PMSG Operation under Grid Faults

Grid Synchronization during asymmetrical faults

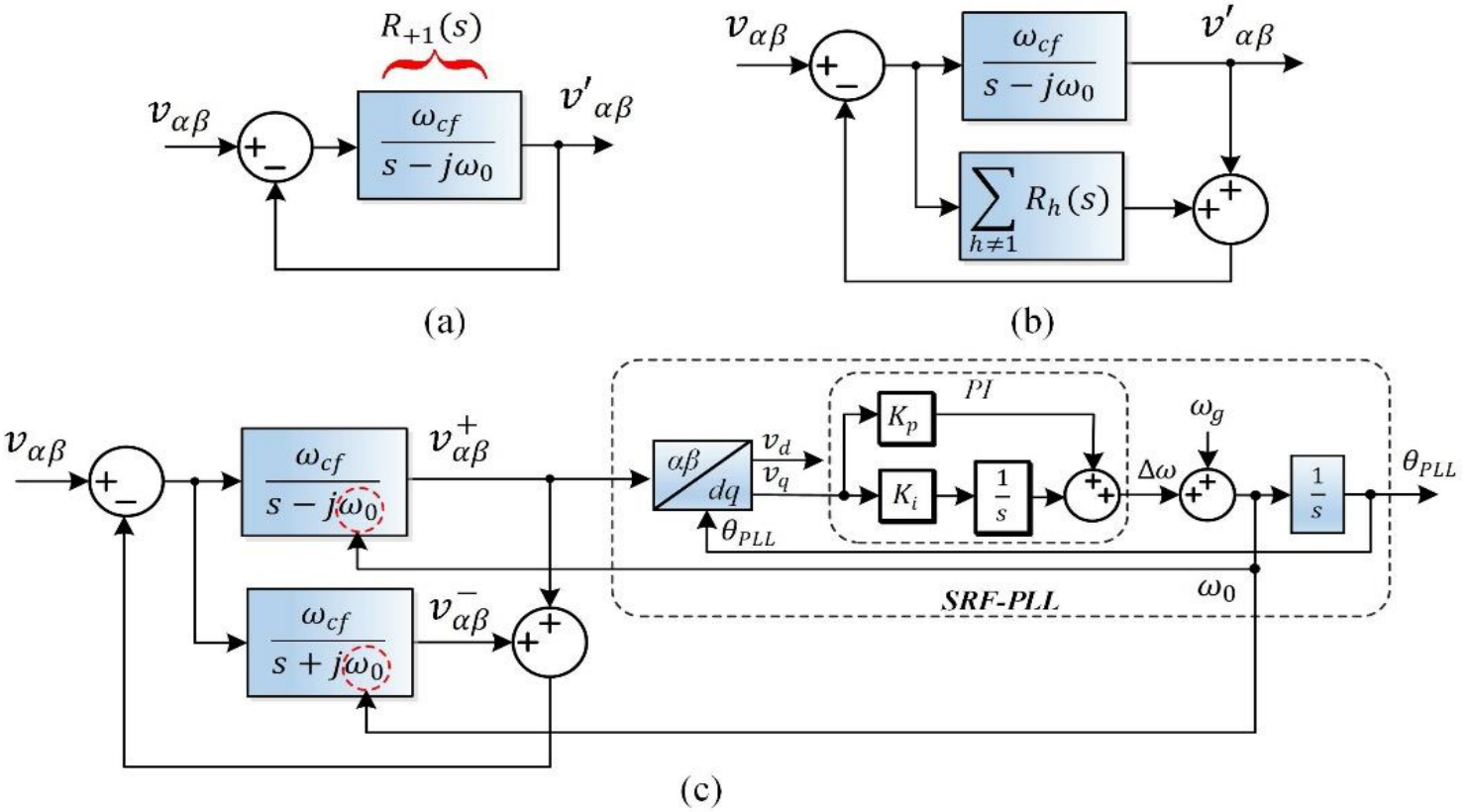

PMSG Operation under Grid Faults

Current-reference generation method

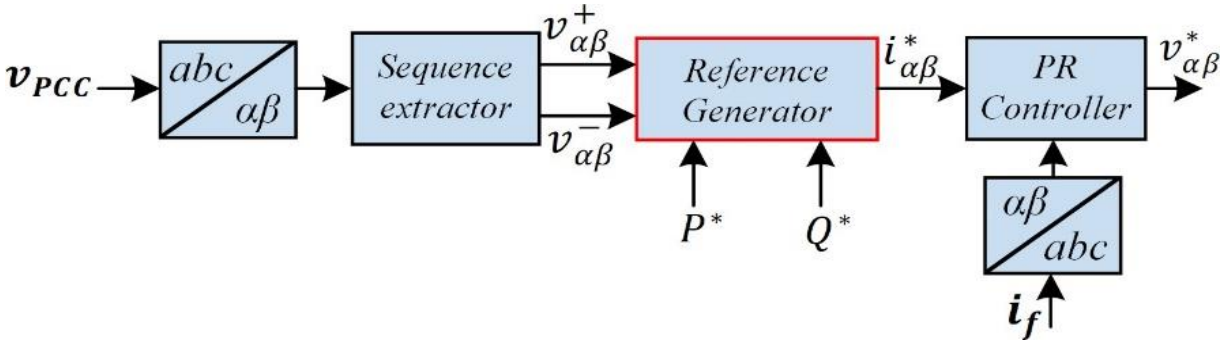

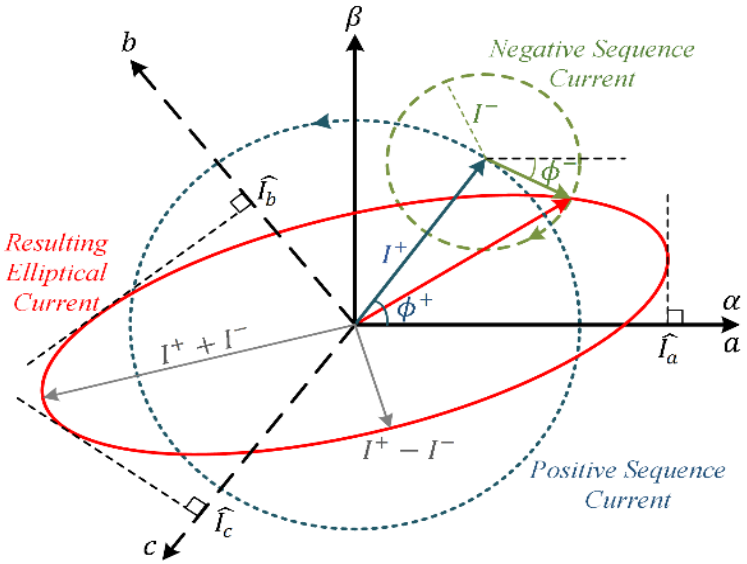

PMSG Operation under Grid Faults

Control scheme during asymmetrical fault

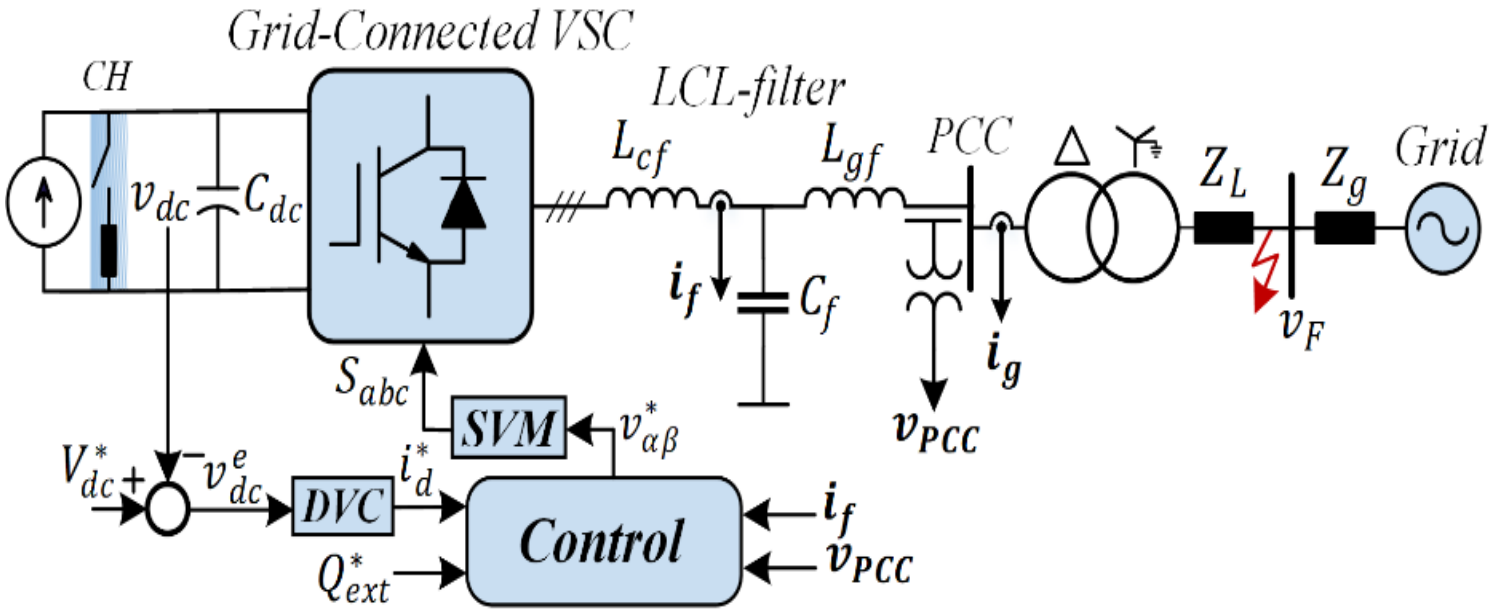

PMSG Operation under Grid Faults

Simulation results

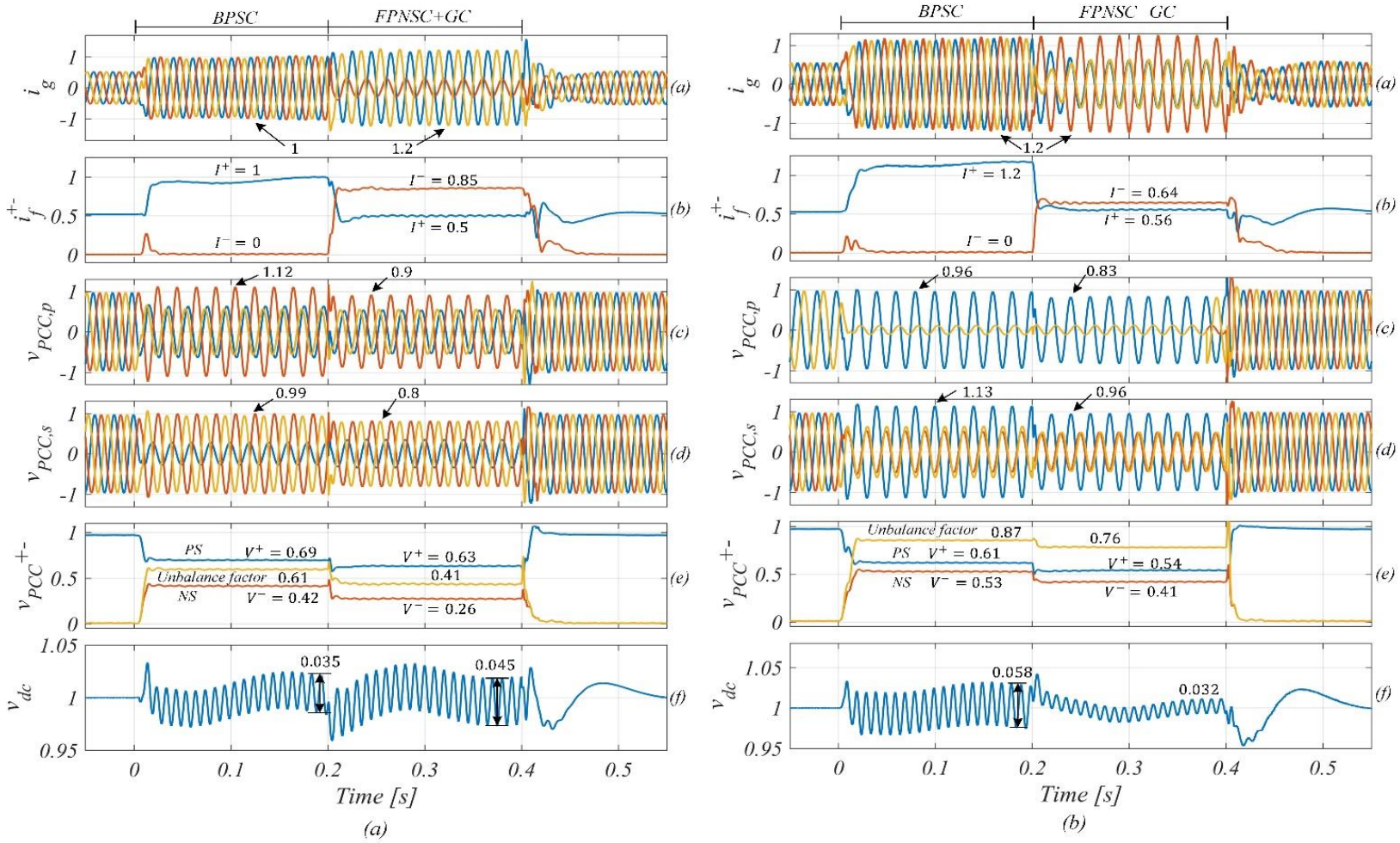

Single line-to-ground fault ***Line-to-line fault***

Summary

- Investigation of **various grid fault types** in power system and **their propagation** through Y/D transformer

- Type III wind turbine:
  - Newly introduced **natural and negative stator flux** may lead to rotor-side converter out-of-control
  - **Demagnetizing control** can be applied to overcome symmetrical/asymmetrical faults

- Type IV wind turbine:
  - Symmetrical faults: advanced PLL to achieve **zero-voltage ride-through**
  - Asymmetrical faults: novel current reference generation method with **dual-sequence current provision**

References

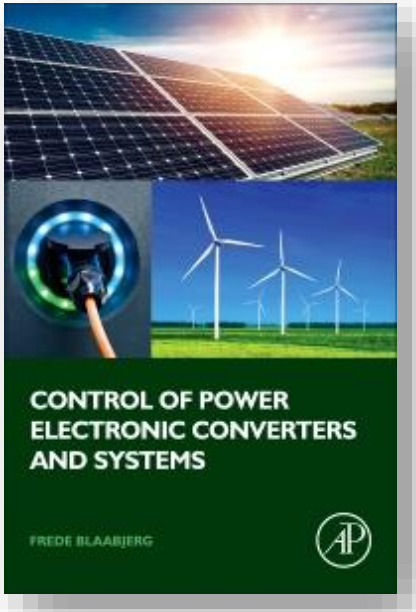

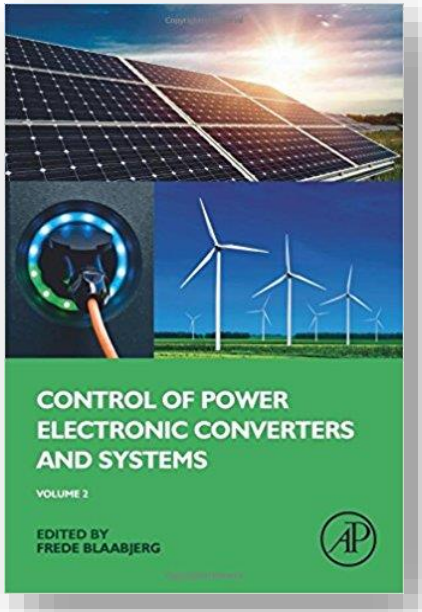

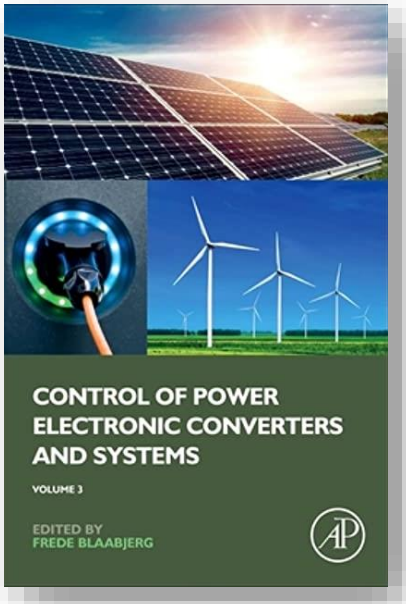

1. D. Zhou, Y. Song, and F. Blaabjerg, Control of Power Electronic Converters and Systems. Elsevier Publisher, 2017. (Chapter 5: Modelling and Control of three-phase ac/dc converter including Phase Locked Loop)
2. D. Zhou, Y. Song, and F. Blaabjerg, Control of Power Electronic Converters and Systems. Elsevier Publisher, 2017. (Chapter 10: Control of Wind Turbine Systems)
3. D. Zhou, and M. G. Taul, Control of Power Electronic Converters and Systems. Elsevier Publisher, 2021. (Chapter 19: Abnormal Operation of Wind Turbine Systems)

Thank you for your attention!

Questions & Comments ?

Dao Zhou

Email: zda@et.aau.dk